

**New and Innovative Equipment and Technologies for the  
Remote Sensing and Surveillance of Oil In and Under Ice**



**Minerals Management Service**  
*Contract Number 1435-01-04-36285*

**March 9, 2005**

# **New and Innovative Equipment and Technologies for the Remote Sensing and Surveillance of Oil In and Under Ice**

March 9, 2005

*Contract Number 1435-01-04-36285*

*Supported by:*

**United States Department of Interior  
Minerals Management Service  
Herndon, Virginia**

*Prepared by:*

**DF Dickins Associates Ltd.,  
La Jolla, CA**

Tel: 858 453-8688 Fax: 858 453-6766

[info@dfdickins.com](mailto:info@dfdickins.com)

*In association with*

Shell Global Solutions (US) Inc.  
Boise State University  
University of Glasgow

Polaris Applied Sciences Inc.  
Exploration Technologies Inc.  
US Army CRREL  
MAR Inc.

**DISCLAIMER**

This report has been reviewed by the U.S. Minerals Management Service staff for technical adequacy according to contractual specifications. The opinions, conclusions, and recommendations contained in this report are those of the authors and do not necessarily reflect the views and policies of the U.S. Minerals Management Service. The mention of a trade name or any commercial product in this report does not constitute an endorsement or recommendation for use by the U.S. Minerals Management Service. Finally, this report does not contain any commercially sensitive or proprietary data release restrictions and may be freely copied and widely distributed.

## **ACKNOWLEDGEMENTS**

This project was contracted through the US Department of Interior, Minerals Management Service, with additional funding support provided by Alaska Clean Seas and Statoil ASA. Crude oil for the experiments was kindly donated and shipped by ExxonMobil.

Shell Global Solutions (US) Inc. participated in the program at substantially reduced rates in order to test the ethane sensor technology in a new application.

In addition to the team members and representatives listed below, the authors would like to acknowledge the enthusiastic support provided by the staff of CRREL and MAR Inc. whose combined resources contributed greatly to the success of the program.

Olga O'Neal of Exploration Technologies Inc. integrated sample locations from a variety of sources into a complete base map, and enhanced the overhead photographs to allow accurate digitizing of oiled areas.

## **PROJECT ORGANIZATION**

### **Contracting Office Technical Representative**

James Lane (COTR)                      U. S. Minerals Management Service

### **Funding Partner Representatives**

John Parson                              Alaska Clean Seas  
Hanne Greiff Johnsen                  Statoil ASA  
Arne Myhrvold                          Statoil ASA

### **Technical Team**

David Dickins                            DF Dickins Associates Ltd. (Prime Contractor)  
Bill Hirst                                  Shell Global Solutions (US) Inc.  
Graham Gibson                          University of Glasgow  
Lee Liberty                                Boise State University (CGISS)  
John Bradford                            Boise State University (CGISS)  
Victor Jones                               Exploration Technologies Inc.  
Edward Owens                            Polaris Applied Sciences Inc.  
Len Zabilansky                           US Army Cold Regions Research Engineering Laboratory  
Dave De Vitis                             Mar Inc.

### **Observers**

Carl-Anne Manen                        NOAA  
Nancy Kinner                              University of New Hampshire

## **SUMMARY AND CONCLUSIONS**

This project positively detected oil trapped in and under ice with two completely independent technologies, both of which have potential for further development and large-scale field-testing. In many respects (limited size of spills, lack of natural cracks and fractures in the ice), the design of this test program represents a worst-case scenario, compared with the expected characteristics of a real spill under sea ice. In this context, the results reported here represent a significant breakthrough, especially when viewed against decades of previous work, resulting in few if any practical solutions to the oil-in-ice detection problem.

There is a worldwide need to develop a practical remote sensing system to detect and map oil in ice. Such systems will facilitate leak detection and improve spill response capabilities for oil and gas operations in Arctic regions. This paper presents results from tests in November 2004 on a 35 cm (14 in) thick sea ice sheet grown at the Cold Regions Research and Engineering Laboratory (CRREL) in Hanover, NH. Two independent technologies were evaluated: high-frequency pulsed Ground Penetrating Radar (GPR), and an ethane gas sensor. The objective was to establish whether off-the-shelf technologies and sensors could detect oil under solid ice.

Fresh South Louisiana crude was injected inside six plastic skirts frozen into the smooth ice. Spill volumes ranged from 49 to 188 liters (13 to 50 gal), representing nominal oil film thickness from 8 to 30 mm (0.3 to 1.2 in). The six spills included an equal mix of trapped oil within the ice sheet and free oil under the ice sheet. A seventh spill was made in rubble ice with a rough undersurface. Analysis of the saturated headspace vapor for the oils used indicated that the ethane concentration ranged from 5000 ppmv before the test to only about 3000 ppmv at the conclusion of the field test.

The radar group completed a series of 2D and 3D experiments, utilizing two radar systems, each with three antenna configurations, ranging from 450 MHz to 1200 MHz. Radar results show a clear reflection from the ice/water interface in both the smooth ice and rough ice areas over the full range of antenna frequencies (including airborne runs up to three meters above the ice surface). At frequencies above 800 MHz, researchers observed clear, well defined frequency, phase, and amplitude anomalies where oil was known to be present at the ice/water interface and trapped within the ice. The agreement of experimental results with initial modeling indicates the potential to accurately predict GPR response to a variety of arctic spill scenarios and radar parameters. Overall, the results clearly demonstrate the potential for detecting oil under sea ice with GPR.

The LightTouch™ ethane gas sensor uses a Tuneable Diode Laser Spectrometer (TDLS), that can measure real-time concentrations to an accuracy of ~50 parts per trillion, approximately 200 times better than gas chromatographic measurements. Results show measurable, but very low, levels of ethane flux being transmitted through the ice sheet within the oiled areas. These measurements were made 2-3 days after the last four spills (under the maximum ice thickness) and 9-13 days following the initial three spills (under thinner ice). Although the ethane flux from oil trapped under these artificial, test-tank conditions was extremely small, the ice coring data demonstrated that the oil and light gases, such as ethane, had penetrated nearly to the surface of the ice within the 14 day program duration (initial spill to final day of testing). Given longer times and natural conditions, where tectonic forces would provide additional migration pathways, it appears likely that an airborne LightTouch™ detection system would be capable of detecting ethane emissions associated with a real oil spill.

## **GLOSSARY AND LIST OF ACRONYMS**

In approximate order of appearance in the report

CGISS	Center for Geophysical Investigation of the Shallow Subsurface
CRREL	Cold Regions Research and Engineering Laboratory
GPR	Ground Penetrating Radar
TDLS	Tuneable Diode Laser Spectrometer
MMS	Minerals Management Service
ETI	Exploration Technologies Inc.
AVO	thin bed amplitude vs. offset (as in change in amplitude with increasing offset or AVO analysis)
TE	transverse electric (polarizations)
TM	transverse magnetic (polarizations)
IARC	International Arctic Research Center (University of Fairbanks)
AFDH	accumulated freezing degree-hours
GC	gas chromatograph
ppb	parts per billion
ppt	parts per trillion
SCADA	Supervisory Control and Data Acquisition
EPA	Environmental Protection Agency
3D	three-dimensional
TDR	time domain reflectometry (probe)
WOW	low frequency transient noise
LSS	proprietary trace interpolation algorithm used in Promax processing software
IR	infra-red
IW	ice/water interface
TDLS	Tuneable Diode Laser Spectrometer
PTFE	Polytetrafluoroethane
SD	standard deviation
h.c.	hydrocarbon

**CONTENTS**

	<b>Page</b>
ACKNOWLEDGEMENTS	ii
PROJECT ORGANIZATION	ii
SUMMARY AND CONCLUSIONS	iii
GLOSSARY AND LIST OF ACRONYMS	v
1.0 INTRODUCTION AND OBJECTIVES	1
2.0 BACKGROUND AND STATE OF KNOWLEDGE	2
2.1 Range of Oil in Ice Scenarios	2
2.2 Oil and Ice Detection	4
2.3 Experiences with Radar	5
2.4 Detection of Hydrocarbon Gases at Low Levels	8
3.0 TEST PLANNING	11
3.1 Facility Description	11
3.2 Crude Oil Selection and Procurement	14
3.3 Ice Sheet Development	14
3.3.1 Rough ice development	15
3.3.2 Smooth ice	15
3.4 Spill Volumes and Containment	16
3.5 Spill Procedures	19
3.6 Flux Chamber Methods	20
4.0 TEST CONDITIONS	23
4.1 Overall Layout	23
4.2 Ice Thickness	26
4.3 Rough Ice Description	27
4.4 Air, Ice and Water Temperatures	38
4.5 Oil in Ice Configurations	29
4.5.1 Lateral oil spreading	30
4.5.2 Vertical oil distribution	34
5.0 GROUND PENETRATING RADAR (GPR)	38
5.1 Experimental Setup	38
5.1.1 3D common offset survey	38
5.1.2 2D profiling	39
5.1.3 Multi-offset data acquisition	41
5.1.4 Airborne radar data	41
5.1.5 Electric permittivity control measurements	41
5.1.6 GPR Data Processing	42

**CONTENTS (cont.)**

	<b>Page</b>	
5.2	GPR Results and Discussion	42
5.2.1	3D common offset survey	42
5.2.2	2D antenna frequency comparison	46
5.2.3	Multi-offset data acquisition	49
5.2.4	Airborne radar data acquisition	49
5.2.5	Electric permittivity control measurements	50
6.0	LIGHTOUCH™ ETHANE SENSOR	51
6.1	Experimental Setup	51
6.2	Ethane Flux Measurements	52
6.3	Results and Discussion	57
6.4	Oil, Ice, Air and Water Sample Analysis	58
6.4.1	Oil chemistry	58
6.4.2	Ice core samples	59
6.4.3	Water samples	60
6.4.4	Air samples	61
7.0	FUTURE DEVELOPMENT	62
7.1	Radar Potential	62
7.2	Ethane Sensing Potential	64
7.3	Alternate Technologies: Seismic Methods	65
7.4	Recommended Research and Development	66
	REFERENCES	68

**APPENDICES**

- A Ground Penetrating Radar (GPR) Data
- B Ethane Flux Data
- C Ice Thickness and Oil Distribution
- D Hydrocarbon Analysis of Independent Oil, Air, Water, Ice Samples
- E Technical Note: Oil Recovery
- F Technical Note: Potential for Seismic Methods

**List of Figures**

	<b>Page</b>	
Figure 2-1	Modeled 1GHz GPR response to a thin layer of oil under ice	7
Figure 3-1	View down the tank to the East with rough ice in the foreground	12
Figure 3-2	New ice forming in the test basin	12
Figure 3-3	Plan view of the Ice Engineering Facilities at CRREL	13
Figure 3-4	Ice growth as a function of accumulated freezing degree hours	16
Figure 3-5	Divers view of a spill containment skirt beneath the ice	17
Figure 3-6	Flux chamber deployed to measure methane emissions	20
Figure 3-7	Flux chamber cutaway view	21
Figure 3-8	Ethane flux chamber fabricated for the project	22
Figure 4-1	Test Layout Map	24
Figure 4-2	Overhead view of surface conditions in the initial three oil skirts	23
Figure 4-3	Overhead view of the second three spill skirts (2-1 to 3-3)	25
Figure 4-4	Surface appearance of ice rubble (Test area 2-4)	27
Figure 4-5	Measured ice temperature profile - November 19, 2004	28
Figure 4-6	Internal ice and surface temperatures - November 18, 2004	29
Figure 4-7	View down the tank with underwater lights	31
Figure 4-8	Vertical photograph looking down on site 2-3	32
Figure 4-9	Example view from the underwater video camera in Site 2-3	33
Figure 4-10	Coring in the center of ethane flux site #26, Site 1-1	35
Figure 4-11	Core extracted from site 1-1	36
Figure 4-12	Oil exposed on the surface from coring in Site 1-2	36
Figure 4-13	Core extracted from site 2-2	37
Figure 4-14	Close up of oiled "brine" channel within the 2-2 core	37
Figure 5-1	Radar team traversing oiled test sites at CRREL	39
Figure 5-2	<i>Sensors and Software</i> system	40
Figure 5-3	<i>MALA Geosciences</i> RAMAC system	40
Figure 5-4	Depth to ice/water interface & surface location of GPR profiles	44
Figure 5-5	Reflection strength of the IW reflection	45
Figure 5-6	GPR reflection data and reflection strength over smooth ice	48
Figure 6-1	The Shell Global Solutions TDLS ethane gas sensor	52
Figure 6-2	Flux chamber pre-test over PTFE sheeting	53
Figure 6-3	Sketch of relative locations of flux chamber measurements	54
Figure 6-4	Flux chamber measurement No. 26a over encapsulated oil	55
Figure 6-5	Asymptotic approach of ethane concentration to equilibrium	56
Figure 6-6	Last 7 minutes of position 26a data	56

**List of Tables**

Table 2-1	Comparison of light hydrocarbon gases in crude oil samples	9
Table 3-1	Spill Sets	19
Table 4-1	Summary of Ice Thickness Measurements	26
Table 4-2	Summary of Spill Volumes and Ice Parameters	30
Table 4-3	Oil Pool Thickness (actual vs. planned)	33
Table 5-1	Ice Permittivity Estimates from Downhole TDR Probe	50

## **1.0 INTRODUCTION AND OBJECTIVES**

As a result of continued interest in oil exploration and development in Alaskan offshore areas, the Minerals Management Service (MMS) as part of their Technology Assessment and Research Program, Oil Spill Response Research, is supporting the evaluation of new and innovative equipment and technologies for the remote sensing and surveillance of oil in and under ice. Additional funding support for this project was provided by Alaska Clean Seas and Statoil ASA, and ExxonMobil donated the crude oil.

The lack of any reliable and practical operational system to detect and map spilled oil in or under ice continues to be a critical deficiency in Arctic spill response (2.0). In addition to needs in the US Arctic, other worldwide areas are rapidly developing with similar oil-in-ice problems (Sakhalin Island, Soviet Barents Sea, North Caspian Sea, Baltic Sea). There is a strong motivation within industry and government agencies to develop a reliable, remote method of detection, which can be carried out economically and safely. Ideally, such a system would have the capability of operating in both airborne and ground-based modes, and have the capability of determining whether oil is present, and to map the boundaries of contamination over potentially large areas. The need for further research and development in this area was recently highlighted in a publication by the Prince William Sound Oil Spill Recovery Institute and the US Arctic Research Commission (Dickins, 2004).

The overall objective of this program was to establish whether off-the-shelf technologies and sensors could detect oil under ice in a controlled meso-scale environment, as a prelude to further development and field-testing.

## 2.0 BACKGROUND AND STATE OF KNOWLEDGE

### 2.1 Range of Oil-in-Ice Scenarios

This section outlines a number of possible configurations of oil-in-ice that could result from spills under solid landfast (also known as simply fast) ice or large pack ice floes. In some cases, oil initially on the ice surface could become trapped internally within thicker ice as individual sheets raft over each other. For a detailed review of the state of knowledge concerning the behavior of oil in all types of ice, the reader is referred to Dickins and Fleet (1992). A detailed description of oil-in-ice scenarios is provided in Dickins et al. (2000).

There are two distinct periods defining oil behavior in and under ice (months refer to typical seasons in the US Beaufort):

- Winter spreading of oil under ice & encapsulation (October to April), and
- Oil migration and surface appearance (May to June).

The fate and behavior of oil beneath solid ice is governed by a number of important processes, which control the extent and thickness of the oil layer:

*Initial Spreading and Natural Containment.* In general, oil spilled under stable landfast ice will not spread beyond hundreds of feet from the spill source, based on basin tests of threshold currents and field measurements of minimal or null currents under the ice in the Alaskan Beaufort (Cox and Shultz, 1980; Intec for BP, 1996 (unpublished), noted in Dickins et al., 2000). The final contaminated area boundaries under smooth ice are controlled largely by natural variations in ice thickness, reflecting the different snow depths. As demonstrated in the CRREL tank, sea ice sheet grown under controlled conditions without snow can still develop significant variations in thickness related to non-uniform rates of heat transfer (Sec. 4.2). These variations in ice thickness allow large volumes of oil to be contained within localized areas (Kovacs et al., 1981).

Areas of ice rubble, rafting, and ridging can lead to a wide variety of mixed oil and ice configurations. Under these conditions, oil can be trapped in localized pockets between blocks or in voids. Oil spreading under relatively smooth ice could be effectively blocked from further movement by under hanging ridge keels.

*Encapsulation and rapid immobilization* This process involves the rapid formation of new ice beneath oil trapped under the growing ice and acts to immobilize the spill within a matter of hours or days (Norcor, 1975; Dickins and Buist, 1981).

*Vertical migration* of oil through the melting ice begins when the expulsion of brine from the warming ice opens pathways to the surface (Norcor, 1975; Dickins and Buist, 1981). Beginning as early as April and continuing through June, oil will naturally rise to the surface from wherever it is trapped within or beneath the ice. Significant migration also occurs in mid-winter with air temperatures still below -15°C. In this case, the oil may rise part way through the ice sheet without surfacing.

The timing of vertical migration effectively changes the character of the oil distribution within the ice sheet in terms of detection. Oil during the active migration period is no longer present in a sharply defined layer with a clear interface between different materials.

Oil from the first two spills in the CRREL basin in this study, reached the surface soon after being spilled under thin (less than 20 cm (8 in)). Initially, it was thought that this early migration was influenced by a combination of spilling oil at room temperature and the presence of slight positive hydrostatic pressure in the basin. Cores taken at the end of the test showed that a similar extent of vertical migration occurred in later spills under thicker ice with the oil at freezing and no positive water pressure. From these observations, it appears possible for light crudes to surface through young sea ice at temperatures well below zero degrees Celsius. .

## **2.2 Oil and Ice Detection**

A 2001 Phase 1 study evaluated and summarized available knowledge about the subject of oil-under-ice detection (Dickins, 2001). The current program represents a logical evolution of this earlier work.

The phrase "oil in or under ice" has been commonly used in the literature to refer to a wide range of situations where oil is for example: trapped within an ice sheet, pooled under sheets or floes, or filling the water or slush-filled spaces between floes in broken ice. As interpreted in this study, "oil in ice" will refer to configurations where the oil is trapped beneath an ice sheet (ice/oil/water interfaces) or within the sheet by means of fresh ice growing beneath the oil following the spill (ice/oil/ice interfaces). The oil can theoretically be trapped at any level within the sheet depending on the thickness at the time of spill (as subsequently demonstrated in this experiment, oil may surface quickly, even at cold temperatures, if spilled under new or young ice).

At present, the only proven operational method of searching for and detecting the presence of oil from an accidental subsurface spill (e.g. leaking at low rates from a marine pipeline during the ice-covered period) involves drilling holes at frequent intervals or in a closely spaced grid pattern to expose any oil which could be trapped in or under the ice. These methods are extremely labor intensive and subject to considerable error in detection. There is a strong motivation within industry and government agencies to identify and develop reliable, remote methods of detection, which can be carried out economically and safely. Ideally, systems need to operate from surface (localized area mapping) and airborne platforms (large areas, fixed wing or helicopter). The ultimate goal is to have a number of complimentary systems (or single system) capable of fulfilling both roles: rapid initial determination of whether or not oil is present in a broad area, and detailed site mapping. This project focuses on proving a number of surface-based systems as a precursor to any future airborne tests.

The problem of remote sensing of winter spills beneath a solid ice sheet is particularly challenging. An operational system needs to accommodate a wide range of oil-in-ice configurations over an equally broad range of ice conditions and water depths. Over the past twenty years, considerable effort has been spent on the research and development of various methods to detect oil trapped under an ice cover or entrapped as a layer within growing ice. To date, none of these technologies has resulted in an operational system. Examples of different systems that have been tried on actual spills in ice include: impulse radar (surface and airborne), infrared and visual photography, and a prototype acoustic system (Butt et al, 1981; SL Ross and DF Dickins, 1987; C-CORE, 1980; Goodman et al., 1985; Fingas and Brown, 2000). Of all these systems, the acoustic technology showed the most promise but was severely constrained by the need to use transducers with an intimate bond to the ice surface. Dickins (2000) concluded that it would be difficult to reconcile this requirement with the need for a portable system capable of mapping potential oil pools over large areas of ice.

Two technology areas were selected in this study as having the best chance to detect oil in a controlled meso scale experiment:

- Ground Penetrating Radar (GPR): contingent on being able to distinguish between the different combinations of interfaces associated with trapped and free oil beneath an ice sheet (depends on contrasting electric permittivity). The potential for positive results was based on demonstrated systems for sea ice thickness profiling and backed by computer modeling that predicted a positive response in the meso scale test situation being planned for this project (see below).
- Geochemical Methods (Hydrocarbon Gas Detectors): contingent on being able to detect direct flux levels of ethane (the most unambiguous hydrocarbon marker) transmitted through the ice above an oil layer in or under the ice.

Both of these technology areas are relatively mature in the sense that off-the-shelf systems are routinely used in a wide range of commercial applications (soil contamination, reservoir mapping, etc.). The intent in this study was to test systems that represent the most advanced state of development for each technology in a primarily surface-based mode (several runs were made along the tank in this study with the radar antenna suspended above the ice). Both technologies have been previously used in an airborne mode, and have the potential to be flown again during later stages of development.

The radar results were modeled in advance of the tests by assuming a representative range of relative electrical properties for ice oil and water (Section 2.2). Without prior knowledge of the possible pathways or likely rate of release of gases from oil entrapped or under ice, it was not feasible to make equivalent predictions of ethane sensor performance prior to the actual test. The potential for using the latest generation of seismic methods to detect oil in ice was also considered (App. F).

The following sections summarize relevant past experience with the two technologies selected for evaluation in this project, including technical issues governing their ability to detect and map oil trapped in sea ice.

### **2.3 Experiences with Radar**

Background and Theory: There is an extensive background in using surface-based and airborne radar systems to profile first-year, multi-year and pack ice thickness. Experimental projects and operational systems have been deployed in areas such as the North Slope of Alaska, Lincoln Sea, Russian Arctic, and the Canadian East Coast/Labrador Sea (e.g., Finkelstein, 1990; Kovacs and Morey, 1992; Todoeschuck and Verral, 1990; Nyland, 2004).

Ground Penetrating Radar (GPR) has been used in numerous arctic studies to image both internal structures within snow (e.g., Harper and Bradford, 2003), the ice/water contact and subsurface geology below freshwater ice (Best et al., 2004; Bradford et al., in press) and the sea ice/sea water contact. In GPR studies, a transmitting antenna generates an oscillating electric field that propagates through the subsurface. This field is then reflected from boundaries separating materials with differing electric properties (electric permittivity and conductivity) back toward a receiving antenna.

The reflected wave field is recorded and used to produce a reflector map in travel time, similar to a cross section of the subsurface. The large permittivity contrast between sea ice and sea water (~6:88) and between sea ice and oil (~6:2.2) suggests that we can derive an accurate map of subsurface boundaries in these conditions using very high frequency GPR antennas (~1 GHz). Consequently, radar is a tool well suited to imaging both the base of ice, and the sub ice conditions for both fresh and sea ice conditions

Desirable System Attributes for this Application: The resolving power of the GPR system limits the thickness of sub ice oil that can be measured directly, i.e. by measuring the travel time difference between wavelets reflected from the top and bottom of a layer. The wavelength of the signal controls the resolution, with a shorter wavelength signal capable of resolving finer features. When a layer is thinner than about 1/4 of the dominate wavelength of the GPR signal, it is impossible to clearly differentiate wavelets reflected from the top and bottom of the layer and a simple reflector map is not sufficient to confidently identify the presence of oil under the ice. In this case, rather than relying on a direct measure of travel time differences, specific attributes of the reflected wave are analyzed such as amplitude, phase or frequency content. Attribute analysis is commonly used in oil and gas exploration to identify relatively thin reservoirs of hydrocarbon in sedimentary rocks. Attribute measurements can be made from typical fixed antenna GPR data, which is relatively fast and inexpensive to acquire.

Another potentially useful measurement is the change in amplitude with increasing offset or AVO analysis. However, this method requires multiple receiver offsets for each source antenna position leading to additional acquisition costs (i.e. time). Although many GPR systems only acquire data at a fixed receiver offset, the setup utilized in this study allows the operator to decouple the source and receiver antennas to acquire such data. Bradford (2004) showed that GPR AVO analysis can be an effective tool for detecting thin layers of hydrocarbons in groundwater studies and we expect that the methods would be more robust in the sea ice/oil system due to decreased stratigraphic complexity.

Model Results: An analytical thin bed GPR model was used to compute the GPR response, at 1 GHz, to a thin oil layer trapped under sea ice, with the layer varying in thickness from zero – 3 cm. In fixed antenna mode, results predict a 24% increase in amplitude and a 20% change in phase for a 2 cm (0.8 in) thick oil layer relative to no oil present. Further, the AVO response in transverse magnetic (TM) antenna configuration shows even greater sensitivity, with a dramatic increase in the AVO gradient. (Figure 2-1)

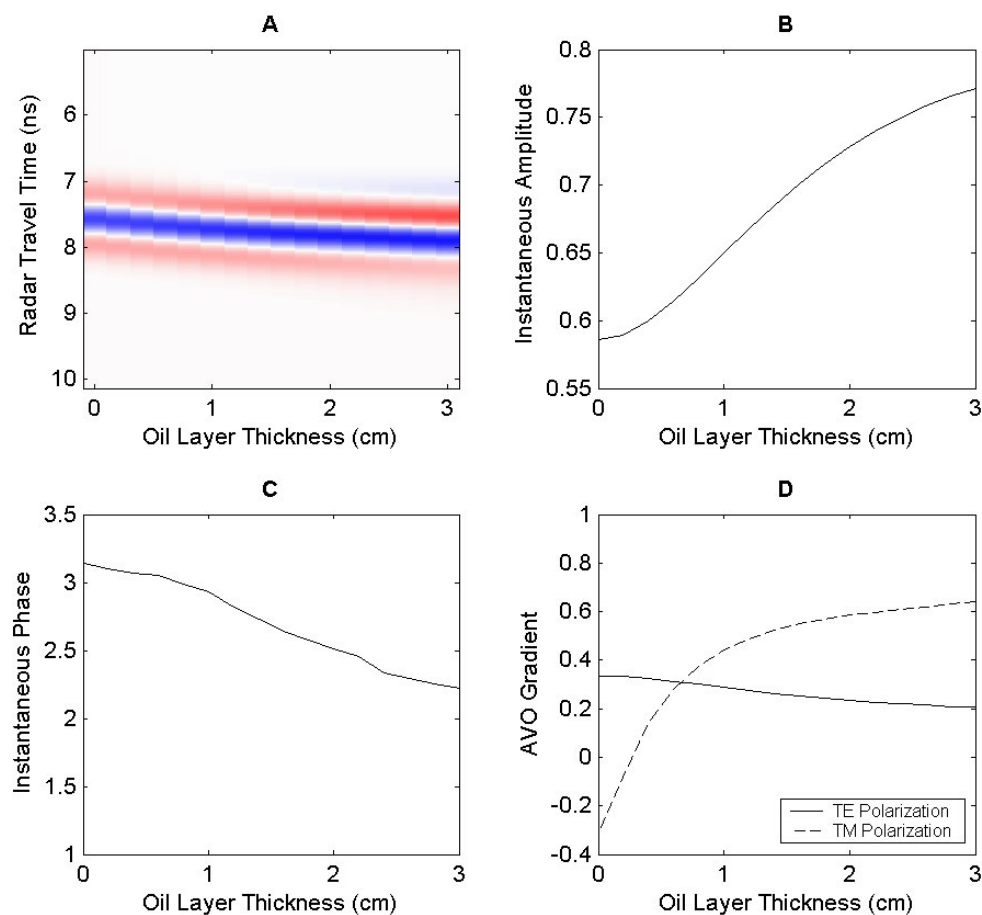


**Figure 2-1** Modeled 1GHz GPR response to a thin layer of oil under ice assuming relative permittivities of 6, 2.2, and 88 for sea ice, oil, and sea water respectively.

FIGURE KEY:

- A) Reflected GPR signal with oil layer thickness varying from 0 - 3 cm (0 - 1.2 in).
- B) Maximum instantaneous amplitude for the model data in A).
- C) Instantaneous phase at peak amplitude for the model data in A).
- D) Thin bed amplitude vs offset (AVO) response for transverse electric (TE) and transverse magnetic (TM) polarizations. The AVO gradient is computed for incidence angles from 0 to 45 degrees. Although amplitude, phase, and AVO data attributes all show a significant response to the trapped oil, the AVO gradient appears to be the most sensitive indicator.

The change in reflection attributes is caused by the interference of wavelets reflected from two closely spaced electric permittivity contrasts. As the frequency of the signal decreases (with a corresponding increase in wavelength), the signal becomes less sensitive to closely spaced permittivity contrasts until, at some limiting frequency, the thin film is “transparent” to radar.

Possible Limitations and Solutions: Water strongly attenuates the radar signal, with the rate of attenuation increasing as the dissolved solid concentration (electric conductivity) increases. Thus, pockets of brine trapped in ice may limit signal penetration. It is important to recognize that entrapped brine and sea ice anisotropy may alter the measured GPR attributes. This problem is minimized in field data analysis by computing attributes relative to a background response that is measured from the data. Multi-offset acquisition can be used to overcome potential problems in field data, such as low signal to noise, variable surface conditions, or ice heterogeneity.

In order to maximize the range and quality of data collected in a limited time, the project plan called for the acquisition of fixed antenna data to analyze travel time, amplitude, and phase information, followed by multi-offset GPR data to characterize the AVO response. Results from the CRREL tests subsequently demonstrated that a satisfactory response could be achieved without having to resort to multi-offset systems (Section 5.2).

## **2.4 Detection of Hydrocarbon Gases at Low Levels**

Background and Theory: All petroleum spills from either man-made or natural conduits contain substantial quantities of dissolved light and gasoline range hydrocarbons. The light gases include methane, ethane, propane, iso-butane and normal-butane and the gasoline range include iso and normal pentane through xylene plus hydrocarbons. The concentrations of biological gases (carbon dioxide and methane) often range upwards to 20 to 50 percent, and are the most volatile components associated with the spill. However, elevated levels of methane (above the natural global background level of ~1.7 ppm) in the atmosphere are possible from a variety of sources, seriously downgrading the use of methane as an unambiguous petroleum marker.

More promising as a positive indicator of the presence of hydrocarbons, are trace levels of the light gases, ethane and iso-butane. These two natural trace components in crude oil are resistant to natural biodegradation and have been found to persist within petroleum spills as old as 60 to 100 years in age (James, 1990). Experiments in bulk diffusion and surface diffusion in ice have shown that the smaller alkanes such as ethane and propane (in contrast to the larger alkanes such as hexane and pentane) may diffuse along the hexagonal shafts into the ice bulk (Livingston et al., 2002).

Recent findings from an international study in Canada utilizing the research vessel Amundsen and ongoing work through the University of Fairbanks International Arctic Research Center (IARC) off Point Barrow, Alaska show that sea ice is much more porous to a range of gases than was previously assumed.

Until recently, the role of the Arctic Ocean in the global CO<sub>2</sub> balance was ignored, as it was thought that sea-ice blocked gas exchange with the atmosphere.

IARC researchers are measuring the partial pressure of dissolved CO<sub>2</sub> in sea-ice and under-ice water in first-year ice. Their results have been surprising as they have found that the Arctic Ocean sea-ice is an active participant in the CO<sub>2</sub> gas exchange (Semiletov) [http://www.iarc.uaf.edu/highlights/Climate\\_Change\\_Clues\\_Under\\_Arctic\\_Sea\\_Ice.php](http://www.iarc.uaf.edu/highlights/Climate_Change_Clues_Under_Arctic_Sea_Ice.php). These findings support the concept of using an ultra sensitive ethane sensor to detect oil trapped under sea ice.

Examples of the analysis of the saturated vapor from four crude oils that have been stored in the laboratory at Environmental Technology Inc. (ETI) for nearly 20 years are shown in Table 2-1. In each case, 2 ml of crude oil was added to a 125 ml glass bottle and allowed to equilibrate at room temperature. The Pierce Junction analysis shows the differences between three different oils from different reservoirs in the Pierce Junction field. In contrast, the Tennessee crude oil shows the variation between analyses on three separate samples prepared from the same crude oil. As shown by this data, each crude oil contains large concentrations of these five light hydrocarbon gases even after being stored in the laboratory for an extended time.

**Table 2-1**

LIGHT C1-C4 HYDROCARBONS (ppmv)

SAMPLE NO.		METHANE	ETHANE	PROPANE	I-BUTANE	N-BUTANE
<b>Pierce Junction Crude Oil</b>						
P-01	SATURATED	34.3	540.473	1662.376	857.325	1802.852
P-02	SATURATED	362.4	704.783	1277.757	69.224	537.440
P-03	SATURATED	57.9	192.952	534.703	409.754	733.966
<b>Tennessee Crude Oil</b>						
Tennessee Crude	SATURATED	13.0	1742.752	16082.720	7915.889	34838.880
Tennessee Crude	SATURATED	13.4	1831.201	15152.750	7525.283	33832.230
Tennessee Crude	SATURATED	13.0	1690.789	16873.360	8148.629	35707.710

The process of vapor migration through the ice may be linked to the natural internal transport of super cooled water films (coating the ice crystals) from the isothermal freezing (warm) interface to the cold ice surface (Jumkis, 1958). The driving force is the vapor pressure difference between the partial water vapor pressure at the warmer end (the freezing surface) and the partial vapor pressure at the upper region of the frozen ice surface.

In theory, there is no reason why light fractions from a crude or (or other oil) trapped under ice would not migrate to the surface where they could be detectable by the current generation of optical ethane sensors.

Anticipated System Performance: Conventional gas chromatograph (GC) methods to detect ethane are limited to the 5-10 parts per billion (ppb) range, thought to be insufficient to detect the presence of oil trapped under a solid layer such as ice. However, detection of ethane gas from oil in ice appeared possible in the planning stages with the latest generation of detectors, represented in this project by the Shell LightTouch™ system. Shell's system, developed with the University of Glasgow, is capable of accurate readings down to a concentration of about 50 parts per trillion (ppt) (Gibson et al., 2002). The Shell system provides a real time graphic representation on site of the ethane concentration in air sampled from above the ice. Elevations in ethane concentration of just a fraction of a ppb relative to the background concentration of the test facility's air could then be used to indicate proximity to a source (oil trapped in the ice). In practice, a more sensible approach is to use a flux chamber to further increase the sensitivity (Sec. 3.6).

The global atmospheric background ethane concentration for Hanover, NH in November during the test period was predicted to be ~1.5 to 2 ppb (Rudolph, 1995). Actual test results confirmed this prediction (Sec. 6.2). The flux chamber concept (Sec. 3.6) was selected as a possible solution to eliminating concerns about cumulative ethane levels in a closed environment affecting the results. The gas sampling procedures further evolved and were modified on site, based on initial experiences (Sec. 6.2).

During the testing phase, the LightTouch team made a series of ethane concentration measurements to derive fluxes of ethane emissions through the test ice sheet. The results are presented in Section 6. The extremely low detection limits of the Shell system allowed elevated ethane flux levels to be measured in real time, something not possible with any other form of available sampling technology. A general technical description of the LightTouch™ system is provided in Section 6.1.

### **3.0 TEST PLANNING**

Physical variables considered in the initial planning stages included:

- Oil/ice configuration (trapped vs. freely exposed under the ice)
- Oil type (light aromatic vs. heavier crude)
- Oil film thickness (mm to cm)
- Ice roughness (smooth sheet vs. induced roughness features)
- Snow cover (bare ice vs. snow covered)

The number of variables that could be practically tested was constrained by the practicalities of working with a man-made ice sheet having fixed dimensions and a finite growth period (limited by time and cost of refrigeration). It was not considered feasible to introduce different oil types and snow within the available ice area and the time limits (two weeks for growth and one week for testing).

The program was subsequently designed around one light crude test oil and two distinct oil in ice configurations (trapped and free) under predominantly smooth ice. A single spill within a 10 m (33 ft) long section of deliberately broken ice was introduced as a contrast to the other six spills in smooth ice. The project team believed that this program design would provide a realistic test of the two systems under conditions representing close-to worst case scenarios (relatively thin oil films and a solid ice cover with no cracks or fractures).

The following sections describe the basic planning elements and targets established for the main parameters: oil selection, oil volume, contaminated areas, number of spills, and oil film thickness.

#### **3.1 Facility Description**

The Ice Engineering Facility at the US Army Cold Regions Research and Engineering Laboratory (CRREL) in Hanover, NH, is a comprehensive research facility designed for developing solutions to engineering and environmental challenges in the higher latitudes. The test basin used in this study was designed for conducting scaled model studies of ice forces on structures e.g. ships and drill platforms. The controlled climatic conditions and expertise in characterizing the ice made this large basin ideal for evaluating the techniques for detection oil under ice. The facility has been utilized in several successful cold climate environmental research programs in the recent past (e.g., creating and supplying ice to Ohmsett in January 2002, and providing an extreme environment for testing survival suits in April 2003).

The large ice test basin is 36.5 m long x 9 m wide x 2.4 m deep (120 ft long x 30 ft wide x 8 ft deep) with the long axis oriented East-West (Figs. 3-1 to 3-3).



**Figure 3-1** Overall view down the tank to the East with rough ice created for this project in the foreground, and oil skirt frames outlined in the smooth ice.



**Figure 3-2** New ice forming in the ice test basin beyond the set-up pool (foreground).

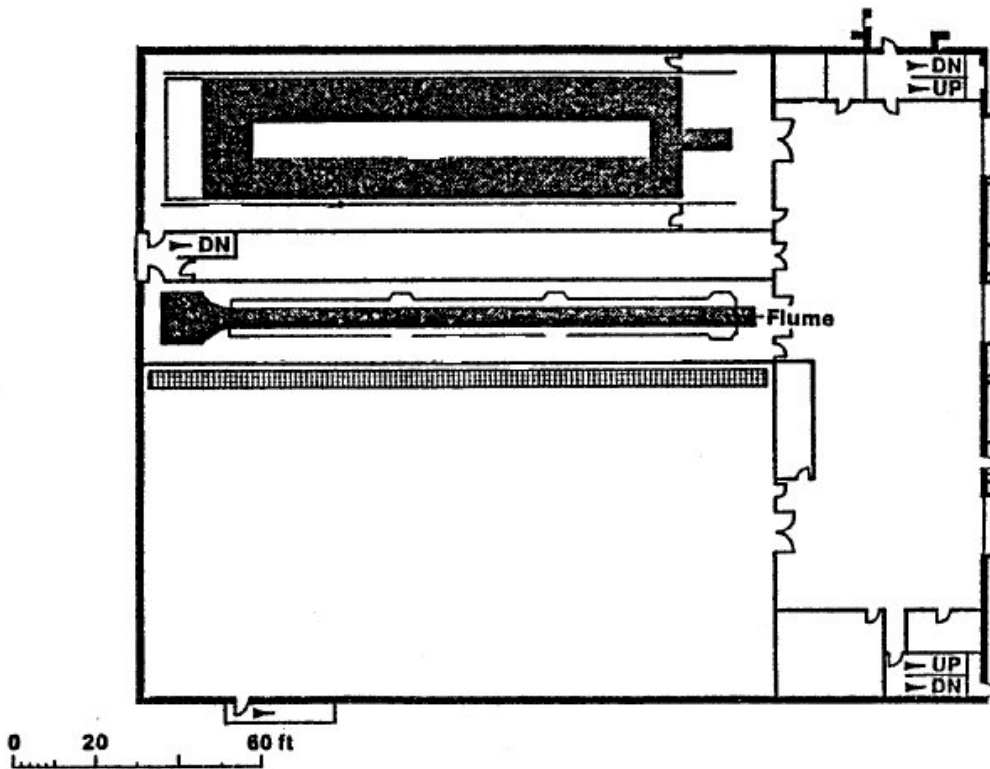


**Figure 3-3** Plan view of the Ice Engineering Facilities at CRREL

The basin is contained within a large cold chamber with a controlled freezing environment down to  $-30^{\circ}\text{C}$ . In order that the engineering properties of the ice correspond to the model scale, the tank is filled with 1% by weight urea water. The crystal structure of the urea-doped ice is very similar to sea ice, with impurities trapped in brine channels. Ice growth rates up to two mm/h can be achieved at  $-29^{\circ}\text{C}$ . Water in the test basin is cooled by using submerged coils and is heated with in-line heat exchangers. For maximum efficiency, waste heat from the refrigeration cycle is recovered and used to heat the Ice Engineering Facility's offices and work areas, and to melt ice and heat water. Performance of the system and the environment within the respective cold room is documented using a Supervisory Control and Data Acquisition (SCADA) System. Air is cooled by recirculating liquid ammonia through ceiling-mounted air units in the cold rooms. A solid one-foot thick ice sheet can be grown over a two-week period prior to the tests. During the test period (one week) the temperature in the cold room can be moderated to provide a more comfortable working environment while still maintaining the integrity of the ice sheet. The 30 to 40 cm (12 to 16 in) ice sheet grown at CRREL for this project was much thicker than the sheet commonly used for structural engineering tests on structures or vessels (typically 5 to 8 cm (2 to 3 in)).

### **3.2 Crude Oil Selection and Procurement**

It was not considered essential to test a particular crude oil in this initial project. Key requirements were that the oil have a low enough pour point to remain fluid in the tank water (-0.3°C) and be light enough to be relatively volatile. From a radar perspective, the key properties of interest (permittivity, conductivity, dielectric constant) do not change significantly between different crudes. In terms of the Shell system performance, it would have been ideal if a crude oil could be selected based on its Ethane content, but there are no readily available properties descriptions to support this selection criterion.

In practice, an operational remote sensing system for detecting oil in ice could encounter a wide range of crude types (e.g., Endicott, Northstar, Chayvo, Kashagan, etc.) with an equally wide range of physical properties, wax content, and chemical composition.

South Louisiana (Gulf of Mexico) was selected as an example of a readily available pipeline crude with properties within a target range of: API Gravity 35 to 45°, Pour Point less than 7°C). ExxonMobil was able to source six drums of this crude from their Baton Rouge refinery, donated the oil to the project and arranged shipping to New Hampshire.

Samples were taken from each drum soon after delivery and subjected to an analysis of the gas concentrations in the headspace. These results proved that the South Louisiana crude was an ideal choice, with high relative concentrations of ethane. Section 6.4.1 and Appendix D provide a comparison of fresh and oil-in-ice samples and analysis sheets.

### **3.3 Ice Sheet Development**

The properties of urea ice grown at CRREL are well documented and have been compared with natural sea ice and ice modeled in other facilities worldwide (Hirayama, 1983; Timco, 1985; Tatinclaux, 1992; Zufelt and Ettema, 1996). The size of the scale models normally used in testing at CRREL dictates the normal ice thickness range from 25 to 60 mm with strength as low as 35Kpa. Due to the limited growth time, thinner ice is uniform across the tank ( $\pm 2\%$ ).

With the much thicker ice and longer growth period utilized in this project, the degree of variability in final thickness related to secondary thermodynamic processes was unknown. As it turned out, there were significant spatial differences ( $\pm 15\%$ ) in ice thickness in the tank at the end of the growth cycle (Section 4.4). This outcome was actually a benefit to the experiment in that the oil tended to spread under the ice in an irregular manner, closely mimicking what has been observed in field spills in the Arctic (e.g. Norcor, 1975).

### **3.3.1 Rough Ice Development**

The test basin was subdivided into two sections, an 8.5 m (28 ft) long area of rough ice (foreground Fig. 3-1) and a 28 m (92 ft) length of smooth ice (background Fig. 3-1). The rubble field was generated to evaluate the sensors' ability to detect oil that would rise between the blocks or collect in much thicker more localized pockets between under hanging ice blocks. This type of ice is found naturally in localized patches of rubble and rafting, common to seasonal ice areas along the Arctic coast.

The rough ice section was created first by breaking up a parent ice sheet that 10 cm (4 in) thick. To control the size of the pieces used to build the rubble field, the ice cover was cut in strips the length of the tank and the room temperature elevated. At the elevated temperature, the strips of weaker ice failed in buckling and the pushers loaded the strips in compression. The larger pieces were on the order of 75 cm (29 in). The oil containment hoop was submerged and positioned below the rubble field before being pulled up into the ice such that the bottom of the containment skirt was lower than the surrounding ice. Once the hoop was in place, the rubble field was confined as it consolidated, by a floating timber boom across the tank. Section 4.5 describes the surface characteristics and appearance of the simulated ice rubble.

### **3.3.2 Smooth Ice**

Once the containment hoop in the rubble field was stabilized (3.3.1), the six remaining test hoops were positioned at intervals down the centerline of the tank, and the room was cooled to  $-23^{\circ}\text{C}$  to commence growing the level ice on October 29. Submerged air bubblers were used to agitate the water to prevent premature ice formation within the hoops. At  $-12^{\circ}\text{C}$ , the air bubblers were turned off and the water surface was seeded with ice crystals. The seeding process insures a uniform ice crystal size and uniform growth rates. Once the level ice cover was established over the full tank, the room temperature was lowered to  $-30^{\circ}\text{C}$  to achieve a target thickness of 31 cm (12 in) by mid-November. On November 3 the room temperature was elevated to  $-5^{\circ}\text{C}$  to facilitate spilling oil in the first three hoops. On the afternoon of November 6, the room temperature was returned to  $-25^{\circ}\text{C}$  and held at that level until November 14 when the air temperature was set at  $-18^{\circ}\text{C}$  for the test period.

The smooth ice sheet reached the target thickness range of 30 to 35 cm (12 to 14 in) over a sixteen-day period. A thicker smooth ice sheet would have been an advantage, but was not possible within the available time and budget. During the test week, the ice continued to grow slowly and eventually exceeded the minimum target thickness by as much as 10 cm (4 in) in some areas. (Sec. 4.2). Figure 3-4 shows the progression in ice growth related to the accumulation of freezing degree hours.

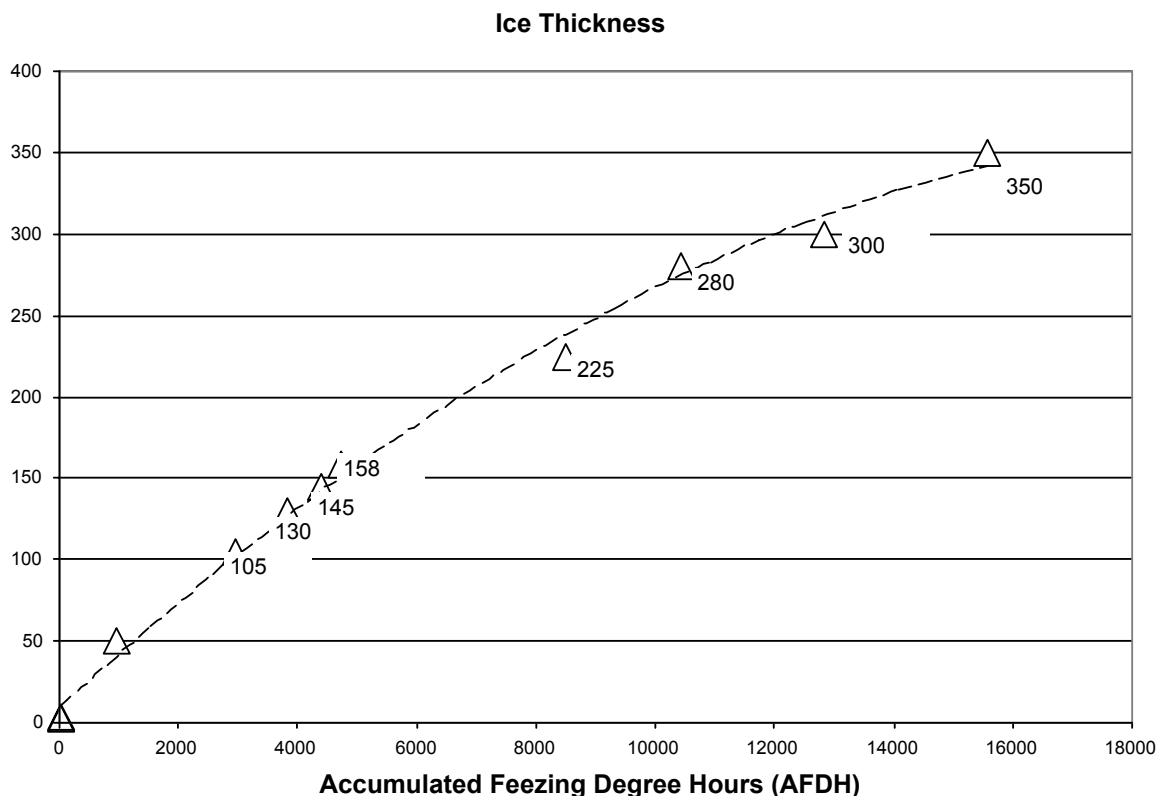


**Figure 3-4** Ice growth as a function of accumulated freezing degree hours (AFDH), Oct 29 to Nov 19. Triangles are data points with recorded thickness in mm. Dashed line is the predicted ice growth from an empirical formula based on AFDH and a coefficient based on experience with previous ice sheets in the CRREL basin.

### 3.4 Spill Volumes and Containment

Spills were contained within seven skirts installed through the ice prior to testing. The technique of inserting flexible fabric skirts through the ice to contain oil has been used successfully in the past on a number of experimental spills in natural sea ice (Prudhoe Bay, Alaska; Spitzbergen, Norway; Balaena Bay, NWT; McKinley Bay, NWT). The hoops or skirts need only to hang a few tens of centimeters under the completed ice sheet to fully contain any oil injected inside the skirt perimeter. Figure 3-5 shows one such skirt (curve of lower edge visible in background) installed through thick first-year ice in the Canadian Beaufort Sea for an experiment with emulsified crude oil (Buist et al., 1983).



**Figure 3-5** Divers view of spill containment skirt hanging beneath the ice during an experimental spill under sea ice in Canada. Emulsified oil appears yellow in color under the ice. Note accumulation of frazil crystals hanging in the upper water column, a common feature of shallow-water landfast ice regimes.

The size and placement of the spill skirts at CRREL were dictated by a number of considerations:

- need for sufficient clearance between test areas and the tank sidewalls to minimize interference effects and overlapping signals
- desire to test three different degrees of oil film thickness in both the entrapped and free-oil configurations
- desire to limit the amount of oil required for the tests to an economically realistic volume (logistics and clean-up cost)
- need for sufficient contaminated area to accommodate the measurement footprints of both the GPR and ethane sensor without boundary conflicts from the skirts.

Each skirt consisted of a 7.5 cm (3 inch) plastic (PVC) tube frame, 2.4 m (8 ft) on a side. A 46 cm (18 in) plastic skirt was hung from the plastic frame and weighted with plastic pipes filled with sand at intervals. The six floating frames in the smooth ice portion of the tank were positioned in line down the centerline of the tank at the onset of ice growth and allowed to freeze-in. The seventh skirt was placed beneath the rough ice end of the tank and cut into the under hanging ice blocks (described above in 3.3.1).

The project test plan called for fresh crude oil to be inserted (injected) beneath the ice at two stages in the growth cycle: into three hoops or spill skirts at a nominal ice thickness of 20 cm (8 in), and into the remaining spill rings once the ice has reached close to its maximum thickness (morning of the first test day). The intent was to end up with a mix of free oil under the ice (ice/water/oil interfaces) and entrapped oil (ice/oil/ice interfaces).

Various field studies have demonstrated that new ice will grow beneath an oil layer within 12 to 24 hours of being spilled under winter climatic conditions (Dickins and Buist, 1981; Norcor, 1975). Similar behaviour was expected in the CRREL basin.

The Test Plan proposed the following distribution of oil spill volumes based on a nominal anticipated availability of 738 l (195 gal):

- Three hoops at a nominal film thickness of 25 mm (one inch) - one in rough ice
- Two hoops at a nominal film thickness of 12 mm (0.5 in)
- Two hoops at a nominal film thickness of 3 mm (0.1 in)

The initial spill plan would have consumed ~4.7 drums. Six drums were actually delivered filled to an average capacity of 80%. Based on the volume available, the following oil volumes and anticipated average oil film thickness were calculated in test planning.

- Total theoretical volume of oil available (6 drums) = 1249 liters (330 US gal)
- Estimated volume available with a 20% air gap = ~1000 liters (264 US gal)

The spill allocations into the different skirted areas were selected to consume almost all of the available oil (leaving ~20 l (5 gal) for radar calibration and miscellaneous sampling.

One skirt in rough ice at an avg. film thickness of 2.4" (62 mm) =	370 liters
Two skirts at a film thickness of 1.2" (30 mm) = 178 x 2 =	356 liters
Two skirts at a film thickness of 0.6" (15 mm) = 89 x 2 =	178 liters
Two skirts at a film thickness of 0.3" (8 mm) = 48 x 2 =	<u>96 liters</u>
<b>TOTAL ESTIMATED SPILL VOLUME</b>	<b>1000 liters</b>

Conversion 1 gal US = 3.785 liters

Each Skirted Area = 5.94 m<sup>2</sup> (64 ft<sup>2</sup>)

**Note:** The revised minimum film thickness of 8 mm (0.3 in) agrees with a number of papers in the literature that define the minimum equilibrium film thickness under sea ice as in the range of 6-8 mm depending on the interfacial tension between oil and sea water (Norcor, 1975). Attempts to create thinner films by spilling smaller volumes of oil would lead to partially oiling the ice within any given hoop - the oil will tend to stop spreading once the equilibrium thickness is reached. As it turned out, small natural variations in the ice thickness were sufficient to create uneven oiling in six of the seven skirts (Section 4.2).

The following sequence was planned for the seven spills.

**Table 3-1 Planned Spill Sets**

<b>Test Number</b>	<b>Nominal Oil Film Thickness mm (inches)</b>	<b>Volume Spilled Liters (US gal)</b>
<b>1- Series: Encapsulated Oil</b> (spilled prior to testing at intermediate thickness) <b>2- Series: Free Oil</b> (spilled during testing at maximum thickness)		
1-1 & 2-1	8 (0.3)	48.1 (12.7)
1-2 & 2-2	15 (0.6)	88.9 (23.5)
1-3 & 2-3	30 (1.2)	177.9 (47.0)
2-4 in rough ice	N/A (expected to be highly irregular depending on local ice geometry)	Dependent on volume remaining after first six spills

### **3.5 Spill Procedures**

The oil was injected under the ice using a "J" shaped piping system that was connected by a rubber hose to a manual pump in the supply drum. A check valve was installed at the delivery end of the supply piping to assure oil was only being delivered only during pumping. The objective was to minimize the spill volume as the piping was removed from under the ice. The oil was injected under the ice by cutting a access hole approximately 50 cm (20 in) long by 20 cm (8 in) wide outside and immediately adjacent to the containment hoop. The J-piping was inserted into the slot far enough to be below the bottom of the skirt before the piping was rotated 90° to get the discharge end within the skirt. To insure the oil was delivered in the center of the hoop, the delivery pipe was then tilted and pushed further under the ice.

On November 6, when the ice as 10 cm (4in) the oil was spilled in hoops 1-1 and 1-2, with the oil injected was at room temperature. In less than hour oil started to appear on the surface. To avoid a similar seepage problem, the oil in hoop 1-3 was not spilled until November 8.

To reduce the affect of the latent heat in the oil, all subsequent spills were pumped from barrels stored in a room just above 0°C. The oil was injected in the four remaining hoops on November 15 with the only mishap occurring in hoop 2-3. The J-piping was oriented horizontal and a portion of the oil was delivered outside of the hoop. This situation (more natural than containing the oil in skirts) was not recognized until the radar systems detected oil outside the northern edge of the hoop. This mishap provided an additional level of confidence in the radar system performance.

### **3.6 Flux Chamber Methods**

The approach selected for measuring the emissions of ethane through the ice sheet was to use an enclosure device such as an emission isolation flux chamber. Klenbusch (1986) provides details regarding the use and operation of flux chambers designed by Radian Corporation for the US Environmental Protection Agency (EPA) (Figure 3-6).



**Figure 3-6** Flux chamber deployed on the ground to measure methane emissions

A cutaway diagram of the EPA flux chamber is shown in Figure 3-7.

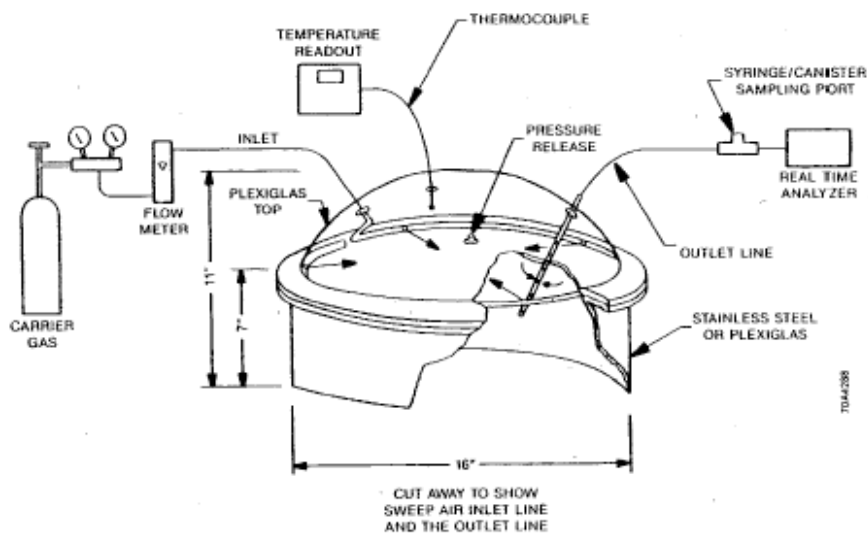


**Figure 3-7** Flux chamber cutaway view

As shown, the EPA flux chamber has a 41 cm (16-inch) OD, giving a surface “footprint” of  $0.130 \text{ m}^2$  ( $0.46 \text{ ft}^2$ ) and a volume of 30 liters (1.1 cubic ft). For flux measurements, the chamber is purged with an inert gas (usually air or nitrogen) at a flow rate of five liters/minute ( $0.18 \text{ cubic feet/minute}$ ). The volumetric flow rate of sweep gas through the chamber is recorded and the concentration of the constituent of interest measured at the chamber’s exit. The emission flux rate is calculated from: the surface area isolated, the volumetric flow-rate of sweep gas, and the steady-state gas concentration resulting. The flux chamber has a vent hole in the top to prevent any pressure build-up in the chamber and rests on the surface of interest.

The primary purpose served by the hemispherical domes is to provide a fixed footprint on the ice for measurement of any ethane gas flux through the ice. A secondary, but equally important reason for using the domes is to prevent any interference from atmospheric contamination that might be present in the ice-testing laboratory. Liquid nitrogen boil-off was used to provide an ethane-free purge gas to the hemispherical domes. The ethane concentration of the extracted carrier gas was then measured using the Shell LightTouch™ instrument (Sec. 6.1). The volume purge rate times the mass concentration gives the flux rate through the dome’s footprint.

The flux chambers used for this project were manufactured by California Plastics and had a volume was  $24.5 \text{ l}$  ( $0.9 \text{ ft}^3$ ) with a cross-sectional area of  $0.158 \text{ m}^2$  ( $1.7 \text{ ft}^2$ ). The flux chambers acquired for the project consisted of three Figure 3-8 shows the 46 cm (18 in) diameter plastic hemispherical dome with Swagelok bulkhead fittings.

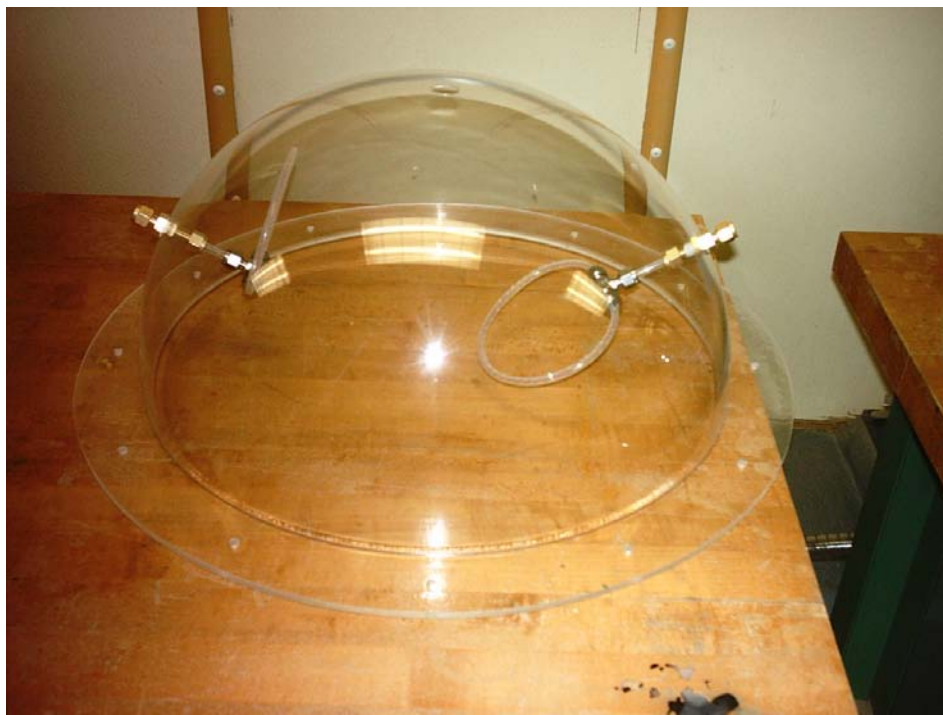


**Figure 3-8** Ethane flux chamber fabricated for the project

The plastic hemispherical dome was placed directly on the ice in order to minimize the internal volume and liquid nitrogen boil-off was used to provide ethane free, ultra high purity nitrogen as a purge gas. Additional operational details are described in Section 6 with Shell's field results.

Shell's LightTouch™ system initially used a 5-liter/minute nitrogen flow to purge the flux chamber and then input this to the gas sensor-sampling cell. Based on experimental results, this purging rate was increased to approximately 7.5 liters/minute (0.26 ft<sup>3</sup>/min) to reduce the influx of ambient air to the test chamber. Shell's very low detection limits (50 pptv) allowed adequate detection levels for the direct measurement of ethane flux through the ice. Flushing the chamber with clean dry nitrogen eliminated problems from atmospheric background intrusion, regardless of the ethane levels in the building, which were very high ~ 100 ppb.

## **4.0 TEST CONDITIONS**

### **4.1 Overall Layout**

The seven skirted spill areas were lined up down the tank in order starting at area 1-1 at the East end and ending with 2-4 in the rough ice field at the West end. Figure 4-1 (page following) shows a plan map of the test basin with locations of individual spill sites, contaminated oil boundaries mapped from overhead photographs (Sec. 4.5.1), and sampling sites.

Figures 4-2 and 4-3 show respective overhead views on Nov 15 of the first (trapped oil) and second (free oil) sets of smooth ice spills. The seventh skirt is not visible on the surface as it was inserted beneath the ice during the construction of the rubble ice (Section 3.4).

Table 4-2 (Sec. 4.5) summarizes the oil volumes, and ice thickness at the time of each spill.



**Figure 4-2** Overhead view of surface conditions in the first three oil sites, in sequence from right to left. Photo taken November 15 (oil spilled November 5 for sites 1-1 and 1-2, November 8 for site 1-3). Evidence of initial oil surfacing in the interior of the first two sites is clearly visible. There is some leakage at the skirt ice interface in all locations (est. much less than 5% of spill volume in each case)

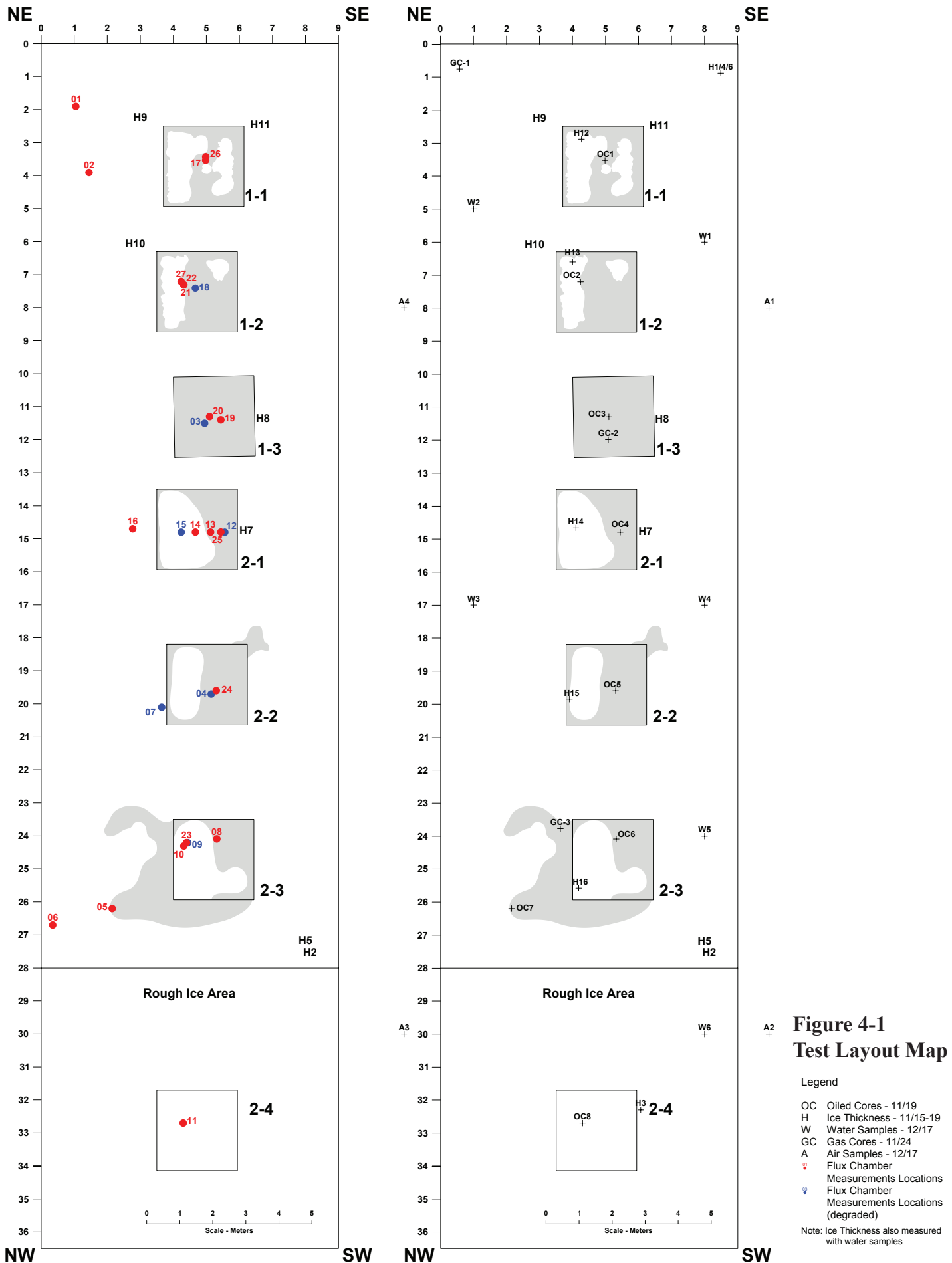




**Figure 4-3** Overhead view of the second set of three spill sites (2-1 to 2-3) on the day of spill, November 15. Note some leakage to the surface at the skirt ice interface in sites 2-1 and 2-2. Flux chamber visible in foreground.

## 4.2 Ice Thickness

The development of the test ice sheet up to November 14 is described in Section 3.3. A series of spot thickness measurements were made throughout the test period in different locations of the tank, in order to gauge the extent of continuing ice growth from November 15 to 19, to assess the degree of natural variability in the sheet ice within the tank, and to compare the thickness in oiled and clean ice areas. Table 4-1 summarizes the ice thickness values from both augur and core holes, taken during the test week. The vertical distribution of oil in the ice is summarized in Section 4.5.2. Appendix C provides a detailed log of ice thickness and coring results.

**Table 4-1**

**Summary of Ice Thickness Measurements During Test Program**

(all measurements from coring or 5 cm (2 in) augur hole except where noted. See Fig. 4-1 and Appendix C for detailed measurements and site locations)

Summary Parameter	Thickness (cm)	Comments
Clean ice outside skirt areas	34 to 40 (avg. 37.7)	Variable locations 11/15-11/9
Clean ice inside oil skirts	41 to 45 (avg. 43.9)	11/19
Oiled ice cores	38 to 44 (avg. 41.1)	11/19
Rubble field	Variable ~ 70	From slots cut for oil insertion 11/15 and coring 11/19

There is no clear explanation for the apparent difference in average thickness between the clean, smooth ice outside the oil skirts and patches of clean ice within five of the skirted areas. On average the uncontaminated ice outside the skirts was ~ 6 cm (2.4 in) thinner than areas within the oiled test sites where oil was not present. Small variations in ice thickness were mapped over ice in the basin in the past (standard deviation of 2% or less of the mean thickness), but at much lower ice thicknesses in the 4 to 8 cm (1.6 to 3 in) range.

Comparing the "clean" ice measurements and oiled core lengths taken within the skirted areas on November 19, confirms that relatively small variations in thickness (less than 3 cm (1.2 in) on average) were sufficient to determine the oil spreading behavior and final contaminated areas shown in backlit photographs (Fig. 4-8 and App. C). In several cases, there was less than a 1 cm (0.4 in) difference between the ice thickness where the oil pooled and the thickness where the ice remained free of oil.

### 4.3 Rough Ice Description and Surface Appearance

Section 3.3.1 describes the creation of an ice rubble area filling the last 8.5 m (28 ft) of the tank at the West end. Figure 4-4 shows a general view of the surface roughness in this area. From observations on November 18, the individual ice blocks height averaged 10-15 cm (4-6 in) elevation above water level. Isolated pieces jugged up to 20 cm (8 in). Approximately 95% of the surface area within the "rubble" section was comprised of irregular ice blocks frozen in at random orientations. Typical block sizes were in the 25-50 cm (10-20 in) range within a base matrix of a smaller number of larger slabs ~1-1.5 m (3-5 ft) across.



**Figure 4-4** Surface appearance of ice rubble (Test area 2-4). Oil on surface was exposed during coring on November 19. Hole was cut to insert camera pole for underwater video.

#### 4.4 Ice Air and Water Temperatures

The tank temperature was raised ten degrees Celsius the day prior to the last spills (November 14) and held at close to the same temperature throughout the test week ( $-17^{\circ}\text{C}$  or  $1.4^{\circ}\text{F}$ ). A continuous record of tank air and water temperatures is available throughout the entire test period.

To achieve uniform ice thickness, air bubblers were used to agitate the water to insure an isothermal thermal mixture at  $0.3^{\circ}\text{C}$ , the freezing point of urea solution. The tank is elevated and heat is gained through the sides and bottom of the tank and without mixing, the water column becomes stratified with the denser warmer water on the bottom. The submerged thermistors used to monitor the water temperature at three elevations at two locations confirmed the water below the ice was at  $-0.3^{\circ}\text{C}$ .

A representative ice temperature profile was acquired at the beginning of coring as the ice started warming on November 19 (Fig. 4-5). Spot measurements of surface and near surface ice temperatures were also made during the test week (Fig. 4-6). As documented by Hirayama (1983), a variation in air temperature of some  $12^{\circ}\text{C}$  results in a variation of only about  $2^{\circ}\text{C}$  in the ice surface temperature.

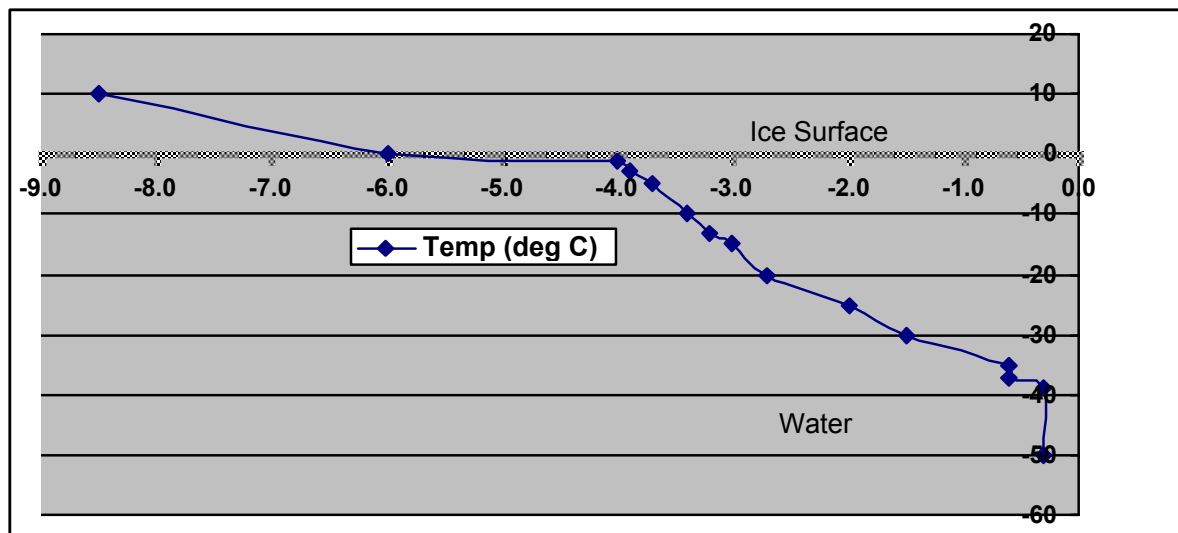


**Figure 4-5** Measured ice and near surface temperature profile - November 19, 2004

**Note:** Water at  $-0.3^{\circ}\text{C}$ , air temperatures measured at 0 depth (probe on ice surface) and +10 cm. Tank ambient temperature  $-15^{\circ}\text{C}$

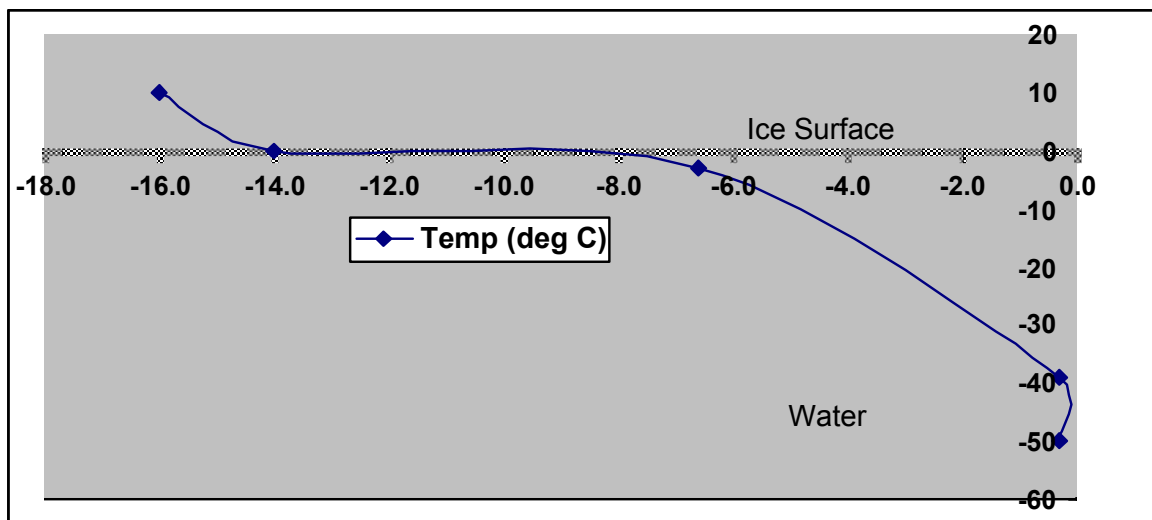


**Figure 4-6** Internal ice and near surface temperatures - November 18, 2004

#### 4.5 Oil in Ice Configurations

The ice sheet was initiated at the beginning of November and reached the target thickness of 16 cm (6 inches) for the first three spills on November 5, 2004. Within approximately 20 minutes after completing the first two spills, evidence of oil appeared on the ice surface in isolated spots and on the inside of the skirt perimeter. The overall percentage volume that surfaced was estimated as no more than 5% in the worst case (Fig. 4-3). Additional photographs of the surface appearance of each spill area during the test period are provided in Appendix C.

Factors contributing to the unexpected oil surfacing in the first two spills include: oil spilled at room temperature (thermal shock), thin ice, and slight positive hydrostatic pressure in the tank (negative freeboard). The presence of oil on the surface in isolated areas in the first two test hoops did not significantly affect the subsequent test program as the ethane sampling areas could be selected to work around the visible oil.

The third spill (Skirt 1-3) was delayed three days until the ice thickened from 17 to 26 cm. At the same time, care was taken to ensure that the tank water level exerted no vertical uplift force on the oil, and the oil was cooled to within one degree of the water temperature. No further problems with premature surfacing were experienced.

The last four spills were carried out on November 15, the first day of the test program, to ensure that the oil remained predominantly in a free state beneath the ice (not encapsulated with new ice growth below the oil as was planned for the first three spills).

**Table 4-2**  
**Summary of Spill Volumes and Ice Parameters**

Test Square	Date and Time	Ice Thickness (cm)	Room Temp (°C)	Oil Temp when spilled (°C)	Volume Spilled Liters (gal)	Target Oil Film Thickness (mm) <u>Section 3.4</u>
1-1	11/5/04 10:30	17	-27	18	48.45 (12.80)	8
1-2	11/5/04 11:00	17	-27	18	88.58 (23.40)	15
1-3	11/8/04 15:00	25.5	-27	1.2	177.9 (47.00)	30
2-1	11/15/04 7:30	34.5	-17	0	48.83 (12.90)	8
2-2	11/15/04 8:00	35.3	-17	0	80.63 (21.30)	15
2-3	11/15/04 9:00	35.1	-17	0	151.4 (40.00)	30
2-4	11/15/04 13:00	~69*	-17	0	164.3 (43.40)	N/A

\* Thickness in the rough ice area was highly variable

The oil naturally pooled in areas of thinner ice creating localized patches where the oil film thickness was significantly greater than the target values shown in Table 4-2. Site 1-3 was the exception in that the entire ice area within the skirt was oiled. Further descriptions of the contaminated areas resulting from naturally irregular oil spreading, and the patterns of vertical oil distribution within the ice are provided below.

#### 4.5.1 Oil Spreading (contaminated areas)

As described above, random variations in ice thickness within the tank caused the oil to run under the ice and accumulate in high spots (thinner areas), leaving the thicker ice portions clear of oil.

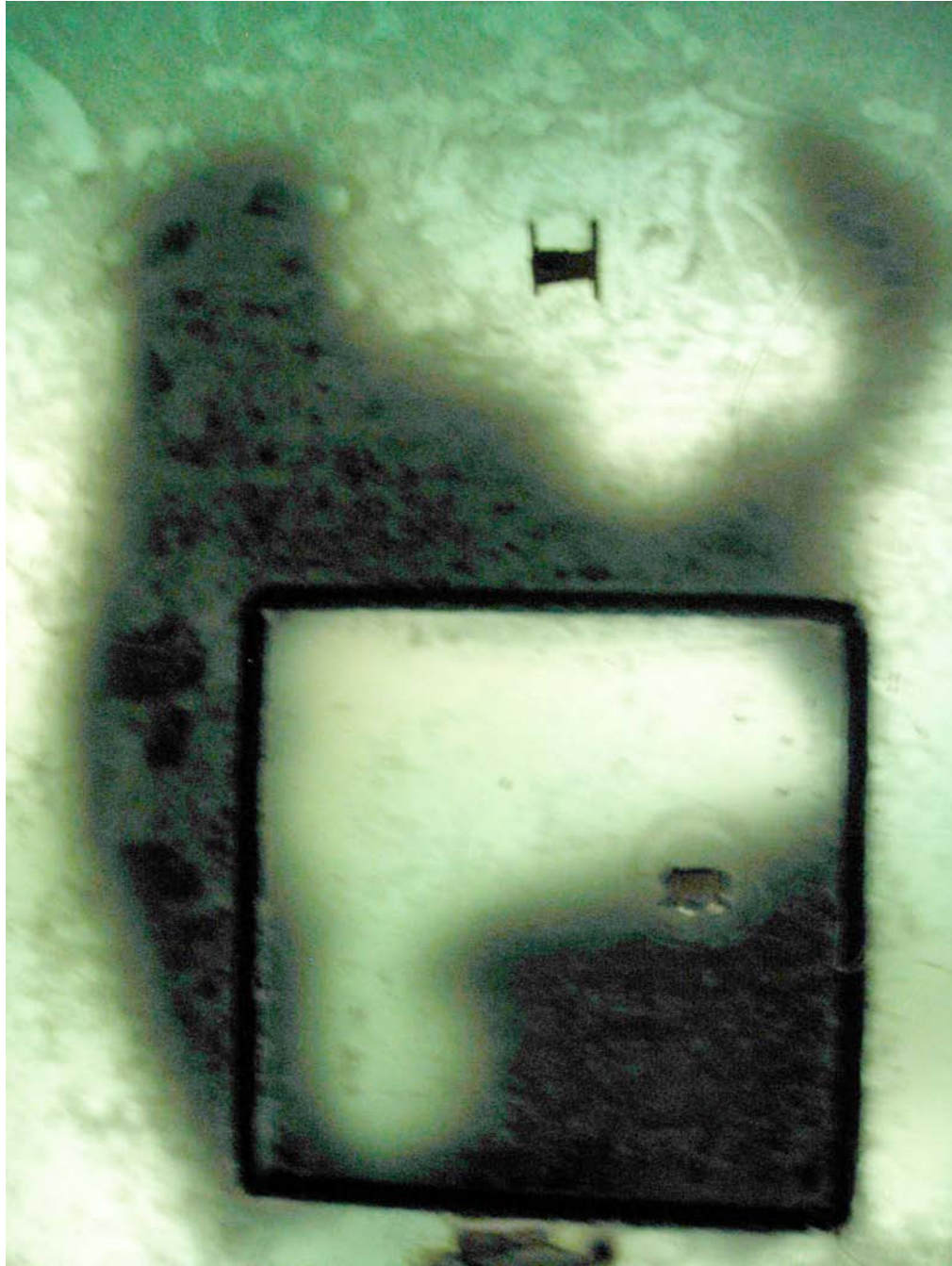
The base maps (Fig. 4-1 and App. D) show the contaminated areas for all six smooth ice sites, digitized from vertical photographs where underwater backlighting clearly revealed the presence of oil trapped in or under the ice (the photos were reprocessed to highlight the oil boundaries).

Figure 4-7 shows an oblique view down the tank under the backlit condition. Oiled areas are clearly visible in all six of the smooth ice sites.

Appendix C contains all of the overhead pictures in their final form. Figure 4-8 shows a representative aerial view of site 2-3. In that spill, a substantial portion of the oil spilled outside the skirt, forming a natural pattern following contours of slightly thinner ice (initially detected on the radar response).



**Figure 4-7** Overall backlit view of all sites from 2-4 in the foreground to 1-1 at the far end (top). Note that the dark area in the thicker rough ice does not accurately reflect the oil distribution. Underwater video in this area showed patchy oil distribution. Oiling in other sites is shown accurately.



**Figure 4-8** Example of under-ice oil distribution in a vertical backlit photograph of Site 2-3 (reprocessed in Photoshop® to accentuate the difference between oiled and clean ice).

The pattern of spreading under the ice was also viewed with underwater video coverage of sites 1-1, 2-2, 2-3 and 2-4. The camera mounted by a controllable hinge joint, was extended beneath the ice on a long pole through trenches cut outside the spill area. Figure 4-9 shows an example still capture from the video segment beneath Site 2-3.



**Figure 4-9** Example view from the underwater video camera in Site 2-3.

Table 4-3 compares: (1) the oil average oil film thickness computed from measured spill volumes (Table 4-2) and digitized oiled areas (Fig. 4-1); (2) the planned oil thickness (assuming complete oiling of the full skirted area in each case); and (3) spot measurements of the actual film thickness from coring (App. C). The ice proved too thick to obtain an accurate picture of the overall oiling in area #2-4. Underwater video under the rubble provided a subjective picture of how the oil in that site tended to be trapped in relatively thick pools between underhanging ice blocks and the skirt.

**Table 4-3**  
**Oil Pool Thickness (actual vs. planned)**

Site	Oiled Area (m <sup>2</sup> )	% Area Oiled Inside Skirt	Volume Spilled (m <sup>3</sup> )	Average Oil Thickness (mm)	Measured Oil Thickness (mm)	Planned Thickness (mm)
1-1	3.27	55%	0.048	14.8	5	8
1-2	4.25	71%	0.089	20.8	10	15
1-3	5.95	100%	0.178	29.9	15	30
2-1	2.82	48%	0.049	17.3	15	8
2-2	3.56	60%	0.080	22.6	8-12	15
2-3	7.42	34%	0.151	20.4	17-25	30

**Note:** The oiled area outside the skirt in spill 2-3 was greater than the oiled area within the skirt boundary

#### **4.5.2 Vertical Oil Distribution Within the Ice**

Eight cores were taken in oiled ice within each spill area on November 19 (two in #2-3 including oiled areas inside and outside the skirt). Where possible, the coring sites were selected to correspond with locations used for the ethane flux measurements (Fig. 4-1). Appendix C contains detailed dimensions and observations from each core and cross references to the ethane site numbers. Close-up photographs are also available for each core, along with selected sectioned views showing internal details of oil inclusions within the ice.

The cores showed that new ice grew beneath the first three spills to a depth of 16 to 24 cm. There was no sign that the presence of oil had a significant effect on the eventual ice thickness reached by the end of the test program in Test areas 1-1 to 1-3.

Ice growth in the second test series was may have been interrupted for a short time by the introduction of an oil insulating layer. However, a comparison of total ice thickness in areas inside the skirt that were clear of oil and areas with a trapped oil pool, showed an average difference of only 2.8 cm (1.1 in) (oiled areas being slightly thinner as expected).

Underwater photography on November 18 showed evidence that new ice crystals (frazil) were beginning to form around the edges of the oil pools in the last four test sites, but the oil in those sites appeared to be still substantially free under the ice (not yet encapsulated). Measurements in the cored holes on November 19 showed a distinct ice/oil/ice interface, even in the three sites where oil was spilled only four days earlier (2-1 to 2-3).

Cores from the first two test sites (1-1 and 1-2) clearly showed that the oil (spilled at room temperature) had fully penetrated up the brine channels to the surface through 17 cm of ice (depth of ice at time of spill). Between 20 and 24 cm (8 and 9.5 in) of new, clean ice had grown beneath the oil in the 14 days elapsed from the time of the spill to taking the ice cores.

The third core (Site 1-3) showed that the oil (spilled at 0°C) had migrated vertically only 5 cm above the initial spill level (27 cm depth). There was 15 cm (6 in) of new ice growth beneath the oil, the top five cm (two inches) of which contained isolated oil inclusions. One possible explanation for the apparent downward migration of oil from the main layer (against buoyancy) is that a few small drops of oil became "speared" on the end of new ice crystals projecting down from the skeletal layer at the time of the spill. The main part of the oil would quickly rise up to form a distinct oil layer, leaving the isolated drops to become incorporated in the new ice as it consolidated and hardened over time, following the spill.

The next three cores (Sites 2-1 to 2-3) showed similar patterns of vertical migration of 14 to 18 cm (5.5 to 7 in) above the oil layer. The ice thickness in clean patches within the test skirts 2-1 and 2-3 was up to 6 cm thinner than the oiled ice, indicating that the ice growth was interrupted or slowed down for a few days by the introduction

of the oil (earlier sites showed little difference in thickness after a few weeks). There is less than a one centimeter difference in ice thickness between the oiled and clean ice in site 2-2.

The following photographs indicate a variety of oil in ice conditions documented through coring on November 19, fourteen days after the initial spills (4 days after the last four spills). Figure 4-10 shows the core barrel, as it penetrates the oil layer in Site 1-1. The core extracted from the same hole, shown in Figure 4-11, illustrates the new clear ice which grew beneath the oil between November 5 and 19. Notably, oil in this site quickly migrated almost to the surface within hours of the spill (heavily oiled core section). A small percentage of the overall spill volume appeared on the ice surface as isolated patches as shown in Figure 4-2.

Figure 4-12 shows the oil left on the surface from coring in Site 1-2. Of particular interest are two other small diameter holes drilled nearby: one showing evidence of light oiling under the ice evidenced by brownish drill cuttings (no free oil) and the other showing essentially clean ice evidenced by completely white cuttings.

Figure 4-13 shows a core from Site 2-2 (free oil at the bottom of the ice). The oil at this site has migrated approximately half way to the surface ~15 cm (6 in). Figure 4-13 shows a close-up of an oiled channel (brine channel equivalent in natural sea ice) exposed by slicing the core shown in Fig. 4-13, vertically in half. The scale is such that the oiled channel is about the width of a pencil lead or a few mm (0.1 in).



**Figure 4-10** Coring in the center of ethane flux site # 26 (Fig. 4-1) spill 1-1. Oiled drill cuttings carried to surface as the drill penetrates the oil pool trapped within the ice.



**Figure 4-11** Oiled core taken in Site 1-1 November 19. New ice growth after spill shown by clean ice in section to the right ("dirty" appearance is due to contamination as the oil is extracted through the oil-filled hole). Oil has penetrated the ice vertically to the surface. Total core length 38 cm.



**Figure 4-12** Oil left on the surface after coring in spill site 1-2. Note two adjacent two inch auger holes: one with very light oiling (beige colored cuttings) to the right of the core hole, and another with no visible oil (clean white cuttings upper left).



**Figure 4-13** Oiled core taken November 19. Oil layer far right, top of ice on left. No evidence of oil in the upper ice section. Total core length recovered 23 cm. Oil migrated internally within the ice for 17 cm above the spill. Measurements in the hole indicated up to 7 cm of new ice growth beneath the oil (too fragile to be recovered by the core barrel).



**Figure 4-14** Close-up of oiled "brine" channel within a half section of the core shown in Figure 4-13. The dimension of the oiled channel is equivalent to the width of a pencil lead or 1-2 mm (0.1 in).

## 5.0 GROUND PENETRATING RADAR

### 5.1 Experimental Setup and Sequence

A series of Ground Penetrating Radar (GPR) experiments tested the response to various radar configurations and compared performance between two different but similar GPR systems. Details of each experiment setup are described below.

#### 5.1.1 3D Common Offset Survey

The objective of this experiment was to measure the GPR response to the three dimensional oil distributions. Data were first acquired using the *Sensors and Software* system with 900 MHz antennas. During this experiment, it was found that the data characteristics changed dramatically over time, an effect interpreted to be a temperature related electronics failure. The survey was subsequently repeated using the MALA system with 800 MHz antennas. The batteries for the *Mala* system failed rapidly (~ 30 min) at the 0°F temperature of the cold room, but the crew was able to complete the survey in segments without any additional equipment problems.

Three-dimensional (3D) surveys were acquired over the smooth ice and rough ice areas separately, but the general layout was common to both. The 3D patch was 4.8 m x 27 m (15.7 ft x 88.5 ft) over the smooth ice, and 4.8 m x 7 m (15.7 ft x 11.4 ft) over the rough ice. In both sections, the data consisted of 25 parallel profiles on 20 cm (7.9 in) centers; utilizing colored string gridlines stretched the length of the tank (visible in Fig. 5-1). Production of a laterally coherent image required correction for cross-line positioning errors caused by odometer wheel slip. It was possible to correct for any possible misplacement during processing by knowing the positions of the oiled cells and the skirt boundaries (discontinuity clearly evident in the GPR data). Figure 5-1 shows the two-person team traversing test site 1-2 line with the *Sensors and Software* system mounted on a towed sled.



**Figure 5-1** Radar team traversing test site 1-2 at CRREL with the *Sensors and Software* system. Note plastic sheets over initial sites to prevent cross contamination with the towed sled.

### 5.1.2 2D Profiling

The objective of this experiment was to test the GPR response for each of six configurations. Hardware configurations consisted of a *Sensors and Software* Pulse EKKO 1000 system with 450 MHz, 900 MHz, and 1200 MHz antennas, and a *Mala Geosciences* RAMAC system with 500 MHz, 800MHz, and 1000 MHz antennas (Figs. 5-1 and 5-2). This not only allowed a comparison of the performance of the two systems, but also provided a backup to ensure completion of the experiment in case of a system failure. Coincident profiles were made with each configuration along a transect that was approximately centered on the test cells. This calibration transect crossed all test cells and spanned both the rough ice and smooth ice areas.

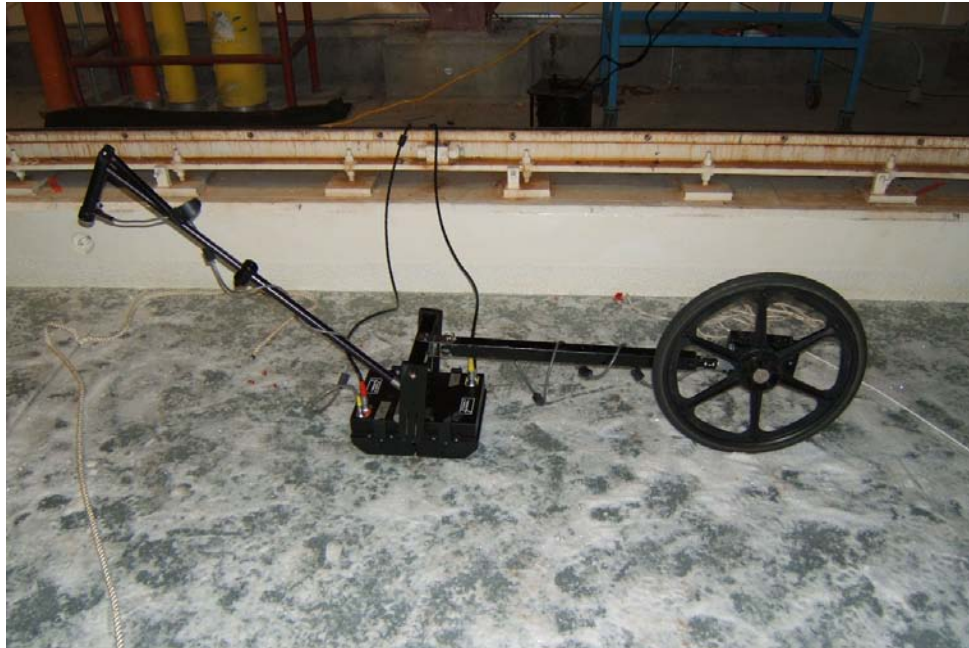


**Figure 5-2** *Sensors and Software system*



**Figure 5-3** *Mala Geosciences RAMAC system. Note colored strings used to establish radar grid survey lines.*

For both systems, an attempt was made to acquire data traces at regular intervals using a studded odometer wheel trigger (a configuration used successfully in previous experiments on ice). Plastic placed over cells 1-1 and 1-2, to prevent spreading the oil that had seeped to the surface soon after being spilled, caused the wheel to slip during data acquisition, causing some errors in data geometry. For the Sensors and Software system, data were acquired at ~5 cm (2 in) intervals, and with the *Mala* system the interval was ~ 2 cm. The spatial aliasing<sup>+</sup> limit at the highest frequency used in this study (1200 MHz) is ~ 6 cm (2.4 in) so the acquisition parameters noted above ensured that data were adequately sampled. Eight radar pulses were stacked at each location to attenuate random noise.

<sup>+</sup>Spatial aliasing means that sampling density of the wave field is too coarse leading to an inaccurate digital representation of the analog waveform. The data are spatially aliased when the spatial sampling interval is greater than 1/2 wavelength at the dominant signal frequency.

### 5.1.3 Multi-offset Data Acquisition

This experiment was designed to measure the GPR amplitude variation with offset (AVO) response to oil trapped at the ice/water interface. It was initially planned to acquire multi-fold data along a continuous transect spanning the smooth ice section. This experiment required the Sensors and Software system, which is designed so that the transmitting and receiving antennas can be separated for multi-offset data acquisition. As mentioned previously, this system had a low temperature induced electronics failure, which prevented the acquisition of a continuous multi-offset profile. However, it was possible to acquire individual common-midpoint, or expanding spread, gathers at six locations; 3 centered in cells 2-1, 2-2, and 2-6, and 3 in the clean ice areas outside each of these test cells. **Note:** The gathers consist of 40 traces at 4 cm offset intervals, and 7 cm near offset.

### 5.1.4 Airborne Radar Data Acquisition

This experiment was designed to test the potential to measure GPR attribute anomalies using an airborne system. Data were acquired with the *Sensors and Software* system with 900 MHz antennas. The antennas were attached to the lab crane that could be moved along at a constant pace. The transect closely coincided with the centerline profile described in section 5.1.1, and spanned both the smooth ice and rough ice sections. Profiles were acquired at acquisition heights of 1 m, 2m and 3 m (3.3, 6.6 and 10 ft) above the ice.

### 5.1.5 Electric Permittivity Control Measurements

The objective of this component of the experiment was to obtain an independent measure of the electric permittivity of the urea ice. Ice measurements used a TRIME Inc. downhole time domain reflectometry (TDR) probe. While the ice was growing, CRREL personnel installed seven vertical 5 cm (2 in) sched. 40 PVC probe access tubes adjacent to each of the test cells. Measurements were made in five probe access tubes (two tubes failed prior to data acquisition).

### 5.1.6 GPR Data Processing

The initial processing flow for all GPR data was similar and consisted of: 1) time-zero shift to correct for instrument drift; 2) bandpass filter to remove the low frequency transient (WOW) and high frequency random noise; 3) spherical spreading correction to approximate true amplitude reflectivity; and 4) ice/water horizon picking, and 5) attribute computation via the Hilbert transform. Additionally, a 3D phase shift migration was applied to the rough ice data to improve spatial accuracy, and 2D kirchoff time migration to the airborne data to improve lateral resolution. The 3D smooth ice data were interpolated to a uniform grid with correct inline positioning using an LSS algorithm available in Promax processing software.

## 5.2 GPR Results and Discussion

A clear reflection was observed from the ice/water contact (IW) in both the smooth ice and rough ice areas with the full range of antenna frequencies we deployed. In addition, GPR attribute anomalies were observed where oil was known to be present at the ice/water interface and within the ice in all data with characteristic antenna frequencies above 800 MHz. The response at lower frequencies and in the rough ice areas is less well defined. A detailed discussion of each experiment referenced above is included below.

### 5.2.1 3D Common Offset Survey.

All 3D data was acquired with the *Mala* system operating with 800 MHz antennas. The IW interface produced a clear, well-defined reflection that enabled mapping of the ice thickness in both the smooth ice and rough ice areas (Fig. 5-4). Overhead photographs of the ice, when illuminated from below provided a clear visual indication of the areal extent of the oil distributions below the smooth ice (App. C). In the smooth ice section, a number of amplitude anomalies were present throughout the survey area, with the largest and most extensive observed in cells 2-1, 2-2, and on the southeast side of cell 2-2 and north and west of cell 2-3 where oil breached the containment skirts. Amplitude anomalies in the GPR data closely followed the photographed oil distribution and instantaneous phase and frequency anomalies correlated with the oil distribution (Fig. 5-5). In the lower figure, the oil distribution, as mapped from the backlit photos, is overlain. A well-defined amplitude anomaly tracks the oil distribution in and around cells 2-1, 2-2, 2-3. Of particular interest are the oil-induced anomalies outside of cells 2-2 and 2-3 where oil breached the containment cells. A null response (oil but no significant amplitude response) is interpreted as the oil film being below the resolution of the signal. Non-oil related anomalies (false positives) also occur. However, the anomalies associated with the presence of oil demonstrate the most consistent response. Note that there is no oil at the ice/water interface in cells 1-1, 1-2, or 1-3.

**Note:** there is even better correlation of the oil distribution with thin ice anomalies in the ice thickness map. This is the expected result, and suggests the possibility of combining the reflection attributes with the ice thickness map to minimize the potential for false positives.

In the rough ice section (cell 2-4), illumination photography was not effective because insufficient light penetrated the thicker ice. However, underwater video showed that most of the oil had migrated to the perimeter of the test cell. This was not surprising since the ice thickness map derived from GPR data clearly showed that the ice was thinner around the test cell boundary, possibly due to ice growth being inhibited by the presence of the containment skirt support frame. While amplitude anomalies in cell 2-4 correlated well with the skirt perimeter, it was not possible to differentiate the amplitude effects due to oil from those due to scattering from the skirt.

In cells 1-1, 1-2, and 1-3, GPR reflections were clearly associated with the trapped oil layer. The area distribution of the oil reflections correlate well with the distribution mapped using illuminated photography (Fig. 4-1 and App. C).

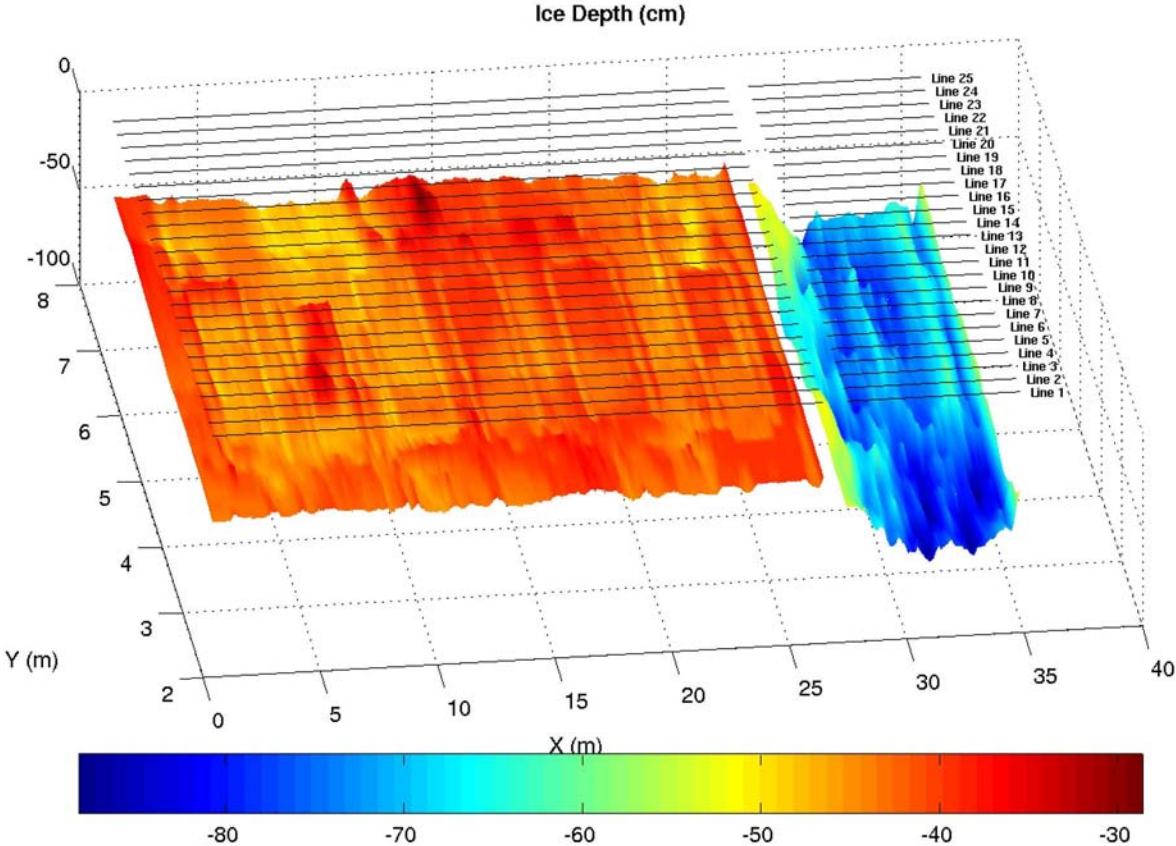


**Figure 5-4** Depth to ice/water interface mapped using 3D GPR and surface location of GPR profiles. The data were acquired using an 800 MHz common offset antenna configuration. Ice thickness anomalies are evident at the boundaries of the containment cells. Image is aligned in the long dimension of the tank, smooth ice on the left (East), rough ice shown in blue on the right (West). Outlines of the six smooth ice spill skirts can be seen in the image.

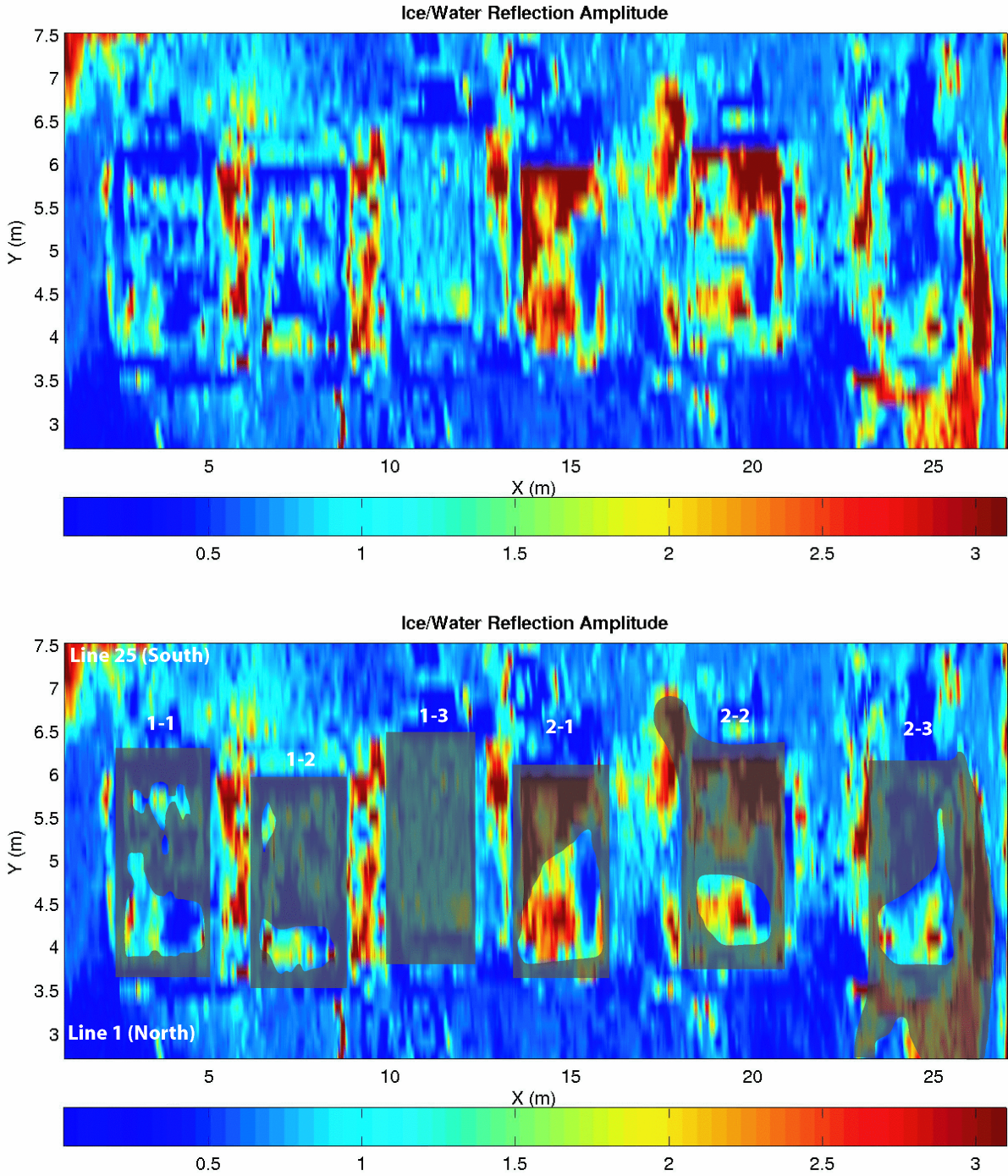


**Figure 5-5** Reflection strength of the IW reflection as the ratio to the background amplitude. The data are taken from the 800 MHz 3D survey

Although the results of the 3D common offset experiment were very positive, three major complications need to be addressed in subsequent development phases.

First, a number of amplitude highs are unrelated to the oil distribution. These are possibly polarization effects due to an irregular ice/water surface, and the containment skirts. The effect of depolarization on GPR amplitudes is discussed by Luzitano and Ulrych (1996). Amplitude variability due to polarization will be a more significant issue in natural sea ice, where GPR amplitude anisotropy due to preferred crystal growth orientation has long been recognized. This issue is covered further in the discussion of future R&D needs in Section 8.4.

Second, there was a null response in some areas: that is no significant amplitude anomaly was observed where oil was known to be present. The null response is interpreted as being indicative of an oil film that is below the resolution of the signal.

Third, the amplitude anomalies associated with the oil are significantly larger than predicted by the model (Fig. 2-1). One potential explanation is that the original model predictions did not consider the effects of electric conductivity. The relatively high conductivity of urea water may account for the deviation between the modeled and measured amplitudes, however a more extensive modeling effort is required to explain this observation. With the existing level of understanding, GPR can be viewed as a promising tool to indicate either the presence or lack of oil. Once the modeling anomalies are explained, it may be possible to extend the technology to provide a quantitative measure of oil film thickness.

### **5.2.2 2D Antenna Frequency Comparison**

**Note:** the 1200 MHz antenna was not available for this test.

Initially, the calibration profile was located at the approximate centerline of the test cells (Line 13 of the 3D survey). This placement assumed that the oil was distributed evenly within the cells. In the profiles, the Sensors and Software system with 900 MHz antennas showed significant amplitude anomalies at the ice/water interface in cell 2-2. Similar results were also observed in cells 2-1 and 2-3, although not as well defined. Anomalies also evident in the 450 MHz data are only marginally above the background level.

Additionally, there are amplitude highs associated with the locations of the oil skirts in all cells. Where the vertical skirt intersects the horizontal ice/water boundary, a lateral permittivity heterogeneity is introduced that results in scattering of the radar signal. This scattered energy interferes constructively with the specular reflection from the ice/water interface causing a local amplitude high. These anomalies were expected and therefore one of the experiment design objectives was to ensure that the cells were large enough to allow for a significant section of data that was free of skirt interference effects. This objective was accomplished successfully.

Over cell 2-4, there are anomalies in both the 900 and 450 MHz data, at the edges of the test cell. Underwater video obtained five days following the spill in area 2-4 showed that most of the oil migrated to the edges. In the rough ice, it is difficult to differentiate the amplitude effect due to the presence of the skirt from the amplitude effect due to the presence of oil. This is discussed in detail in section 5.2.3.

Clear reflections were evident in the 900 and 450 MHz data from the trapped oil layer present in cell 1-3. Additionally, reflections from the trapped oil are present in the 900 MHz data for cells 1-1 and 1-2, although not as clearly defined. At less than 1 cm measured, the oil film thickness in cells 1-1 and 1-2 may be below the resolution limits of the 450 MHz data (see Table 4-3).

Similar results were obtained with the MALA system, with the 1000 MHz and 500 MHz systems being comparable to the 900 MHz and 450 MHz antennas of the Sensors and Software system. The most notable exception is that the 500 MHz antenna of the MALA system is significantly narrower in bandwidth than the Sensors and Software 450 MHz antenna. Narrowing the bandwidth results in a pulse that has an increased number of side lobes making the data appear “ringy”. Resolution is inversely proportional bandwidth so that a narrower bandwidth signal has lower resolution potential.

By the time the 1200 MHz *Sensors and Software* antenna arrived on site, the team had mapped the oil distribution using backlighting of the ice. Recognizing that the oil distribution was biased toward the south side of the tank, the 2D acquisition was repeated with the Sensors and Software system along Line 16 in the smooth ice.

Comparisons of the 450, 900, and 1200 MHz antennas are shown in Figure 5-6. The relative amplitude anomalies associated with oil in cells 2-1, and 2-2 is evident in all three profiles, but decreases in relative strength with decreasing frequency, as expected. Very little oil was present in cell 2-3 along this profile and, as expected, there is no amplitude anomaly. A reflection from the intra-ice oil film in cell 1-3 is evident at all three frequencies, with resolution improving with increasing frequency. Very shallow reflections from films in cells 1-1 and 1-2 are evident in the 900 MHz data but not well separated from the surface waves (direct air wave and direct wave through the ice). Oil induced amplitude anomalies at the IW interface in cells 2-1 and 2-2 are clearly defined at 900 and 1200 MHz. At 450 MHz, these anomalies are present but only marginally above the background level. Little oil was present in and near cell 2-3 along this profile.

# Oil-in-Ice Detection

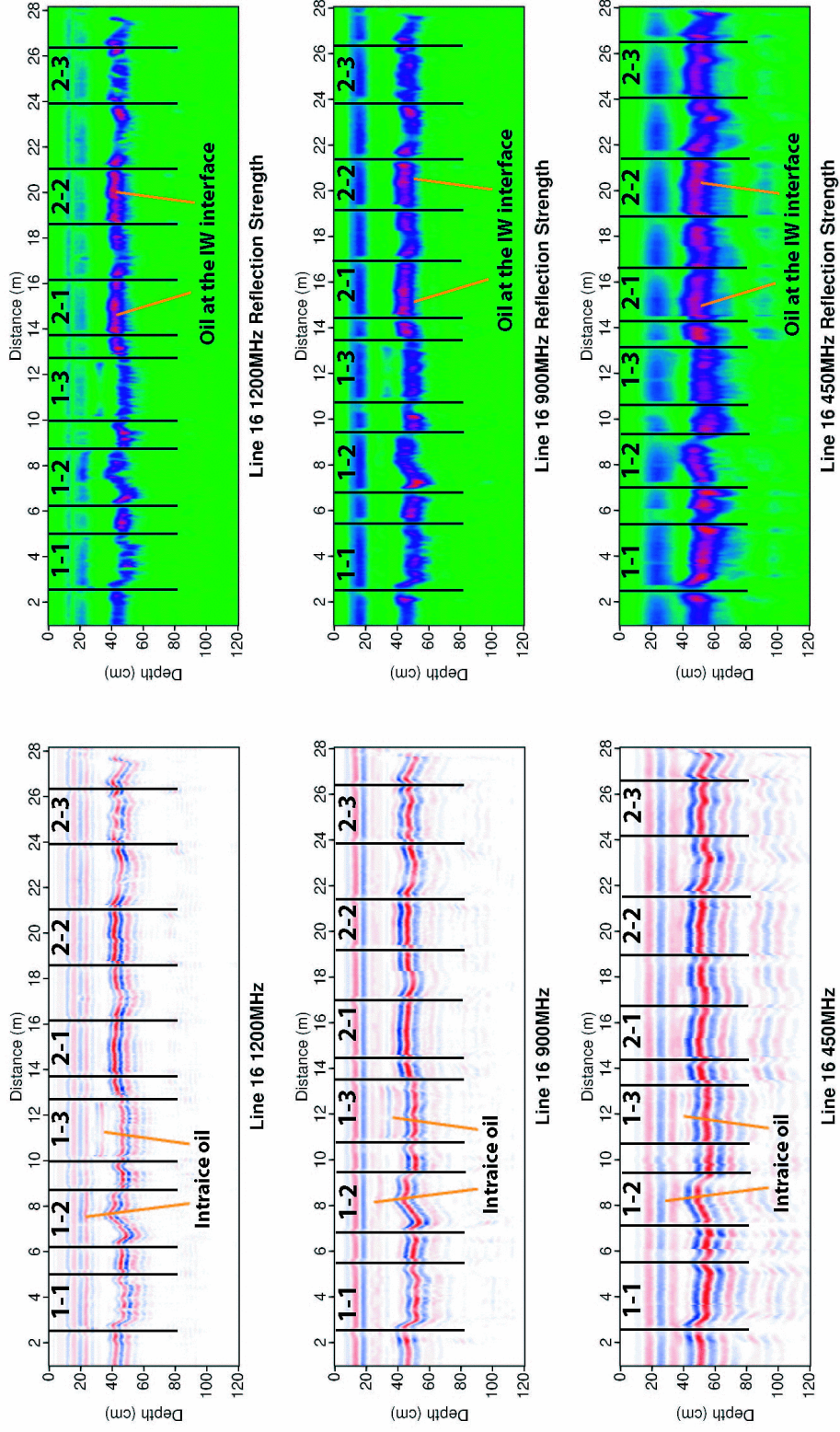


**Figure 5-6** GPR reflection data and reflection strength (absolute value of the Hilbert transform) at 450, 900, and 1200 MHz over the smooth ice section (See Fig. 5-4 for position of Line 16).

It is evident from these tests that radar operating at ~1000 MHz is highly effective for imaging oil films trapped in and beneath sea ice. Radar operating at ~500 MHz still images the oil, but appears to be at the low end of practical resolution limits. The amplitude vs. frequency response is scale dependent so that a thicker oil film will produce a larger response at lower frequencies. The thickest oil film produced during this experiment produced a marginal amplitude response at 500 MHz, but a strong response at 1000 MHz. Other variables, most notably the dielectric permittivity of the ice, which varies by salinity, liquid brine content, and temperature, will impact the amplitude response.

### **5.2.3 Multi-offset Data Acquisition**

The trend of the GPR AVO response to the presence of oil at the ice/water interface closely matches the trend predicted in the modeling study (Figure 2-1). Clearly GPR AVO analysis has significant potential for identifying oil under sea ice, and based on previous work in sedimentary systems (Bradford, 2004; Bradford et al., in press) may prove beneficial in making oil detection more robust. However, given the clarity of the response observed in the common-offset data, the added cost in processing and acquisition may not balance the added value.

### **5.2.4 Airborne Radar Data Acquisition**

Data acquired in the airborne configuration showed a clear reflection from the ice/water interface, but did not repeat the oil-induced amplitude anomalies present in the surface data. This is likely a resolution problem. Lateral resolution is a function of the distance from the source and receiver to the target, and is given by the function  $(lz/2)^{1/2}$  where  $l$  is the signal wavelength and  $z$  is the distance to the target. Consequently, raising the radar unit decreases the lateral resolution potential. The radar footprint at the ice/water interface ranged from ~ 1 to 1.5 m (3.3 to 4.9 ft) at 1 m to 3 m (3.3 to 10 ft) above the ice respectively. A second limiting factor was that the crane, which was used to elevate the GPR system, was biased toward the north side of the cells, but the spill distribution was biased toward the south side of the cells, so the configuration was not optimal. With a laterally extensive spill, this will not be an issue, but the spatial limitations of the lab experiment, coupled with the irregular oil distribution created a non-ideal test for an airborne experiment (not part of the original test design).

**5.2.5 Electric Permittivity Control Measurements.**

Electric permittivity of the urea ice was measured with the 20 cm TDR wave-guide centered in the ice. The results of these measurements are shown in Table 5-1. The resulting average relative permittivity of  $K=4.17 \pm 0.09$  was used in the thin layer model to predict the reflection attributes and to compute radar velocity in the ice for depth conversion.

**Table 5-1**  
**Ice Permittivity Estimates from Downhole TDR Probe**

<b>~1.5 m S of Cell 1-1</b>	<b>~1.5 m S of Cell 1-2</b>	<b>~ 1.5 m S of Cell 1-3</b>	<b>~ 1.5 m S of Cell 2-2</b>	<b>~1.5 m S of Cell 2-4</b>	<b>Mean</b>
K=4.09	K=4.17	K=4.31	K=4.12	K=4.15	K=4.17±0.09

## **6.0 LIGHTTOUCH™ ETHANE GAS SENSOR**

The Shell Global Solutions' LightTouch™ sensor was used in combination with a flux chamber (Sec. 3.6) to measure the surface ethane mass flux rates produced by oil trapped beneath ice in the CRREL tests. These flux values can then be used to assess whether an airborne LightTouch™ survey would be capable of detecting and mapping the fluxes resulting from a full-scale oil spill trapped in or under ice.

### **6.1 Experimental Setup and System Description**

The ethane gas sensor used at CRREL was a Tuneable Diode Laser Spectrometer (TDLS), operating as a second derivative modulation spectrometer scanning over a single ethane CH transition in the mid infra-red (IR) region. The gas sample is introduced into a multi-pass optical sample cell, controlled at low pressure. The ethane gas concentration is determined from the measured total optical absorption at the selected transition wavelength; the automated system continuously recalibrates itself using ethane-free N<sub>2</sub> boil-off gas to fix the zero, and a glass cell, sealed ethane sample to provide a constant fixed known concentration reference.

The sample gas is continuously replenished along pipes connected to the flux chamber, which is continuously flushed with ethane-free N<sub>2</sub> carrier gas until the equilibrium concentration is achieved. The chamber's equilibrium ethane concentration is determined by the chamber's "footprint" area, the mass flux through that surface, and the carrier gas volume flow rate. The ethane gas sensor can accurately measure concentrations to a precision of ~50 parts per trillion (ppt), which is approximately 200 times better than gas chromatographic measurements. Furthermore, the TDLS measurements are available continuously every second. The TDLS instrument enclosure and associated Liquid N<sub>2</sub> source with pump are shown in Figure 6-1. The system is further described in Hirst et al. (2004) and Gibson et al. (2002) and at the following web sites

<http://www.physics.gla.ac.uk/Optics/projects/oilProspection/>  
[http://www.shellglobalsolutions.com/products\\_services/lighttouch.htm](http://www.shellglobalsolutions.com/products_services/lighttouch.htm)

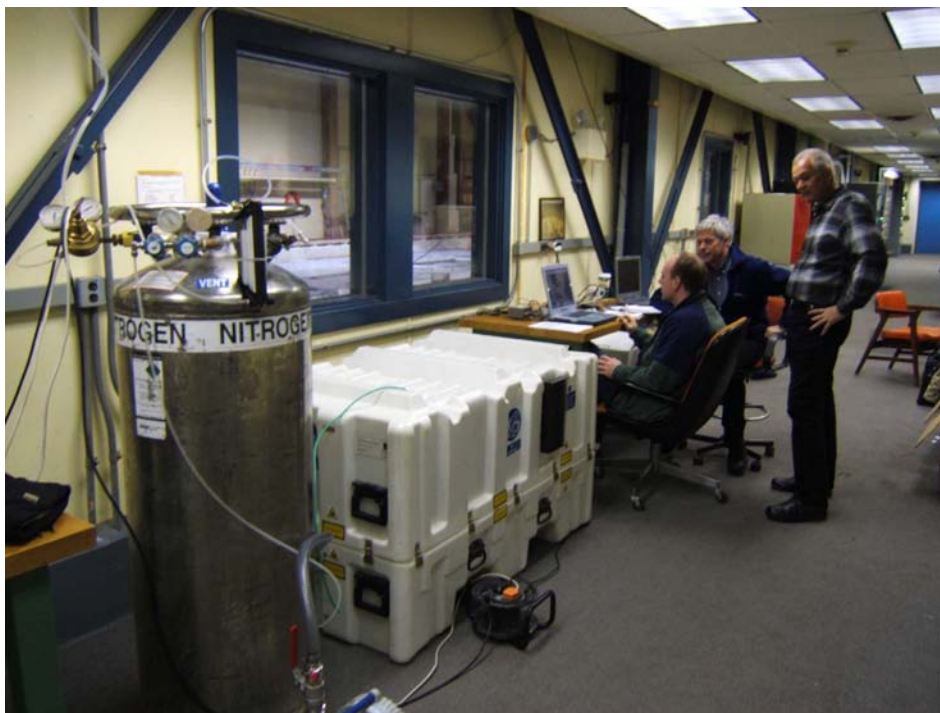


**Figure 6-1** The Shell Global Solutions TDLS ethane gas sensor (inside white box) with Liquid N<sub>2</sub> Dewar, vacuum sample pump and associated piping and flow controls; the spectroscopy and data collection is all controlled by the laptop.

## 6.2 Ethane Flux Measurements

The atmospheric background ethane concentration was measured at ~2 ppb, which is normal for November and the latitude of New Hampshire (Rudolph, 1995). Within the cold room containing the ice sheet concentrations were ~100 ppb at the beginning of the first day of flux measurements (November 17), dropping progressively to 70 ppb at the start of day 2, and 23 ppb at the end of day 2. The cold room conditions were continually changing: with unavoidable variations in ventilation, recirculation and temperatures throughout the experiments; but these do not compromise the flux values obtained via the flux chamber methodology.

Before starting the experimental programme, the flux chamber was tested over an inert Polytetrafluoroethane (PTFE) sheet, checking the flux value was zero and that no ethane was being evolved from any of the surfaces within the chamber or associated gas flow circuit. The test was perfect and yielded zero flux to within the experimental accuracy (Fig. 6-2). The chamber volume was 24.5 litres (0.86 ft<sup>3</sup>) with a cross-sectional area of 0.158 m<sup>2</sup> (1.7 ft<sup>2</sup>).



**Figure 6-2** Flux chamber pre-test over PTFE sheeting proved no surfaces were contaminated or producing ethane and the flux chamber equilibrium concentration was zero to within experimental accuracy of <100 ppt.

The team made flux chamber measurements at 27 locations over 2 days. Each measurement comprised 30 to 50 minutes of concentration data collection at one-second intervals, with one minute averaging and recording of all standard deviations. The exact locations of all flux chamber measurements are shown to scale in Figure 4-1 superimposed on the oiled areas. Figure 6-3 shows an overall sketch of locations and respective concentrations created early in the program (later to be converted to fluxes). Greater red saturation signifies greater concentration.

Some of the earlier concentration measurements were discarded in the full analysis as influx of background air was detected. The experimental methodology was progressively refined to improve reliability. For example, it became clear how important it was to ensure a continuous outflow of carrier gas from the chamber. This was achieved by providing a good seal between the lip of the flux chamber and the ice, and by increasing the carrier gas flow rate from an initial value of 5 litres/min (0.18 ft<sup>3</sup>/min) to the maximum feasible with the flow monitoring equipment: 7.74 litres/min (0.27 ft<sup>3</sup>/min). The vent area in the roof of the flux chamber was shielded without creating any back pressure, by incorporating a diffuse tissue filter: this prevented ingress of high ethane concentration background air from the turbulent-recirculated atmosphere of the cold room into the flux chamber.

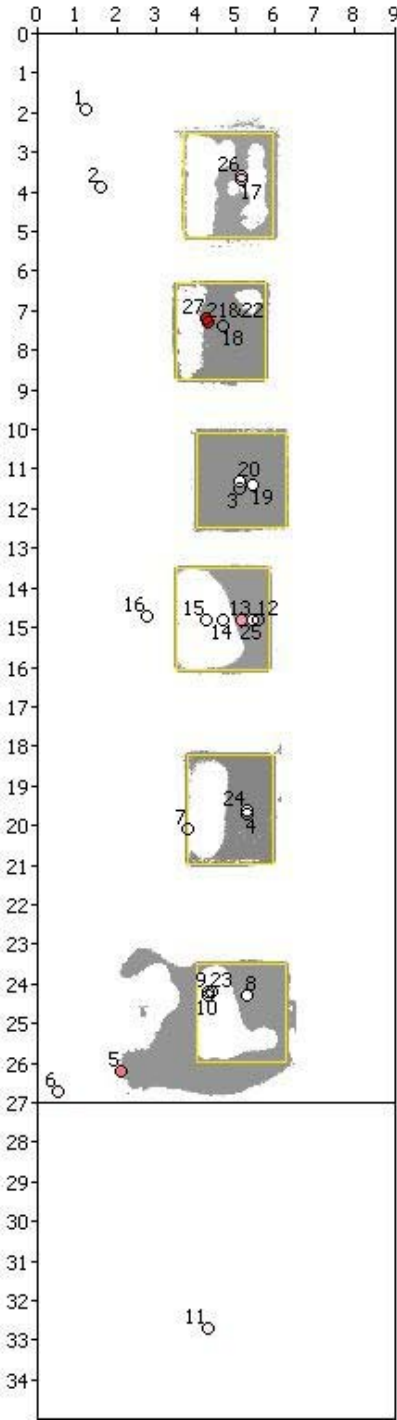


**Figure 6-3** Sketch of relative locations of the 27-flux chamber measurements superimposed on the spill areas. Strength of red is proportional to equilibrium ethane concentration. Refer to test maps in Figure 4-1 and Appendix D for exact locations oil areas digitised to scale.

Figure 6-4 shows the flux chamber in place over a trapped oil spill 15 cm (6 in) below the surface of the ice. The ethane-free N<sub>2</sub> carrier gas input is on the right of the chamber, via a hoop of perforated PTFE hose. The sample gas is collected from the left side via a similar hose. The rim/ice contact is sealed with snow to prevent ingress of background ethane contaminated air; the air in the test room was quite blustery when the test room fans were on. This measurement was repeated as a consistency test, yielding very similar values after a much prolonged equilibration period. Flux chamber measurement location 26a (photo subject) yielded an equilibrium concentration of 0.71ppb with a standard deviation of  $\pm 130$  ppt. Following Figures 6-5 and 6-6 show the stabilization of the measurement with time and subsequent stability during the sampling phase.



**Figure 6-4** Flux chamber measurement No. 26a over encapsulated oil spill, 15 cm (6 in) below the ice top surface. The flux chamber is positioned directly above a discoloured portion of the ice, above oil trapped in the ice but with no evidence of free oil on the surface.

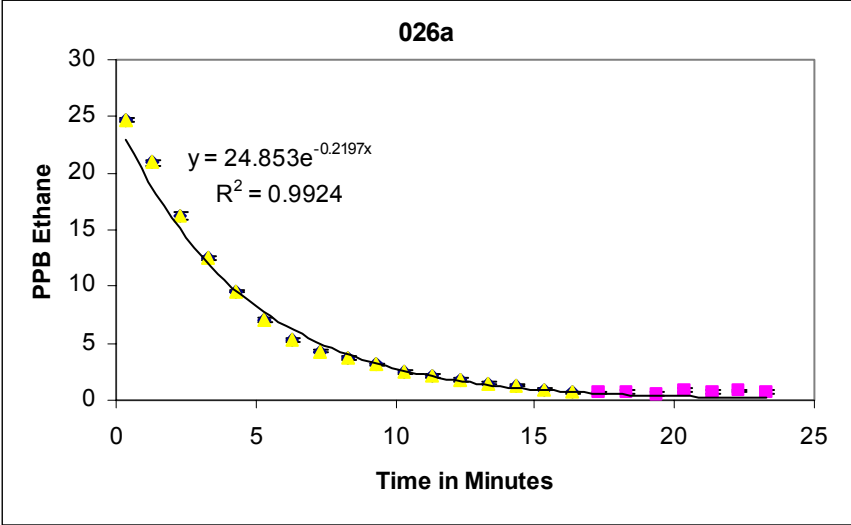


**Figure 6-5** Asymptotic approach of the flux chamber ethane gas concentration (ppb) to its equilibrium value for measurement position 26. The background room concentration was >25 ppb at the commencement of the measurement. Once at equilibrium concentration, the ethane influx through the base area of the flux chamber is equal to the rate of removal by the carrier gas flow.

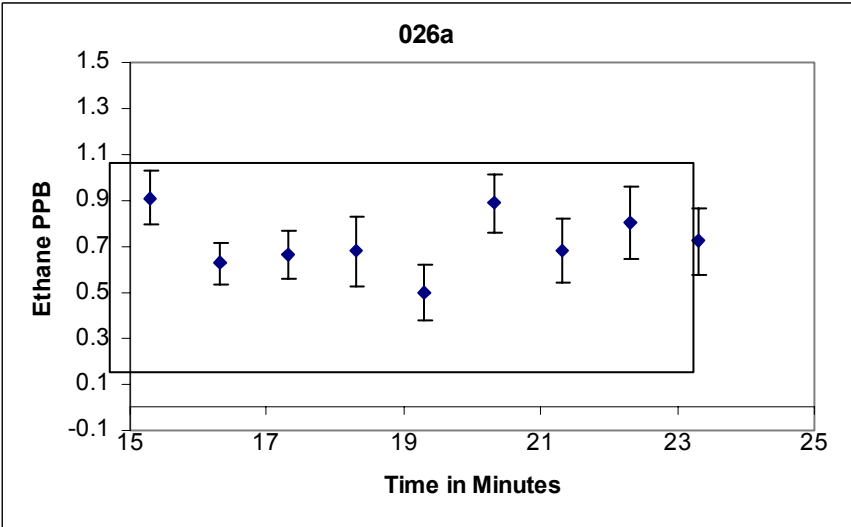


**Figure 6-6** Last 7 minutes of position 26a concentration data (ppb), stable to well within the standard deviation (SD) of the results. The mean concentration here is 0.71 ppb with SD of 130 ppt.

### 6.3 Ethane Flux Results and Discussion

The equilibrium ethane concentration is linked to surface ethane mass flux rate by the equation:

$$(\text{Mass Flux}) \times (\text{Area}) = (\text{density}) \times (\text{carrier gas volume flow rate}) \times (\text{Concentration by Vol.})$$

This report presents measured flux values or upper limits of flux for the different ice thickness and spill types. Flux values are also presented for ice that shows oil “weeping” to the surface (isolated spots of surfaced oil within the test skirts, principally in sites 1-1 and 1-2).

For measurement 26a (Figs. 6-5 and 6-6) the measured surface mass emission flux of ethane through the ice above the trapped oil layer was  $8.4 \times 10^{-13} \text{ kg/(s.m}^2\text{)}$  with a standard deviation of 18%.

For LightTouch™ exploration surveys over natural seepage sources, Shell normally quotes fluxes in  $\text{kg/(hr.km}^2\text{)}$  as a useful practical unit. One (1)  $\text{kg/(hr.km}^2\text{)}$  is regarded as a significant flux value, which is detectable from several kilometers distance (one mile or more) (for example from an aircraft). Using measurement 26a as an example, the corresponding flux is  $3.0 \times 10^{-3} \text{ kg/(hr.km}^2\text{)}$  with SD of 18%. This value is approximately three orders of magnitude lower than the fluxes normally detected in exploration surveys.

All of the flux results are tabulated in Appendix B, with the results grouped in relation to the spill locations shown in Figures 4-1 and 6-3. Dubious measurements are omitted where the flux chamber was inadequately sealed against ambient air ingress.

The flux data shows a consistent picture of higher fluxes closer to where oil is present. An exception of site 1-3, where the ice had been sealed with a skim coat of fresh ice. This was done to guard against a repeat of experiences with the first two spills. Although the top layer of the ice was scraped clean for flux measurements 19 and 20, it appears that the underlying ice in site 1-3 still remained less permeable.

Overall, the flux values for similar regions are consistent to within the standard deviations quoted. Background flux was not significantly different from zero at position 1 (the lowest reading obtained). A number of the supposed background measurement sites yielded flux values greater than zero (e.g., #2, 6 and 16). These values are however consistent with the ice core and water measurements made after the flux measurements. These indicated that some free oil (with associated gases) had migrated extensively within the tank.

## **6.4 Oil, Ice, Air and Water Sample Analysis**

A series of independent oil, ice core, water and air samples were collected in support of the ethane-sensing component of the project (the application of GPR technology is not affected directly by oil, ice, or water chemistry). Samples taken before, during and after the flux measurements include:

1. Fresh oil samples from each drum on delivery
2. Oil samples from core holes in each test area on November 19
3. Upper layer (top 25 cm) clean ice cores for trapped gas analysis, in two oiled sites and a control area of clean ice, November 24
4. Water samples from holes drilled in the melting ice cover on December 17

In addition, a series of air samples were collected during the course of the ethane flux measurements and at the time that the water samples were collected. All of these samples were subsequently analyzed for comparison with the ethane flux results (Sec. 6.2) and to determine any changes that might have occurred in the oil components during the testing period.

Figure 4-1 shows all sample locations. Data tables and interpretive notes are contained in Appendix D. Results are summarized below.

### **6.4.1 Oil Chemistry**

Pre-spill fresh oil samples were collected from the individual drums soon after arrival at CRREL. Spills took place on November 5, 8 and 15. Radar and ethane flux measurements were made between November 15 and 18. At the time of collecting the post-test oil samples, the oil had resided in or under the ice for between 4 and 14 days (Table 4-1).

Table 3 in Appendix D contains the analytical light gas headspace data for the saturated vapors in the South Louisiana Crude Oil samples, as initially received before injection under the ice and after the oils were recovered from under the ice after the field testing. As shown by the analytical data, the headspace ethane concentrations in the original oil samples are significant and uniform, ranging from 4000 to 5000 ppmv in the saturated vapor headspace in contact with the six oils. These concentrations are in the upper quartile when compared with examples of other oils (Table 2-1), indicating that South Louisiana Crude Oil was an excellent choice for this study.

As expected, the oil in the ice lost only a small quantity of its light and C<sub>5+</sub> gasoline range gases after injection and residence under the ice for four days. Methane is down about 40% and ethane, propane and butanes are down about 60% after their recovery from underneath the ice. The C<sub>5+</sub> gasoline range components appear to be

lower by less than 20% from their original values. This data shows that, in spite of their exposure and handling, these oils still contained significant levels of light C<sub>1</sub> – C<sub>4</sub> and C<sub>5+</sub> hydrocarbons when they were removed from underneath the ice.

#### **6.4.2 Ice Core Samples**

The pattern of oil spreading under the ice revealed by underwater backlighting indicates that a substantial portion of the oil escaped through (or was initially spilled outside) the skirt in spill 2-3 and a much smaller portion in spill 2-2 (Fig. 4-8 and App. C).

In order to determine whether the escaped oil might have impacted the ice sheet outside of the skirts, several ice cores were taken within the upper portion (top 25 cm of the ice sheet), following the test program. Three locations (GC-1, GC-2, and GC-3) were selected for these supplementary ice cores (Fig. 4-1 & test map App.D). One was a background core (GC-1) where six core segments were collected from the upper 25 cm (10 in) of the ice sheet. The other two locations (GC-2 and GC-3) were placed directly over areas where the injected oil was visible under the ice sheet.

The ice core samples were collected on Nov 24, and kept frozen until transported to ETI's lab for analysis of light C<sub>1</sub> – C<sub>4</sub> and C<sub>5+</sub> hydrocarbons. Detection limits for this data are in the 5 to 10 ppbv (0.005 to 0.010 ppmv) range, and each ice core samples was run in triplicate in order to define the variance between samples. The analytical data from the melted core segments is contained in Table 2 in Appendix D with further explanatory notes.

The results are interesting in that measurable hydrocarbon (h.c.) concentrations were observed within all of the ice cores, including the so-called background area (GC-1), located in visibly clean ice more than 3.5 m (11.5 ft) from the nearest oil spill area (1-1). Even more striking than the presence of light hydrocarbons, is the vertical hydrocarbon concentration gradient in the upper ice layer in all three areas, including GC-1 ("background"). As expected, the concentrations of light gases within the ice cores are greatest within the two areas that overlie the encapsulated oils. Although the background area is less impacted than the oil spill areas, it is significant that all three areas (including the "control" core in visibly clean ice) were clearly impacted by the presence of the oil.

This ice core data demonstrates a vertical hydrocarbon gradient in the ice from the surface towards the bottom, and suggests that perhaps either the air or the underlying water might have provided an avenue for migration of these light gas oil components to these ice core locations.

Four air samples and six water samples were collected from the ice/water interface on December 17 to evaluate any relationship that might exist between the air and underlying water. These air and water samples are discussed in the following sections.

The light gases in the underlying oil were sufficiently mobile to spread over the entire tank area. Given additional vertical pathways such as natural cracks and fractures, it appears likely that in a real spill, these dissolved oil components would reach the surface with much higher flux levels, compared to values measured in this project with a completely solid ice sheet.

### **6.4.3 Water Samples**

Water samples collected from holes drilled in the melting ice sheet on December 17 were analyzed for their light C<sub>1</sub> – C<sub>4</sub> hydrocarbons. The water sample analysis and ambient air data is shown in Table 4 in Appendix D.

With the exception of one invalid leaking sample, the remaining water samples contained large headspace concentrations. Laboratory detection limits for these samples is ~30 ppb.

As shown by Table 4 (in App. D), the water samples have very large, nearly uniform magnitudes of light h.c. gases that have to be derived from the spilled oils. For example, ethane and propane concentrations range upwards to 35,692 ppb and 79,819 ppb, respectively. The regional distributions of these water samples would imply that all of the water in the ice tank has been similarly impacted. The high concentrations of light gases found in these water samples conforms the presence of a sub-ice oil source that appears to underlie the entire ice sheet. This would explain the wide-ranging impact and the vertical distribution of oil contamination found in the ice cores (7.2.1).

Further analysis of the water samples for their C<sub>5+</sub> gasoline range hydrocarbons produced component signatures in the headspace waters that were very similar to the whole oil sample analysis (as opposed to dissolved phase). The fact that the water samples are dominated by the less degradable and less soluble gasoline range components implies that the source of the h.c. vapors in these water samples are probably very small droplets of free oil that has migrated to the locations where the water samples were collected.

In this project, the light gases derived from the spilled oil, impacted the surface water (immediately sub-ice) over the entire tank. On this basis, the oiled under ice water area would be much larger in a real arctic spill. Significant vertical gas concentration gradients were established in the ice core samples in only two weeks (previous discussion). Therefore, it appears probable that ethane would escape to the surface within a short time under natural conditions. This would provide a suitably broad target area for remote detection.

#### **6.4.4 Air Samples**

When using an instrument, such as the Shell LightTouch™ system that measures only one component, it is important to be able to confirm this single component (ethane) by an independent method, such as gas chromatography. In addition to confirmation of the Shell LightTouch™ system results, the collection of ambient air bottle samples also provided backup should the real-time Shell LightTouch™ system fail during the testing phase. In addition to ethane confirmation, the GC method also allowed for the detection of other oil-related light hydrocarbon gases, such as propane and butanes.

A series of seven air samples were collected during the first two days of field-testing for analysis by conventional GC technologies. Although only limited data is available for comparison, in all cases excellent agreement was obtained between Shell and ETI's ambient air data. For example, the initial laboratory air sample collected adjacent to Shell's instrument was 29 ppbv (Shell's system at the same time reporting 30 ppbv) and dropped to 17 ppbv on the second day (Shell reporting 10 ppbv). The initial ethane concentration reported by Shell in the ice-testing chamber was 100 ppb (ETI measured 115 ppb). This concentration dropped to 70 ppb on the second day (ETI measured 67 ppb).

Ambient air samples collected after field-testing were also analyzed for light C<sub>1</sub> – C<sub>4</sub> hydrocarbons. Results showed that the ambient air in the chamber had become considerably more contaminated (particularly by propane and butanes) during the collection of the ice core and water samples. However, the gas concentrations in these samples are not nearly large enough to represent a credible source for the light gas concentrations found in the upper ice layers. In addition, the consistent vertical h.c. concentration gradients in the ice cores are inconsistent with air contamination, and can only be explained by a sub-ice oil source (Section 6.4.2).

## **7.0 FUTURE DEVELOPMENT**

The next logical step, given the very promising results in the CRREL tank tests, would be to explore the potential for field tests under natural conditions. The ultimate long-term goal is to develop reliable ground-based and airborne surveillance systems that could be deployed to check for the presence of oil trapped in ice under a variety of scenarios. This project focused on proof of concept, with ground-based technologies being used as the first step in the overall development process. Recommendations are put forward in the following sections to further develop the technologies proven at CRREL, with the goal of deploying the next generation of systems in a larger scale field experiment and collecting additional field measurements of ethane levels over natural sea ice, required to evaluate the future potential of geochemical methods.

### **7.1 Radar Potential**

In the analysis of data acquired in the CRREL test basin, anomalies were found in GPR amplitude, spectrum, and phase that closely tracked the known distribution of oil under ice. Based on the clarity of the results discussed here, GPR is considered to have significant potential for detecting oil in and under sea ice. The following priority issues are selected for further testing and evaluation (see program outline in Sec. 7.3).

1. One of the more important requirements will be ensuring that high frequency radar ( $> 450$  MHz) can penetrate the range of thickness encountered in naturally occurring first-year sea ice (up to 2m (6.6 ft) in level ice, 4 m+ (13 ft+) in rubble ice). In the CRREL tests, radar frequencies up to 1200 MHz penetrated close to 1 m of rough urea ice. Without entrained liquid brine, frequencies in the range of 450 - 1200 MHz should easily image through  $\geq 2$  m (6.6 ft) of sea ice.
2. A second issue involves resolving the polarization effects due to sea ice anisotropy and irregularities in the ice/water interface in natural sea ice. Presently, the hardware is available to efficiently acquire multidirectional GPR data. Gathering this type of data will account for polarization effects, thereby minimizing the potential for false positives or missed detections. Additionally, multi-polarization acquisition has the added benefit of measuring the direction of sea ice anisotropy, which may prove valuable in characterizing future sea ice environments. Depending on the clarity of the ice/water reflection in real sea ice, it may be possible to automate the data analysis, which would enable real-time interpretation and open the use of the technology to a greater number of field users. Implementing this analysis methodology will require a moderate level of software development.

3. Since it is clear that multiple reflection attributes, such as the amplitude and spectrum, and mapped sea ice thickness profiles are potential indicators of oil presence, there may be significant added benefit in developing combined attributes. Combining multiple attributes has the potential to make the analysis more robust. For example, based on the results of this experiment measuring coherence between ice depth and high reflection amplitude clearly has potential to eliminate some false positives.
4. In principal, it should be no more difficult to detect amplitude or other attribute anomalies from an airborne platform, and the results of this experiment do not rule out the potential for oil detection with an airborne GPR system. However, a more extensive spill is required to test this effectively. Preliminary modeling indicates that minimum spill areas of 10 m x 10 m (33 ft x 33 ft), 18 m x 18 m (59 ft x 59 ft), and 23 m x 23 m (75 ft x 75 ft) would be required for airborne tests at elevations of 10 m, 30 m and 50 m (33 ft, 100 ft, and 164 ft) respectively. The important issue of minimum spill size will be considered in planning any future field tests (Sec. 7.3).
5. Finally, some additional effort is necessary to test the latest generation of available GPR systems under Arctic conditions. Both older systems tested at CRREL in 2004 suffered from a variety of electronics and battery failures at the relatively mild zero °F temperature of those experiments. The manufacturer claims a system rating to -40°F. Additional work is needed to evaluate the consistency of this claim and answer the question as to whether the electronics malfunctions experienced in NH were unique to the particular systems employed in that project. If problems persist in this next phase, additional engineering may be required to develop radar systems that will perform consistently under Arctic climatic conditions.

Additional questions related to field implementation of the GPR methodology include:

- Limiting ice thickness: The thinnest ice in which GPR can be effective is limited by the resolution of the signal. At 1 GHZ, the expected limit is ~ 10 – 15 cm. The thick ice limit is more difficult to define, and requires additional study of real sea ice. Based on the results presented here, investigations of ice at > 2m are reasonable.
- Effect of rafted ice: Rafted ice will introduce stratigraphic complexity into the ice pack. However, internal boundaries caused by this scenario will likely be substantially lower than the contrasts at the ice/oil/water interface and identifying oil trapped below the ice pack will not be significantly impacted. Since the effect is subtler, the identification of intra-ice oil films will be complicated by rafted ice, and not likely possible in all conditions. This complicated problem depends on ice and oil permittivity and the thickness of the oil layer, so the interpretation will be case dependent

- Oil dispersed through the ice sheet (i.e. late winter conditions): The attribute analysis methods presented here are effective when there is a well-defined oil film, either beneath or within the ice. Vertically dispersed oil will alter the electric permittivity structure of the ice pack, and therefore likely alter the reflection amplitudes at the air/ice interface (for an airborne system), and at the ice/water interface. Therefore, it is possible that radar can be used to identify dispersed oil as well.
- Oil film thickness: Based on the results of this experiment, it appears that it is possible to identify oil films, in and under ice, as thin as ~ 1 cm. This lower limit is given with the caveat that it is difficult to directly correlate oil film thickness measured in the cores with the GPR data due to the irregular ice thickness, and the difficulties in measuring film thickness beneath the ice.

## **7.2 Ethane Sensing Potential**

The results obtained with Shell's LightTouch™ ethane gas sensor at CRREL show measurable, but very low, levels of ethane flux being transmitted through the ice sheet within the last four oiled areas within two days of spilling. Although the ethane flux from oil trapped under these artificial, test-tank conditions was extremely small, the ice coring data demonstrated that the oil and light gases, such as ethane, had penetrated nearly to the surface of the ice after 14 days: the time elapsed between the initial two spills and flux measurements. Given longer migration times and natural conditions, where tectonic forces would provide additional migration pathways through the ice, it appears feasible that airborne detection systems could detect ethane associated with a real oil spill. It is not known at this stage whether ethane flux levels over a trapped spill in natural sea ice would reach levels sufficient to support an airborne survey: namely ~1kg/(hr.km<sup>2</sup>).

Remaining questions and issues include:

1. Whether the pathways for gas migration through natural sea ice will be sufficient to generate substantial surface flux values, potentially enabling some form of airborne sensing system as the ultimate goal. At this stage, it is thought that the pattern of micro cracks and fractures in real ice, related to forces of wind stress, and tidal variations, will provide greatly enhanced opportunities for ethane to migrate to the surface from a trapped oil layer.
2. Whether the flux values would have remained the same if the tests had taken place a week or a month later. As demonstrated by the analysis of the trapped hydrocarbon gases within the cores, there is likely a critical time for light ends to migrate through a given thickness of ice, which is possibly also affected by internal ice temperature and the related percentage of liquid brine. The presence of measurable light and gasoline range gases within every ice core and water sample analyzed suggests that the hydrocarbons were moving upward through the ice sheet and would likely have reached the ice surface given more time.

Aided by the presence of natural discontinuities in sea ice, it appears likely that ethane and other gases from a real spill would eventually vent into the atmosphere, where they could be measured by an airborne instrument.

3. Understanding the mechanisms for lateral oil spreading in the water column outside of test skirts. Hydrocarbon gases and free oil migrated from the oil pools under the ice via mechanisms that remain undefined. The ice core and water signatures of the migrated hydrocarbons suggest whole oil migration, rather than solubility and/or diffusion. There could also be some form of low-rate convective stirring of the water within the tank due to slight temperature gradients. This phenomenon would influence future detection limits for an accidental spill, as it appears that even clean ice outside the actual spill boundaries can contain significant levels of trapped ethane.

Even without being able to deploy an airborne system at this stage, further ground-based options could prove useful, especially compared with the present state of the art requiring hundreds of labor-intensive drill holes. For example, a centrally located LightTouch system in a controlled environment could rapidly process large numbers of bagged air samples collected by field personnel in sensitive areas (e.g. along a pipeline route). It may also be possible to detect meaningful ethane flux levels through conventional GC analytical methods, once sufficient time has elapsed after the spill, or with added pathways for gas migration in natural sea ice. In this regard, the continuous "perfect" ice sheet at CRREL was very much a worst-case in terms of impeding gas migration to the surface. The Shell team considers that the LightTouch™ technology stands a good chance of detecting through-the-ice flux from trapped oil spills in a field environment.

### **7.3 Alternative Technologies: Seismic Methods**

Seismic reflection methods showed promise in past imaging through sea ice (e.g., Jones and Kwan, 1984; Jones et al., 1986). The primary challenge in acquisition comes from the need to couple the source and receiver to the ice surface. Once achieved, seismic frequencies upwards of 200 kHz that produce cm-scale wavelengths have been documented to penetrate sea ice (e.g., Jones et al., 1986). Although these earlier studies concluded that simple reflection methods to identify amplitude anomalies due to the presence of oil under sea ice was not possible, improvements in acquisition and processing technologies prompted a reconsideration of the potential use of seismic methods to address this problem. Appendix F reviews the physical properties of each material involved and includes results of modeling the response of the presence of oil under sea ice under various conditions. The modeled results show that seismic methods can identify the presence of oil under sea ice. Although the amplitude effects diminish when oil thickness or oil densities decrease, increased dynamic range of new acquisition systems coupled with advanced processing routines to address thin bed problems should provide adequate resolution to distinguish the presence of oil under ice when compared to an ice/water interface. The challenge to the use of seismic methods in the future hinges on solving the challenge of efficiently and quickly coupling the seismic source and receivers to the ice surface.

## **7.4 Recommended Research and Development**

The findings from this project are extremely promising. Positive oil-in-ice detection was achieved by both the ground penetrating radar (GPR) and the ethane sensor.

The results reported here justify further research into systems and procedures to detect oil ice through both radar anomalies and ethane sensing. In order to build on the success achieved in the current project, the following near-term (four month time span) tasks are recommended as a means of further developing and proving GPR as the technology area that shows the most potential in being developed in to an airborne off-the-shelf system in the near future (next two years).

The means to achieve the immediate goal focus on two key areas: (1) increasing the level of confidence in reliability by using the system in an Arctic sea ice environment with variable sea ice thickness and roughness, and cold temperatures; and (2) developing the necessary software to automatically interpret the radar response, given known parameters (e.g., ice properties and temperatures) and oil-in-ice configurations associated with different Arctic spill scenarios.

Although the existing ultra-sensitive ethane detection system is relatively heavy and bulky for Arctic field applications, future developments will no doubt lead to the development of units that are more portable as well as operational airborne systems. The option of using a central LightTouch system to process intra-field samples could be an attractive alternative to winter ice drilling. These possibilities deserve further longer-term evaluation as to their economic and technical feasibility. The key uncertainty remaining is the likely ethane flux over a real oil spill under ice; this will determine the feasibility of routine remote detection by the LightTouch method.

The development activities outlined below will lead to a more reliable and easier-to-use GPR system for possible field tests with oil during the winter of 2005/06. The objective of these tests would be to test the radar over natural sea ice in both surface and airborne modes, over much larger oiled areas than are possible in a cold basin. At the same time, large-scale field trials would provide an ideal opportunity to obtain representative ethane flux values in a realistic natural setting. This data will support a more reliable assessment of the prospects for an operational airborne ethane sensor system.

The following recommended follow-on work items were funded by MMS on March 1, 2005 (PO Number 0105PO39137):

1. Hardware evaluation and configuration for multi-polarization data acquisition
2. Field testing over a variety of sea ice conditions at Prudhoe (April 2005)
3. Software development aimed at real-time or close to real-time data analysis
4. Preliminary planning for a full field test with oil, winter 2005/06

## REFERENCES

- Best, H., McNamara, J., and L. Liberty. 2004. Detecting Relationships between Ice and Hydraulic Geometry in an Arctic River Using Ground Penetrating Radar - *Journal of Arctic, Antarctic, and Alpine Research*.
- Bradford, J.H. 2004. 3D Multi-offset, Multi-polarization Acquisition and Processing of GPR data: A Controlled DNAPL Spill Experiment. SAGEEP 2004 Proceedings, Symp. Appl. Geophys. Env. Eng. Prblm: Colorado Springs, CO, Env. Eng. Geophys. Soc.
- Bradford, J.H., McNamara, J.P., Bowden, W., and M. Gooseff. *in press*. Measuring Thaw Depth Beneath Peat-Lined Arctic Streams Using Ground Penetrating Radar, *Hydrological Processes*.
- Buist, I.A., Potter S.G., and D.F. Dickins. 1983. Fate and Behaviour of Water-in-Oil Emulsions in Ice. Proc. 6<sup>th</sup> Arctic Marine Oilspill Program Technical Seminar, Environment Canada, Ottawa, ON.
- Butt K., O'Reilly, P. and E. Reimer. 1981. A Field Evaluation of Impulse Radar for Detecting Oil in and Under Sea Ice. C-CORE, St. John's, 1981 (Appendix K to Vol II of the Oil and Gas Under Sea Ice Experiment, Dickins and Buist (1981), APOA Contract Report 169, Calgary, AB.
- C-CORE. 1980. An Oilspill in Pack Ice - Chapter 8: Remote Sensing of Bunker C in Dynamic Pack Ice. C-CORE Contract Report C80-2, St. John's, NF.
- Cox, J.C. and L.A. Schultz. 1980. The Transport and Behaviour of Oil Spilled Under Ice. Proc. 3<sup>rd</sup> Arctic Marine Oilspill Program Technical Seminar, Environment Canada, Ottawa, ON, pp. 45-61.
- DF Dickins Associates Ltd. and Fleet Technology Limited. 1992. Behaviour of Spilled Oil at Sea (BOSS): Oil-in-Ice Fate and Behaviour. Draft report submitted to Environment Canada, Ottawa, ON.
- Dickins, D.F. 2004. Advancing Oil Spill Response in Ice Covered Waters. report prepared by DF Dickins Associates Ltd. for the Prince William Sound Oil Spill Recovery Institute (OSRI), Cordova, AK (published in conjunction with the US Arctic Research Commission, Washington, DC).
- Dickins, D.F. October 2000. Detection and Tracking of Oil Under Ice. Final report submitted by DF Dickins Associates Ltd. to Minerals Management Service, Herndon VA.
- Dickins, D.F. and I.A. Buist. 1981. Oil and Gas Under Sea Ice Study. COOSRA Report CV-1 (Vols. 1 and II), prepared by Dome Petroleum Limited, Calgary, AB.

- Dickins D.F., Vaudrey K. and S. Potter. 2000. Oil Spills in Ice Discussion Paper: A Review of Spill Response, Ice Conditions, Oil Behavior and Monitoring, prepared by DF Dickins Associates Ltd., Vaudrey & Associates Inc., and SL Ross Environmental Research Limited for Alaska Clean Seas, Prudhoe Bay, AK.
- Fingas, M.F., and C.E. Brown. 2000. The Detection of Oil in and Under Ice. Proc. International Oil & Ice Workshop 2000, Anchorage, AK.
- Finkelstein, M. I. 1990. The development of geophysical subsurface radar in the USSR and its practical uses: Proc. Third International Conference on Ground Penetrating Radar, U.S. Geological Survey Open File Report #OF90-0414.
- Gibson, G., Monk, S.D., and M. Padgett. 2002. A Field-portable Laser-diode Spectrometer for the Ultra-sensitive Detection of Hydrocarbon Gases, *J. Mod. Opt.* v. 49, pp. 769-776.
- Goodman, R., Jones, H., and M. Fingas. 1985. The Detection of Oil Under Ice Using Acoustics, Proc. Vol.2 of the Conference on Port and Ocean Engineering Under Arctic Conditions (POAC), Narssarsuaq, Greenland, pp. 903-916.
- Harper, J.T., and J.H. Bradford. 2003. Snow stratigraphy over a uniform depositional surface: Spatial variability and measurement tools, *Cold Regions Science and Technology*.
- Hirayama, K. 1983. Properties of the Urea-doped Ice in the CRREL Test Basin. CRREL Report 83-8, Hanover, NH.
- Hirst, B., Gibson, G., Gillespie, S., Archibald, I., Podlaha, O., Skeldon, K.D., Courtial, J., Monk, S., and M. Padgett. 2004. Oil and Gas Prospecting by Ultra-sensitive Optical Gas Detection with Inverse Gas Dispersion Modelling. *Geophys Res. Letters*, v. 31, pp. 112-115.
- James, A. T. 1990. Correlation of Reservoired Gases Using the Carbon Isotopic Compositions of Wet Gas Components. *AAPG Bulletin*, v. 74, pp. 1441 - 1458.
- Jones, H.W., and H.W. Kwan. 1982. The Detection of Oil Spills Under Arctic Ice by Ultrasound, Proc. 5<sup>th</sup> Annual Arctic Marine Oil Spill Program Technical Seminar, Environmental Protection Service, Ottawa, ON, pp. 391-411.
- Jones, H.W., Kwan, H.W., Hayman, T., and E.M. Yeatman. 1986. The Detection of Liquids and Viscoelastic Substances Trapped Under Solid Surfaces. *Journal of Acoustical Society of America*, v. 79(1), pp. 84-90.
- Jumikis, A. R. 1958. Some Concepts Pertaining to the Freezing Soil Systems. National Research Council Highway Research Board Special Report No. 40.

- Klenbusch, M.R. 1986. Measurement of Gaseous Emission Rates from Land Surfaces Using an Emission Isolation Flux Chamber, User's Guide. *EPA Contract No68-02-3889. EPS/600/8-86/008.*
- Kovacs, A., Morey, R.M., Cundy, D.F. and G. Decoff. 1981. Pooling of Oil Under Sea Ice. Proc. POAC 81: Sixth International Conference on Port and Ocean Engineering under Arctic Conditions, Quebec, PQ, pp. 912-922.
- Kovacs, A., and R.M. Morey. 1992, Estimating Sea Ice Thickness from Impulse Radar Sounding of Flight Time Data. Geological Survey of Canada Report # 90-04, pp. 117-124.
- Livingston, F.E., Smith, J.A.. and S.M. George. 2002. General Trends for Bulk Diffusion in Ice and Surface Diffusion in Ice. *J. Phys. Chem*, v. 106, pp. 6309-6318.
- Luzitano, R.D., and T.J. Ulrych. 1996. The Value of Two-Component GPR Data: Identifying the Polarization Contribution in Amplitude Anomalies. Proc. *SAGEEP 1996 Symposium on the Application of Geophysics to Environmental and Engineering Problems*, Environmental and Engineering Geophysical Society, Keystone, CO, pp. 1179-1187.
- Norcor Engineering and Research Ltd. 1975. The Interaction of Crude Oil with Arctic Sea Ice. Beaufort Sea Technical Report No. 27 , Dept. of Environment, Victoria, BC.
- Nyland, D., 2004. Profiles of Floating Ice in Arctic regions Using GPR: *The Leading Edge*, v. 23, No. 7, pp. 665-668.
- Rudolph, J. 1995. The Tropospheric Distribution And Budget of Ethane, *Journal of Geophysical Research*, v. 100, pp. 11369-11381.
- S.L. Ross Environmental Research Limited and DF Dickins Associates Ltd. 1987. Field Research Spills to Investigate the Physical and Chemical Fate of Oil in Pack Ice. Environmental Studies Revolving Funds Report No. 062, Ottawa, ON, 118 p.
- Tatinclaux, J.C. 1992. Tests in Ice on an Antarctic Research Vessel Model. CRREL Report No: SR 92-03, U.S. Army Cold Regions Research and Engineering Laboratory, Hanover, NH.
- Timco, G.W. 1985. Flexural Strength and Fracture Toughness of Urea Model Ice. 4th Proc. International Offshore Mechanics and Arctic Engineering Symposium, Dallas, Texas, TX, Vol.2, p.199-208.

- Todoeschuck, J.P., and R. I. Verral. 1990, Radar Ice Thickness Measurements in the Lincoln Sea: Third International Conference on Ground Penetrating Radar, U.S. Geological Survey Open File Report #OF90-0414, p.65.
- Verrall, R.I., and J.P. Todoeschuck. 1990. Multiyear Landfast Sea Ice: Observations and Models. Third International Conference on Ground Penetrating Radar, U.S. Geological Survey Open File Report #OF90-0414, p. 71.
- Zufelt, J.E., and R. Ettema. 1996. Model Ice Properties, CRREL Report No: CR 96-01, U.S. Army Cold Regions Research and Engineering Laboratory, Hanover, NH.

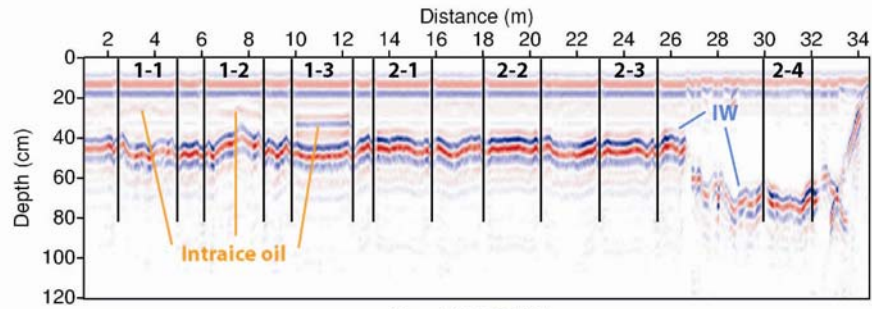
# **Appendix A**

## **Ground Penetrating Radar (GPR) Data**

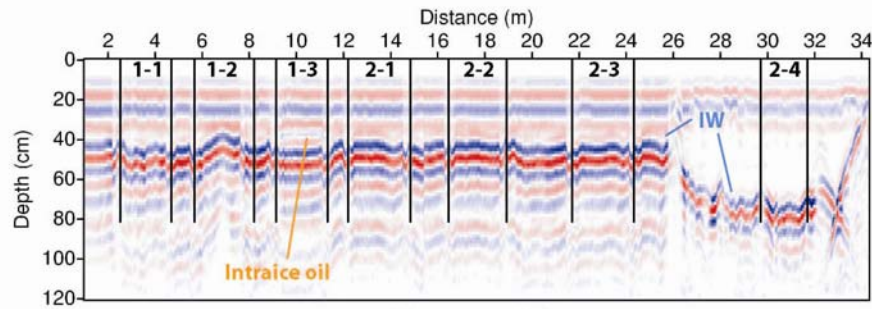
John Bradford & Lee Liberty

Boise State University

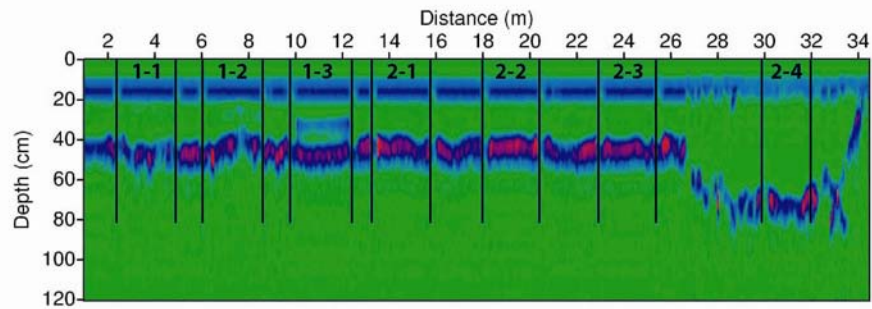
Center for Geophysical Investigation of the Shallow Subsurface (CGISS)



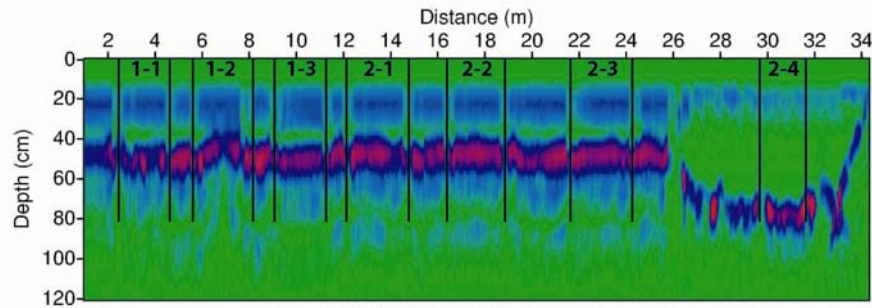
Line 13 900MHz



Line 13 450MHz

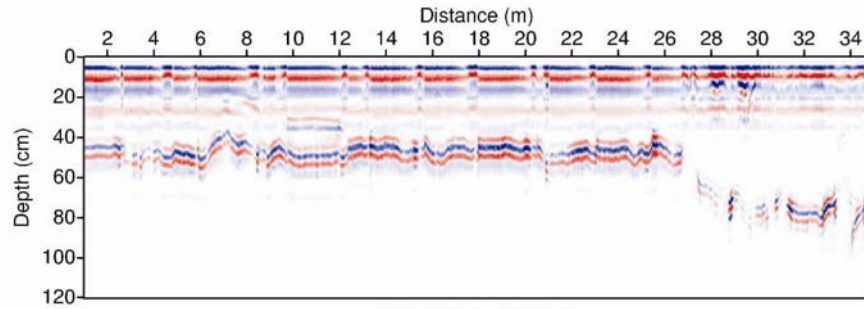


Line 13 900 MHz Reflection Strength

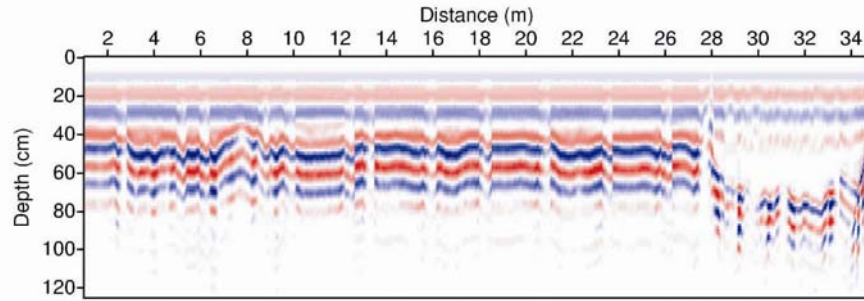


Line 13 450 MHz Reflection Strength

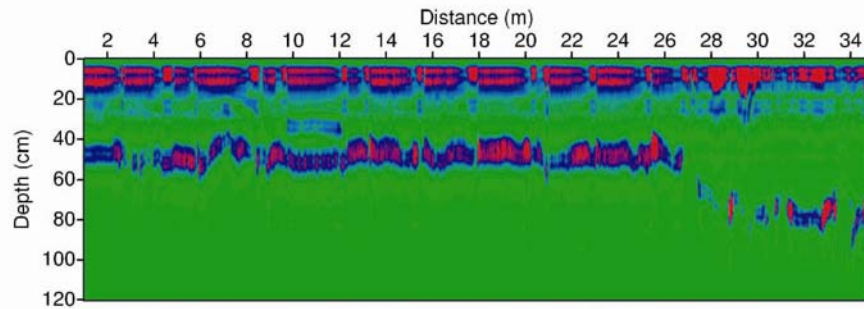
Figure 1. 2D profiles acquired along Line 13 with the Sensors and Software system with 450 and 900 MHz antennas. Oil induced amplitude anomalies are evident in the 900 MHz data, but not well defined in the 450 MHz data.



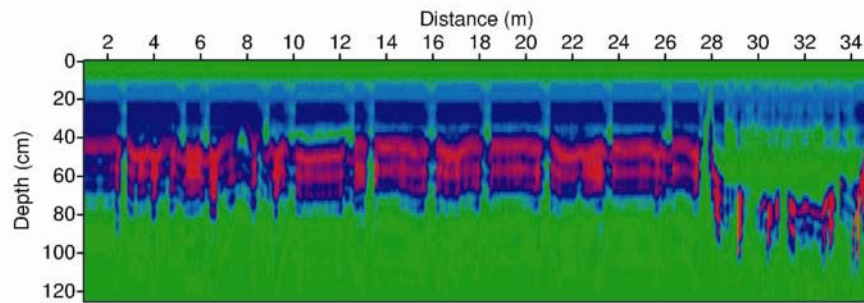
**Line 13 1000MHz**



**Line 13 500MHz**



**Line 13 1000 MHz Reflection Strength**



**Line 13 500 MHz Reflection Strength**

**Figure 2. Profiles acquired along Line 13 using the Mala Geosciences system with 500 and 1000 MHz antennas. Results are comparable to the Sensors and Software system with 450 and 900 MHz antennas. The narrow bandwidth at 500 MHz with this system results in a “ringy” appearance and poorer resolution.**

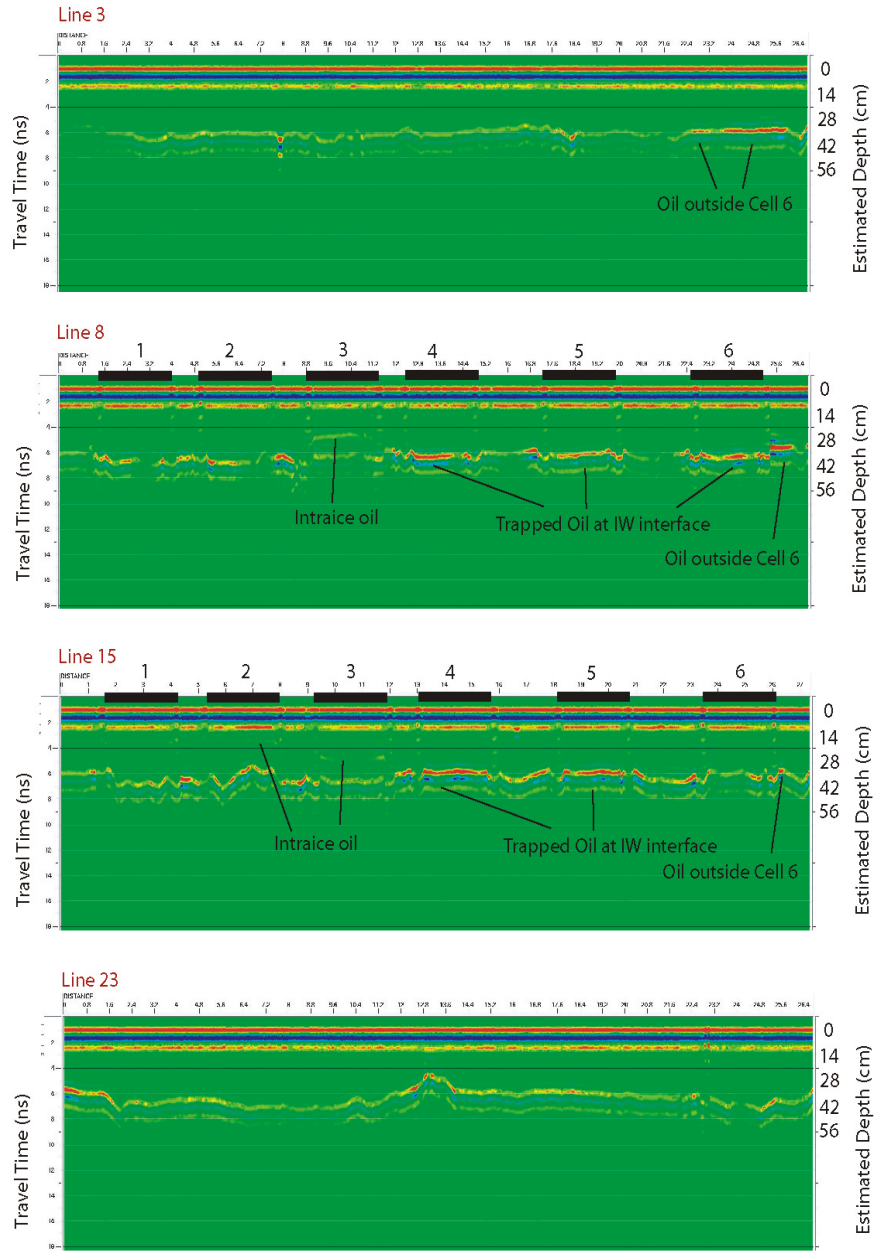


**Figure 3. Profiles taken from the 800 MHz 3D GPR survey. Lines 8 and 15 pass within the containment cells while Lines 3 and 23 lie outside the cells. Well-defined GPR amplitude anomalies are evident where oil is present under the ice. Further, intraice reflections are present in cells 2 and 3 where oil is trapped within the ice.**

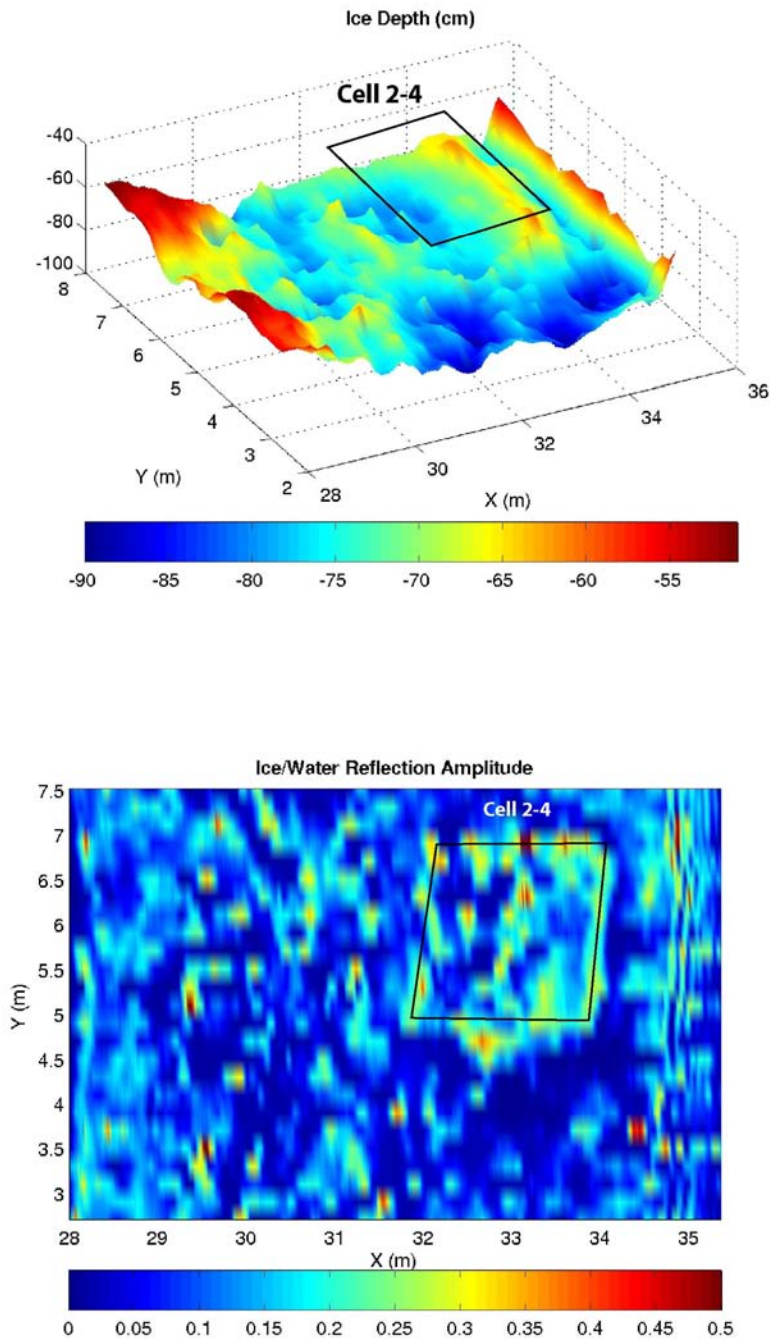


**Figure 4** Ice depth in the rough ice section mapped with the Mala 800 MHz 3D survey. There are systematic high amplitude anomalies that define the position of cell 2-4, particularly at the boundary. Underwater video identified that most of the oil had accumulated in the shallow ice section around the periphery as suggested by the radar amplitude image. However, we cannot definitively separate the amplitude effects due to oil from those caused by the containment skirt. However, given the strong response seen in the smooth ice section, there is likely a significant oil related contribution. There are many point like amplitude anomalies present that are likely related to 3D tuning and polarity effects.

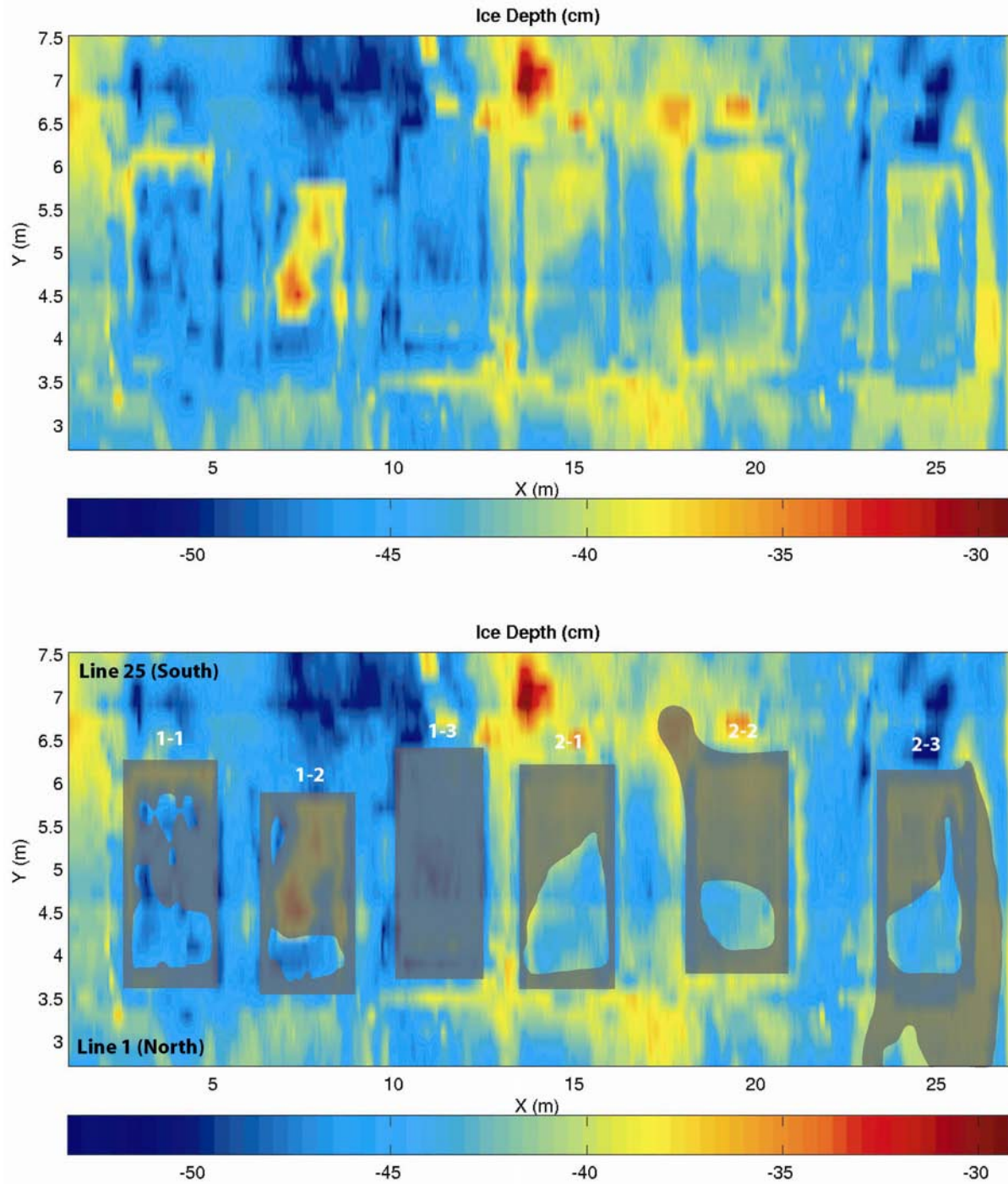


**Figure 5. Ice depth in the smooth ice section mapped with 800MHz 3D GPR. The oil distribution is overlain in the lower image. Note that the distribution of oil correlates very well with sections of relatively thin ice.**

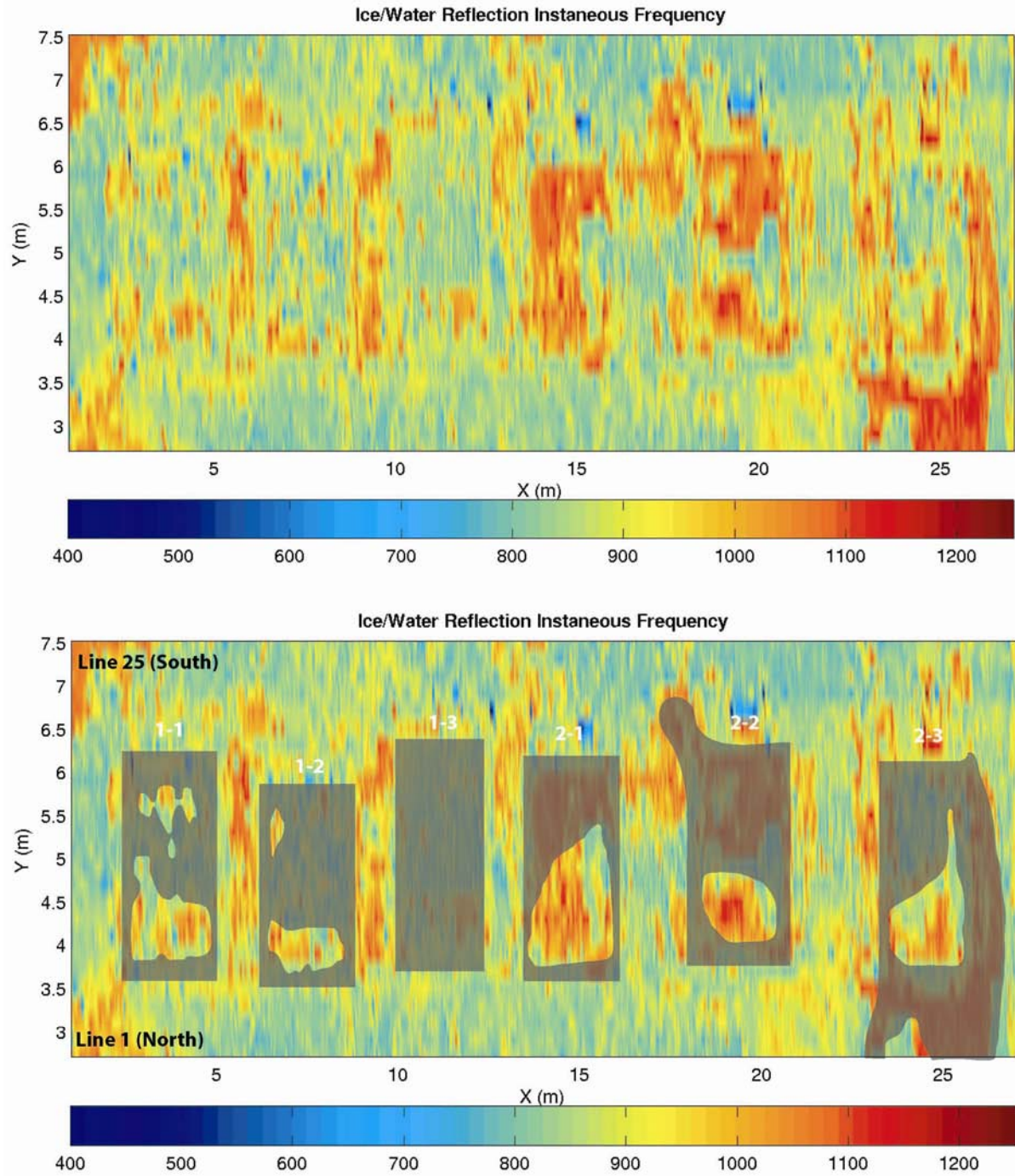


**Figure 6. Instantaneous frequency at the IW interface in the smooth ice section. Generally, high frequency anomalies correlate with the oil distribution. This is due to frequency dependent reflection or “tuning” caused by the thin film of oil. The signal is relatively noisy however, and not as robust as the amplitude attribute.**

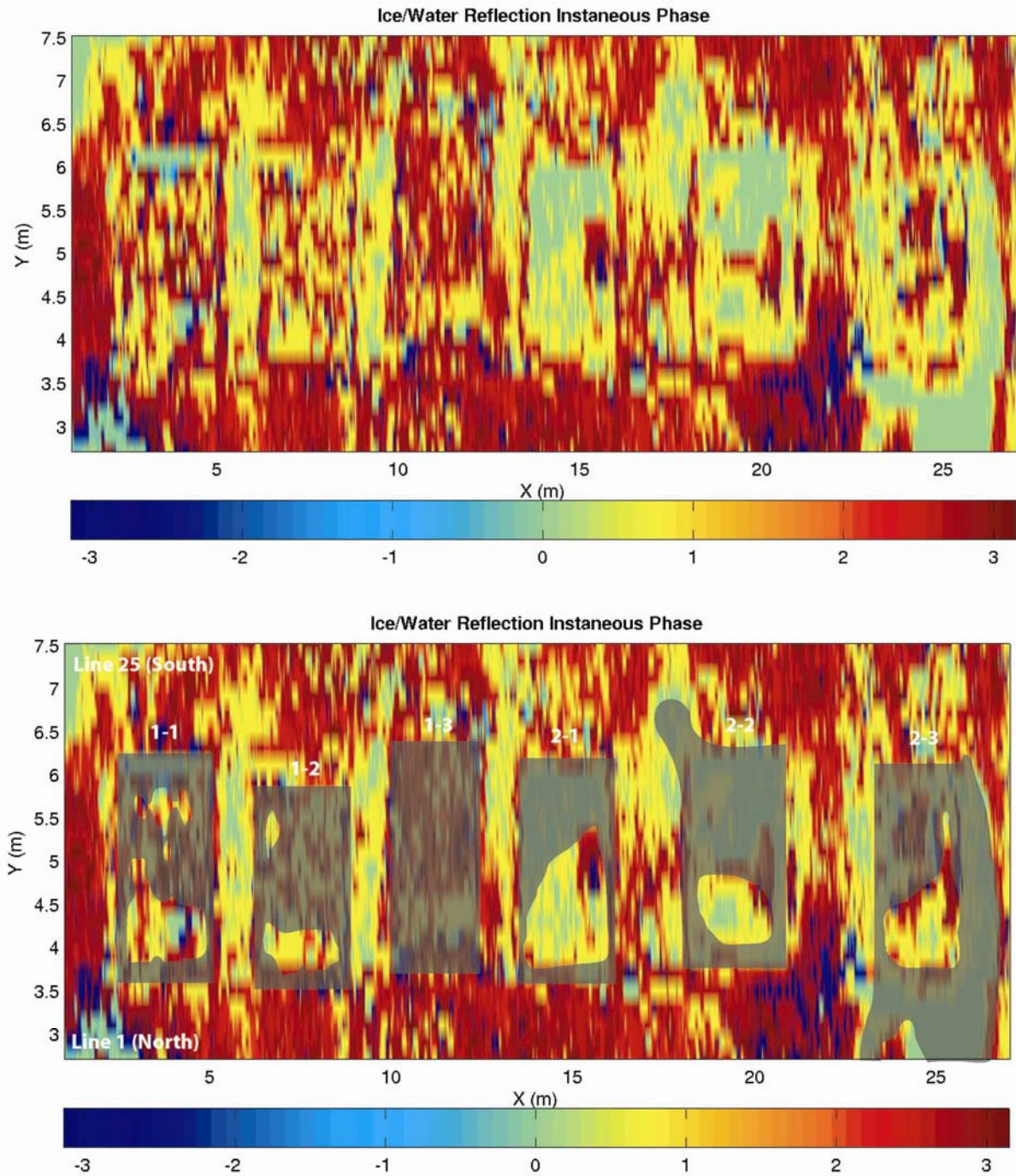


**Figure 7** Instantaneous phase at the IW interface with oil distribution overlain in the lower image. A significant anomaly correlates with the oil distribution. As with the frequency response this is a tuning effect caused by the presence of a thin film of oil.

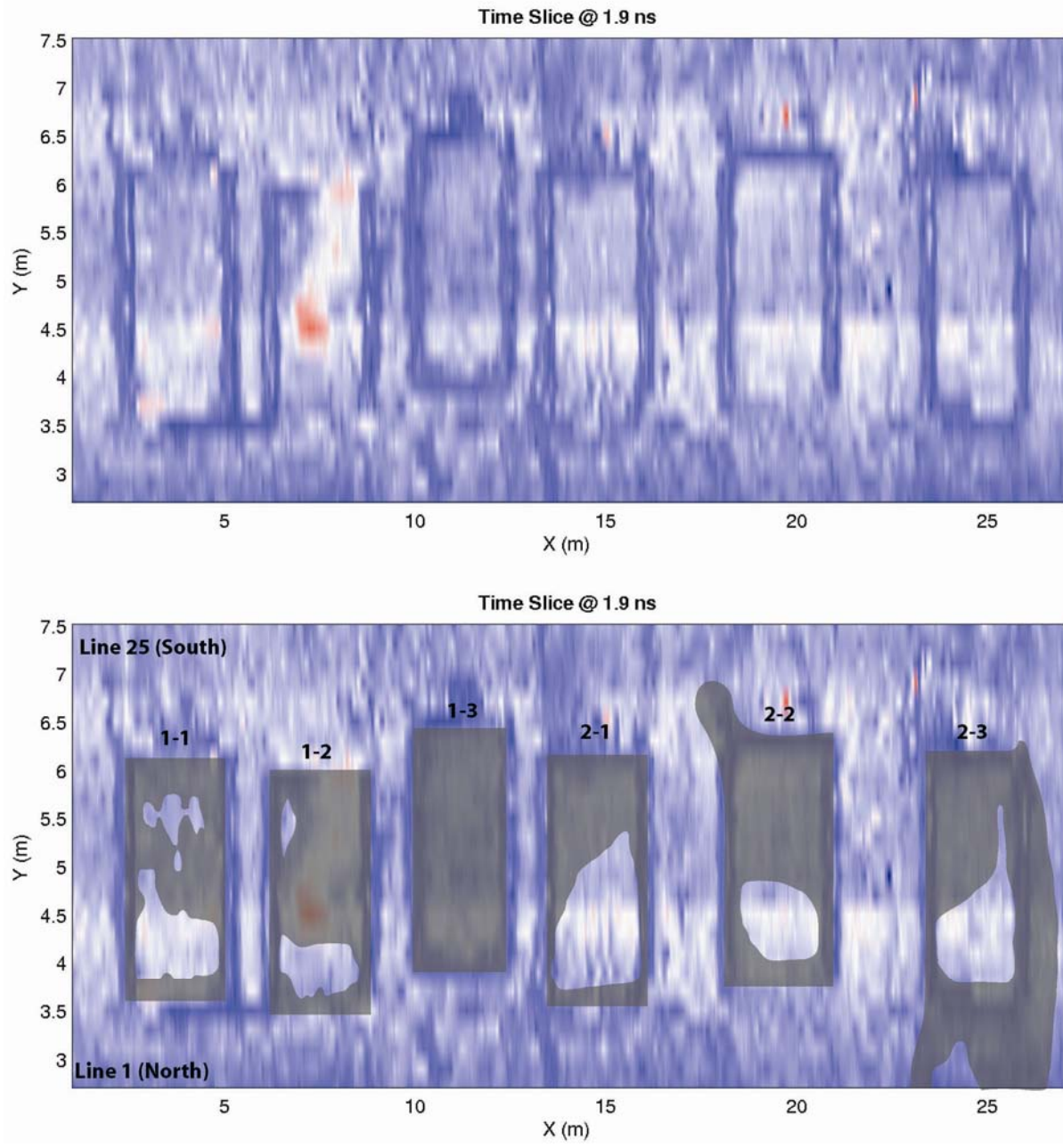
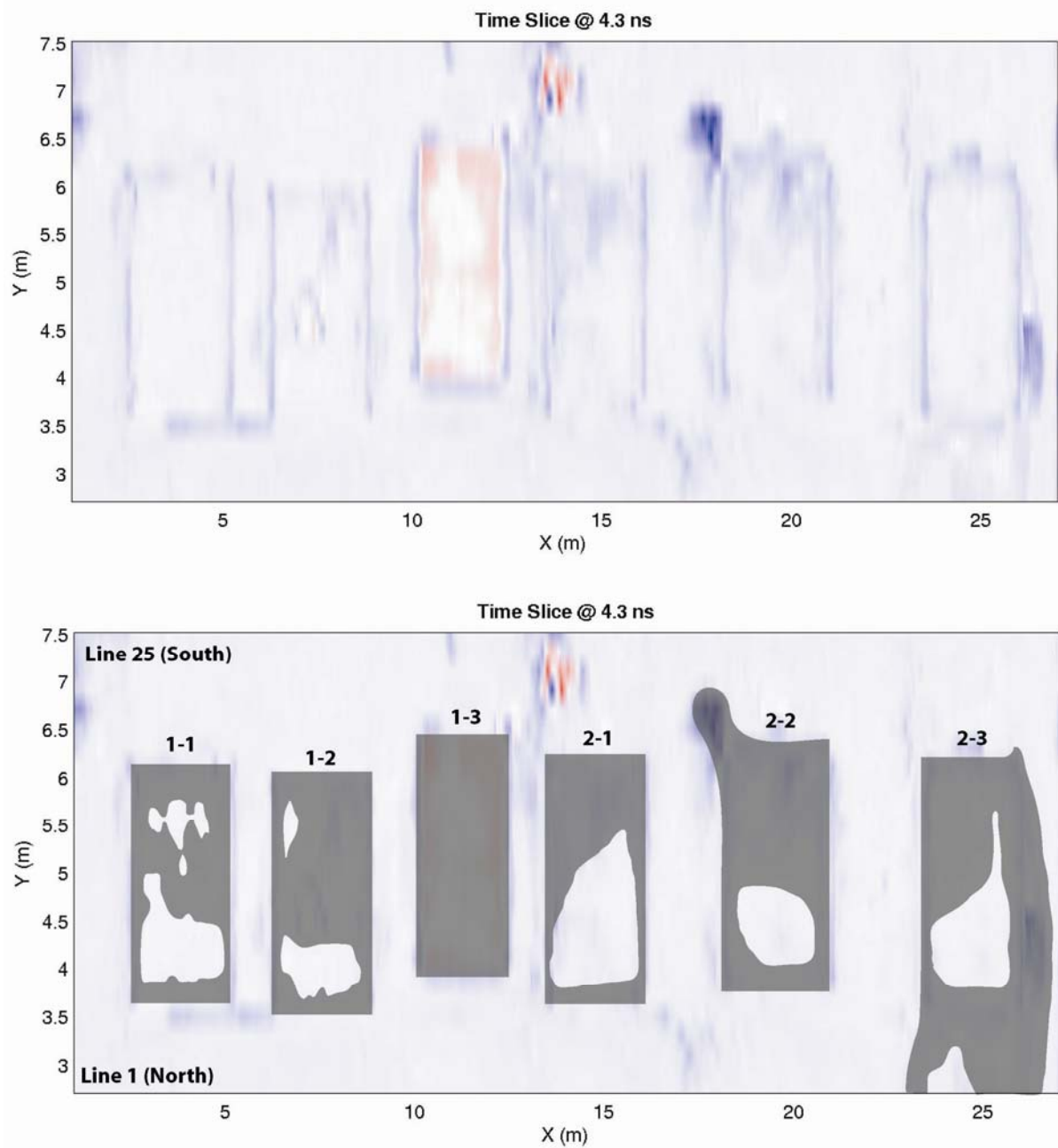
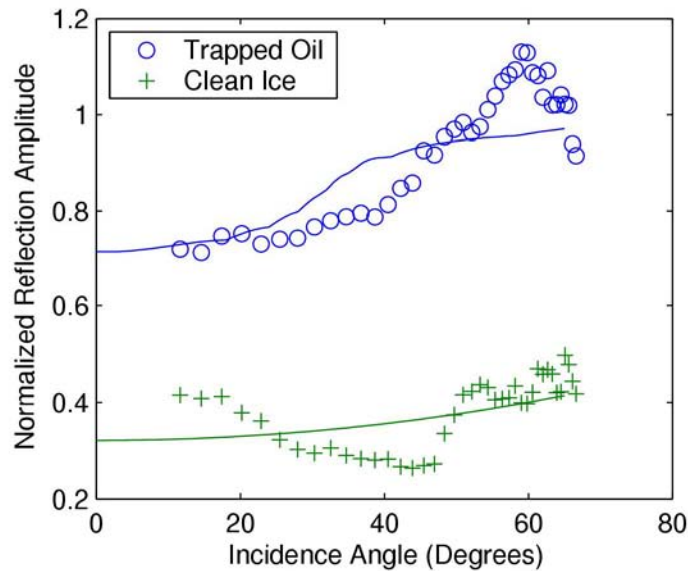
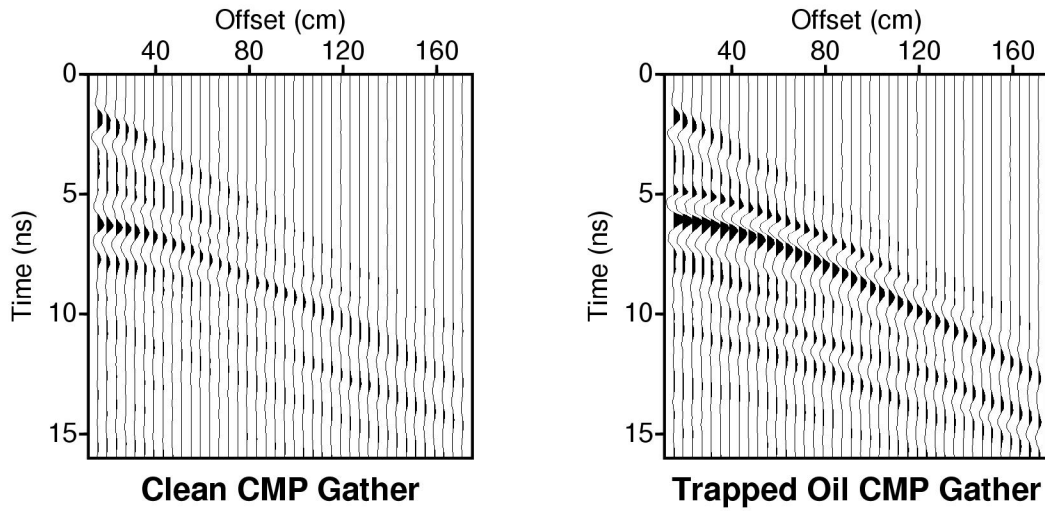


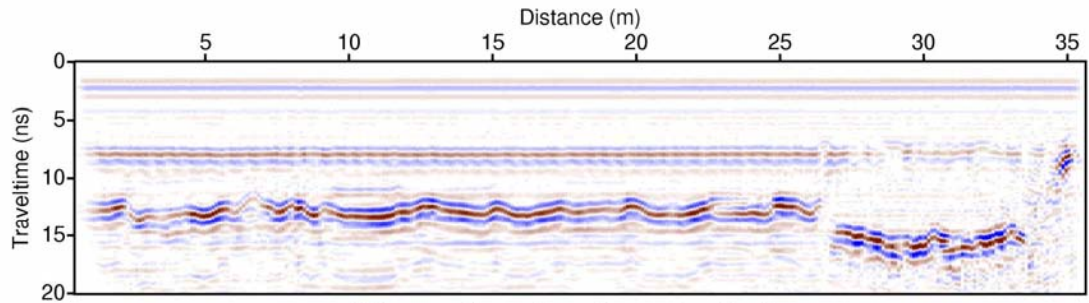
Figure 8 A time slice through the 800 MHz 3D volume at 1.9 ns ( 14 cm, 5.4 in) shows reflectivity that tracks the oil distribution in cell 1-2.



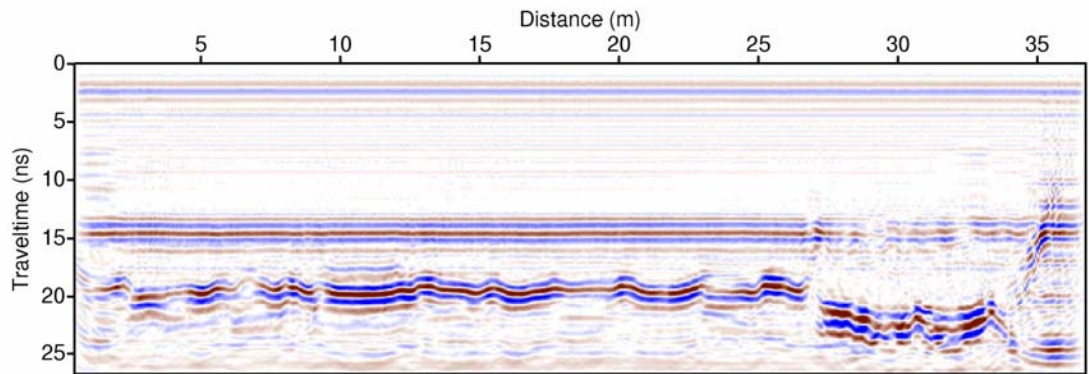
**Figure9.** A time slice through the 800 MHz 3D volume at 4.3 ns ( 31 cm, 12 in) shows reflectivity that tracks the oil distribution in cell 1-3.



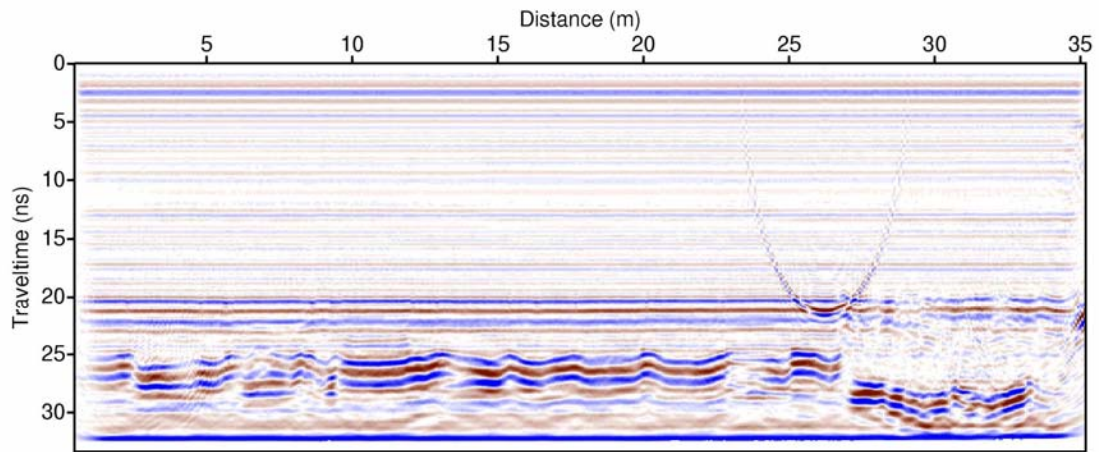
**Figure10.** Trapped oil test TE CMP gather (centered on Cell 2-2), control gather acquired in the clean ice area adjacent to Cell 2-2, and IW reflection amplitudes corrected for wave spreading and radiation patterns. The antenna frequency for this test was 900 MHz. Model AVO curves for a 6 cm thick oil layer trapped at the IW interface are shown with solid lines. Over this range of incidence angles, reflection amplitudes increase more rapidly when oil is present at the IW interface. The model data reasonably predict the AVO trend of the experiment data, although the amplitude difference between the two scenarios is underpredicted.



**Airborne Run - 1 m Above Ice Surface**



**Airborne Run - 2 m Above Ice Surface**



**Airborne Run - 3 m Above Ice Surface**

**Figure 11** Airborne GPR data acquired with the Sensors and Software system with 900 MHz antennas. No amplitude anomalies associated with the oil trapped under the ice are evident. This is likely due to decreased lateral resolution with increasing distance above the ice and the profile not being directly over the thickest oil films. Additionally, in the lab environment, coherent noise caused by scattering from surface objects becomes more prevalent as the antennas are raised above the ice. This noise interferes with the target reflection altering the amplitude characteristics. The intraice oil film in Cell 1-3 is evident.

# **Appendix B**

## **Ethane Flux Data**

Bill Hirst  
Shell Global Solutions Inc.

Graham Gibson  
University of Glasgow

Victor Jones  
Exploration Technologies Inc.

## Ethane Flux Values from CRREL Oil in Ice Experiments Nov 2004

Position	Flux in kg/m <sup>2</sup> .sec	Flux SD kg/m <sup>2</sup> .sec	Location	Comments
1	4.53E-14	6.0E-14	well away from Area 1-1	ice background reference
2	4.65E-13	6.3E-14	near Area 1-1	
17	1.22E-12	9.2E-14	Area 1-1	discoloured surface
26	8.41E-13	1.5E-13	Area 1-1	discoloured surface
21	1.48E-11	4.3E-13	Area 1-2	heavily discoloured surface
22	1.29E-11	7.3E-13	Area 1-2	heavily discoloured surface
27	1.10E-11	3.3E-13	Area 1-2	heavily discoloured surface
19	1.32E-13	1.2E-13	Area 1-3	After removal of fresh ice seal layer, post oil spill
20	1.15E-13	1.2E-13	Area 1-3	After removal of fresh ice seal layer, post oil spill
16	3.25E-13	9.3E-14	outside Area 2-1	
14	3.74E-13	1.9E-13	Area 2-1	
13	1.60E-12	9.3E-14	Area 2-1	at ice/oil boundary?
25	3.03E-13	1.3E-13	Area 2-1	
24	3.73E-13	1.0E-13	Area 2-2	
6	5.07E-13	1.5E-13	away from Area 2-3	Possibly over spilled oil/gas, against walls?
5	1.89E-12	1.6E-13	nearer Area 2-3	at ice/oil boundary?
8	3.59E-13	1.5E-13	Area 2-3	
10	2.80E-13	2.0E-13	Area 2-3	
23	3.83E-13	1.3E-13	Area 2-3	
11	≤ (5.61E-13)	8.2E-14	Rough Ice	upper limit estimate only

Bill Hirst, Shell Global Solutions International BV

# **Appendix C**

## **Ice Thickness and Oil Distribution**

David Dickins  
DF Dickins Associates Ltd.

Len Zabilansky  
US Army Cold Regions Research Engineering Laboratory

**Table C-1****Ice Thickness Measurements During Test Program**

(all measurements from coring or 5 cm (2 in) augur hole except where noted)

<b>Date</b>	<b>Sample # Fig. 4-1</b>	<b>Thickness (cm)</b>	<b>Location</b>	<b>Comments</b>
11/15	H1	36.5	East end	
11/15	H2	37.7	West end	
11/16	H4	38.8	East end	same location as 11/15
11/16	H5	34	West end	different point than 11/15
11/17	H6	38	East end	same location as 11/16
11/16	H7	25-28	just outside south skirt for area 2-1	area highlighted as thin on radar trace - two holes separated by 40 cm
11/16	H8	36-39.5-41	just outside south skirt for area 1-3	three holes in a line separated by 20 cm
11/18	H9	38	just outside NE corner of area 1- 1	thickness measured in chainsaw slot cut for underwater video
11/18	H10	40	just outside NE corner of area 1- 2	" " "
11/19	H11	38	just outside SE corner of 1-1	Core drilled for temp. Soft skeletal layer - 2cm. Milky band (air intrusions) between 19.5 and 24 cm depth. Thin band of opaque ice at 17 cm. Rest of core clear ice.
11/19	OC1	43	inside area 1-1, ethane flux site 17	oiled core
11/19	H12	45	inside area 1-1	clean ice area 75 cm NE of the oiled core
11/19	OC2	44	inside area 1-2, ethane flux site 27	oiled core
11/19	H13	44.5	inside area 1-2	relatively clean ice close to the N side of the skirt (faint trace of oil - beige drill cuttings)
11/19	OC3	43	inside area 1-3, ethane flux site 20	oiled core (note no clean ice measurement as entire area inside skirt oiled)

Date	Sample # Fig. 4-1	Thickness (cm)	Location	Comments
11/19	OC4	38	inside area 2-1, ethane flux site 25	oiled core
11/19	H14	44	inside area 2-1	clean ice in N half of skirt
11/19	OC5	40.5	inside area 2-2, ethane flux site 24	oiled core
11/19	H15	41	inside area 2-2	clean ice close to N side of skirt
11/19	OC8	39.8	inside area 2-3, ethane flux site 8	oiled core
11/19	H16	45	inside area 2-3	clean ice close to NW corner
11/19	OC7	40.2	outside area 2- 3, ethane flux site 5	oiled core where oil escaped the skirt
11/19	OC8	66 - 69	inside area 2-4, ethane flux site 11	oiled core in rough ice, slab cut to insert underwater camera

**Note:** "OC" and "H" Sample numbers refer to Oiled Core and Ice Thickness measurement locations shown on the site base map in Figure 4-1 (main report)

**Table C-2**  
**Oiled Core Measurements, 11/19/04 (in cm)**

Test Site	H Ice Total	Core Length	Dist. to Top of Oil Layer	Oil Layer Thickness	Vertical Oil Migration		New Ice Growth Following Spill	Comments
					(-) Below oil layer	(+) Above oil layer		
1-1	43	37.5	17	<0.5 cm	None	17	25.5 (est.)	Ice from the oil layer to the ice surface saturated with oil
1-2	44	41	17	~1 cm	None	17	26	First 6.8 cm oil migration saturated, followed by isolated oiled channels to the surface
1-3	43	42	25.5	1.5	5	7	16	(+) migration saturated, (-) migration in isolated channels 2-3 mm dia
2-1	38	34.5	34.5	1.5	Not known	20.5	2	first 3.5 cm ice above oil saturated, remaining 17 cm migration as isolated channels
2-2	40.5	32	32	0.8-1.2	Not known	17	~7	oil migration as discrete channels, 1-2 mm dia.
2-3 #1	39.8	35.	35.	1.7	Not known	17	3.1	Saturated ice 5.8 cm above the oil layer, remaining migration separate channels

Test Site	H Ice Total	Core Length	Dist. to Top of Oil Layer	Oil Layer Thickness	Vertical Oil Migration	New Ice Growth Following Spill	Comments
2-3 #2	40.2	35.8	32.4	2.8	3.4+	4.2	Saturated for 10 cm above the oil layer, followed by 5 cm isolated channels. (-1) migration isolated oil inclusions 1-2 mm dia x 10 mm long
2-4	69	69	38-40.5	not measured <3 mm	None	5	Oiled layer at an angle following junction between ice blocks. Isolated oil brine channel segments (1-2 mm X 1 cm) for about 5 cm above the oil layer

**Notes:**

Difference between the total ice thickness and the total core length + oil layer thickness = bottom portion of the core often missing due to the soft, easily broken skeletal layer of the ice undersurface.

Difference between distance to top of the oil and (+) migration indicates the depth of clean ice from the surface down.

Refer to OC (Oiled Core) locations marked on the site base map for exact locations within each test site (Fig. 4-1, main report)

## Site Photographs

- Oiled areas
- Surface appearance
- Oiled Cores

### Notes:

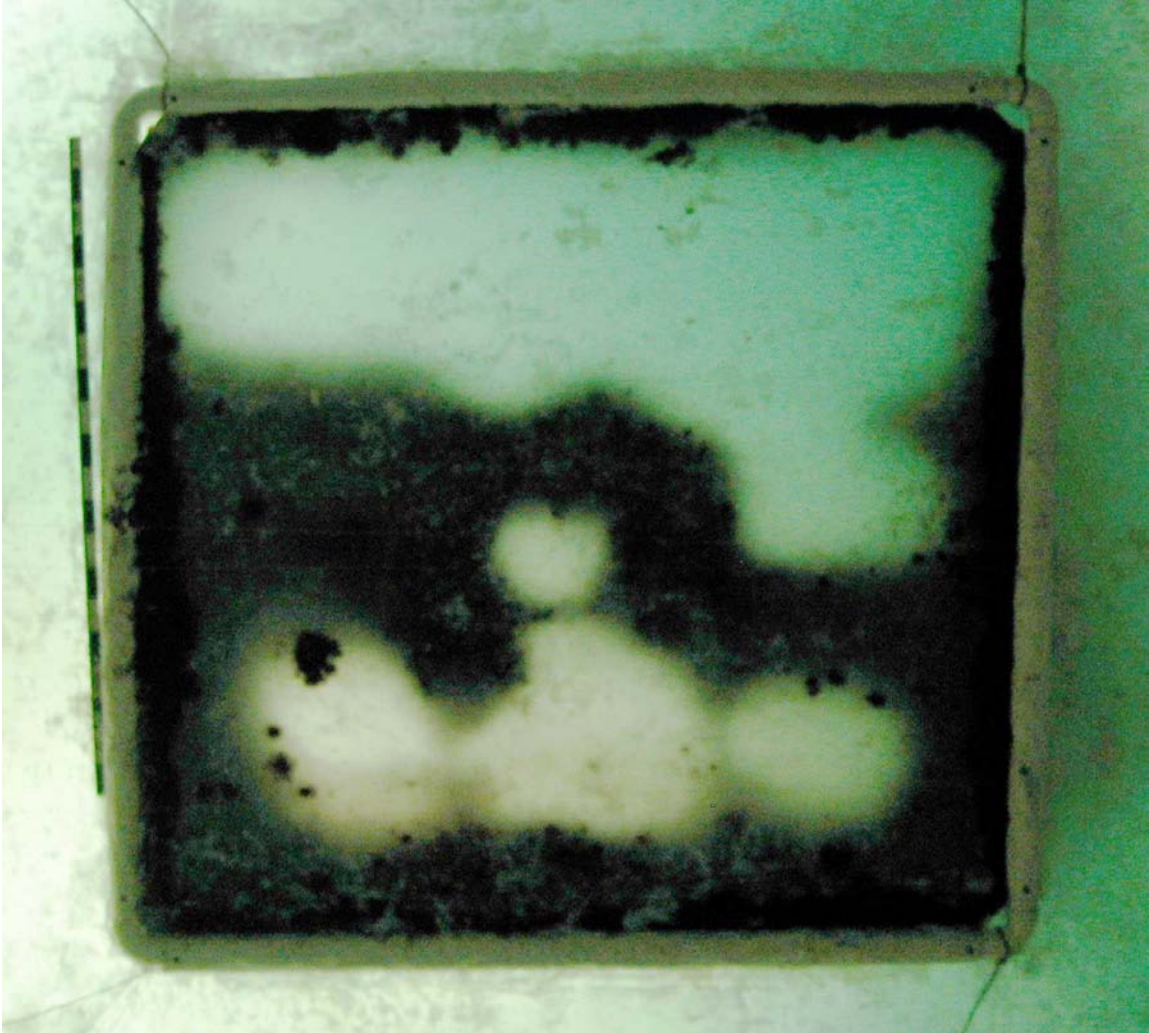
Figure 4-1 (main report) contains a site map to scale with all coring locations and digitized oil boundaries (from photographs shown here).

Table C-2 (preceding) contains detailed observations and measurements made from each core.

Backlit vertical photographs reprocessed to improve clarity by Olga Sandria, Exploration Technologies Inc., Houston.



Coring Site 2-2



**Test site 1-1:** Overhead view of under-ice oil, Nov 18. Skirt box is 2.43 m (8 ft) on each side. Photo is close to vertical.



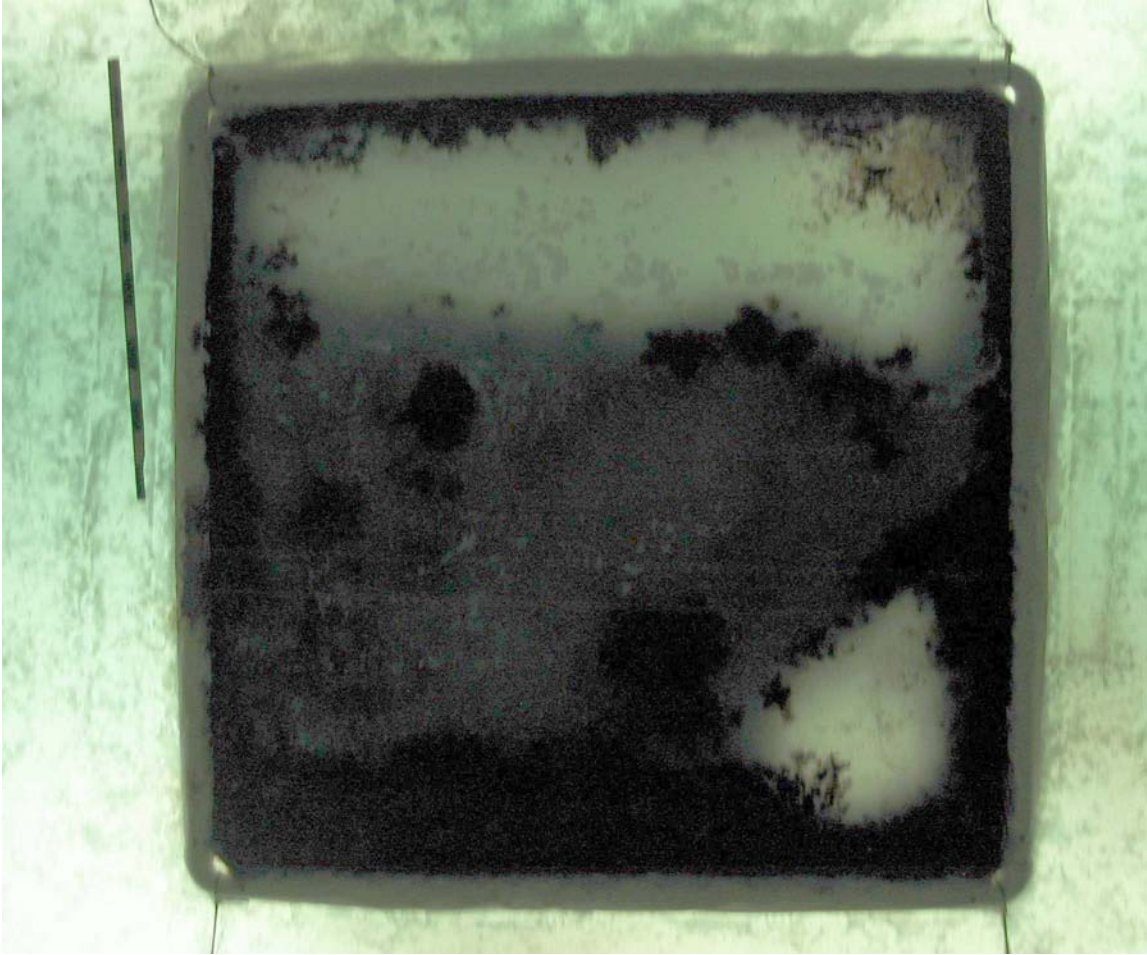
**Test Site 1-1:** Overhead view of surface oil leakage at skirt edges, Nov 8 (3 days post-spill). Note shadow of oil trapped under the ice. Most of the leakage occurred immediately following the spill (tens of minutes to hours).



**Test Site 1-1:** Oblique view SW to NE showing surface appearance after removal of protective plastic sheet installed for radar surveys, Nov 17. Note the lack of any significant further leakage to the surface (compared with surface view from Nov 8 - above).



**Test Site 1-1:** Oiled core taken Nov 19. New ice growth after spill shown by clean ice in section to the right. Oil has penetrated the ice vertically to the surface. Total core length 38 cm.



**Test Site 1-2:** Vertical backlit view showing oil under the ice, Nov 18. Skirt box is 2.43 m (8 ft) on each side. Photo is close to vertical. Note what appear to be areas of thick (blackest tone) and thinner oil with image at 87% brightness and contrast. The blackest parts of the image close to the edges correspond to the surface oiling shown below and do not necessarily reflect thicker oil trapped within the ice.



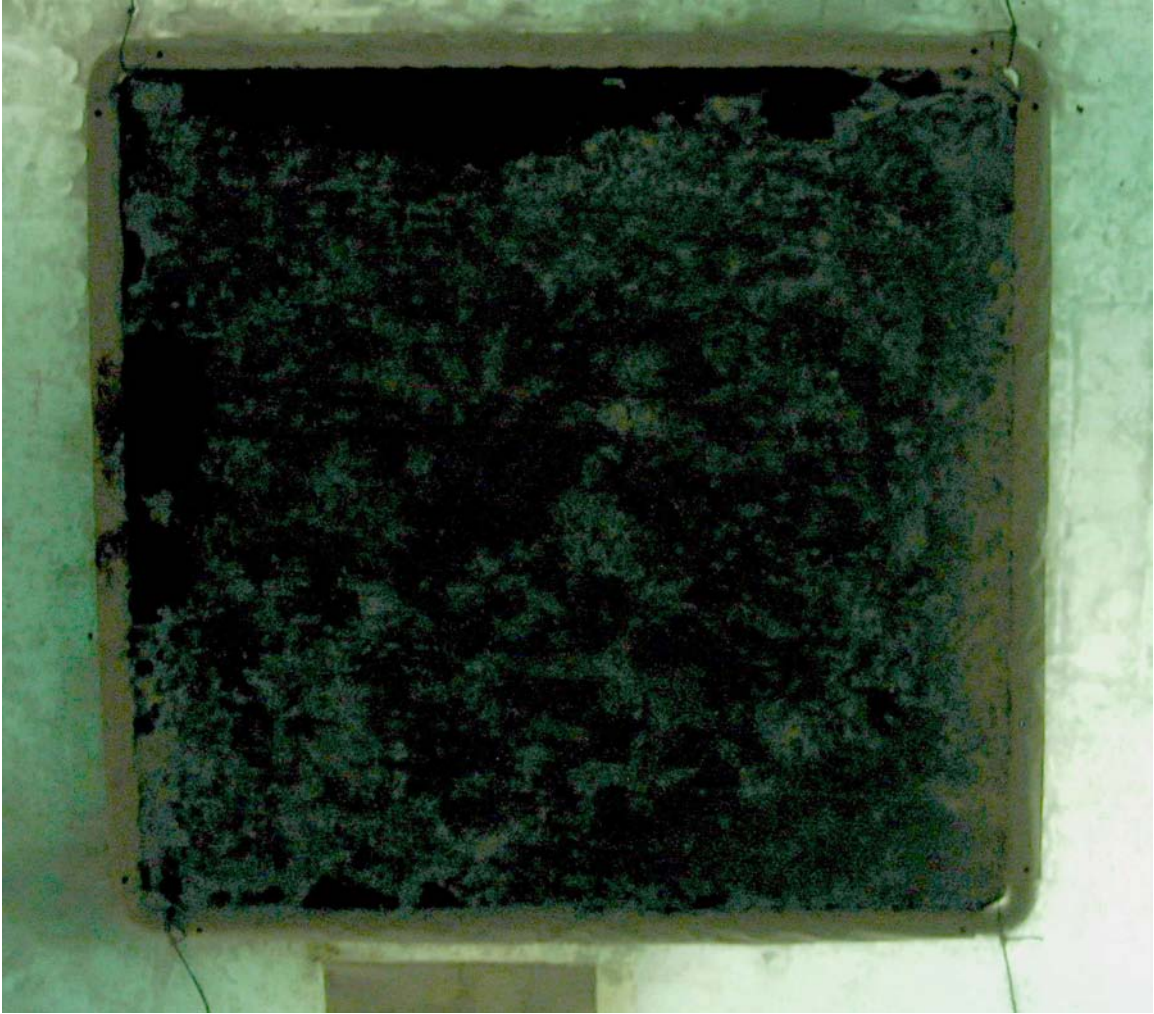
**Test Site 1-2:** Overhead view of surface oil leakage at skirt edges, Nov 8 (3 days post-spill). Note shadow of oil trapped under the ice. Most of the leakage occurred immediately following the spill (tens of minutes to hours). Ropes at four corners used to hold frame in place during freeze-up.



**Test Site 1-2:** Oblique view SW to NE showing surface appearance after removal of protective plastic sheet installed for radar surveys, Nov 17. Note the lack of any significant further leakage to the surface (compared with surface view from Nov 8 - above). Some surface smearing of oil occurred because of towing the radar sled back and forth.



**Test Site 1-2:** Core showing new ice after spill to the right. Oil layer was trapped in the ice at the right end of the small section (heaviest oiled). Note that dirty appearance of core section to the right is surface contamination from the coring process (ice internally is clean). The oil is distributed throughout the ice from the depth at time of spill (Nov 5) to the surface. Total core length 41 cm.



**Test Site 1-3:** Vertical backlit view showing oil under the ice, Nov 18. Skirt box is 2.43 m (8 ft) on each side. Photo is close to vertical. The blackest parts of the image (along top and left sides) correspond to the surface oiling from leakage up the skirt ice interface following the spill.



**Test Site 1-3:** Oblique view SW to NE showing surface appearance Nov 17.  
Leakage occurred at the ice to skirt interface after the cold room was warmed-up on Nov 14.



**Test Site 1-3:** Core taken Nov 19, 2004. Clean ice growth after the spill (Nov 8) shown in section to the left (oiled appearance is surface contamination from coring). Vertical migration through internal ice channels visible in section to the left (towards the surface). Total core length is 42 cm.



**Test Site 2-1:** Vertical backlit view showing oil under the ice, Nov 18. Skirt box is 2.43 m (8 ft) on each side. Photo is close to vertical. The blackest parts of the site (bottom left of center) likely show an area of thicker oil.



**Test Site 2-1:** Overall oblique view down the tank on Nov 17 showing Test Site 2-1 on the far left. Note no sign of any significant surface leakage in this test area. Oil spilled Nov 15.



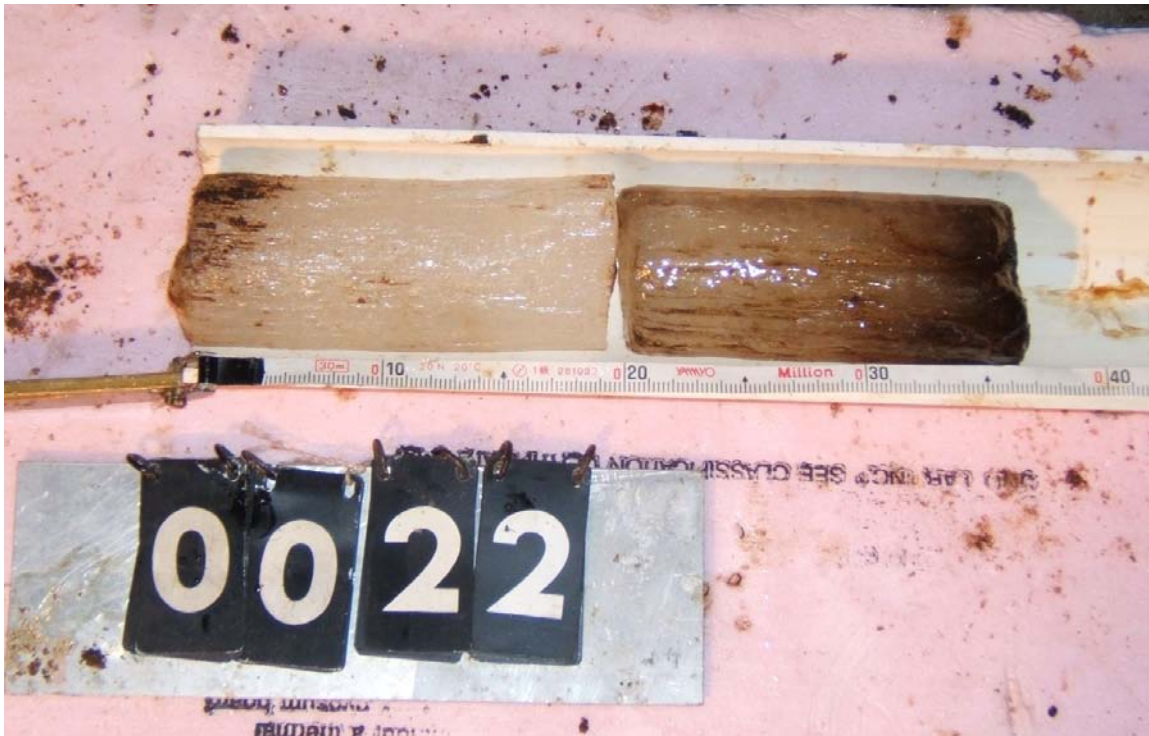
**Test Site 2-1:** Oiled core taken Nov 19, showing no visible new ice under the oil layer (far left) from spill on Nov 15. Measurements of the hole indicate the presence of up to 2 cm of new ice crystals as a skeletal layer of new growth beneath the oil (impossible to recover with the core barrel). Total core length 34.6 cm. Evidence of vertical migration of oil up to 20 cm. No visible oil in the upper 15 cm (oiling of the upper ice section in the photo is caused by surface contamination in the extracting the core through the oiled hole).



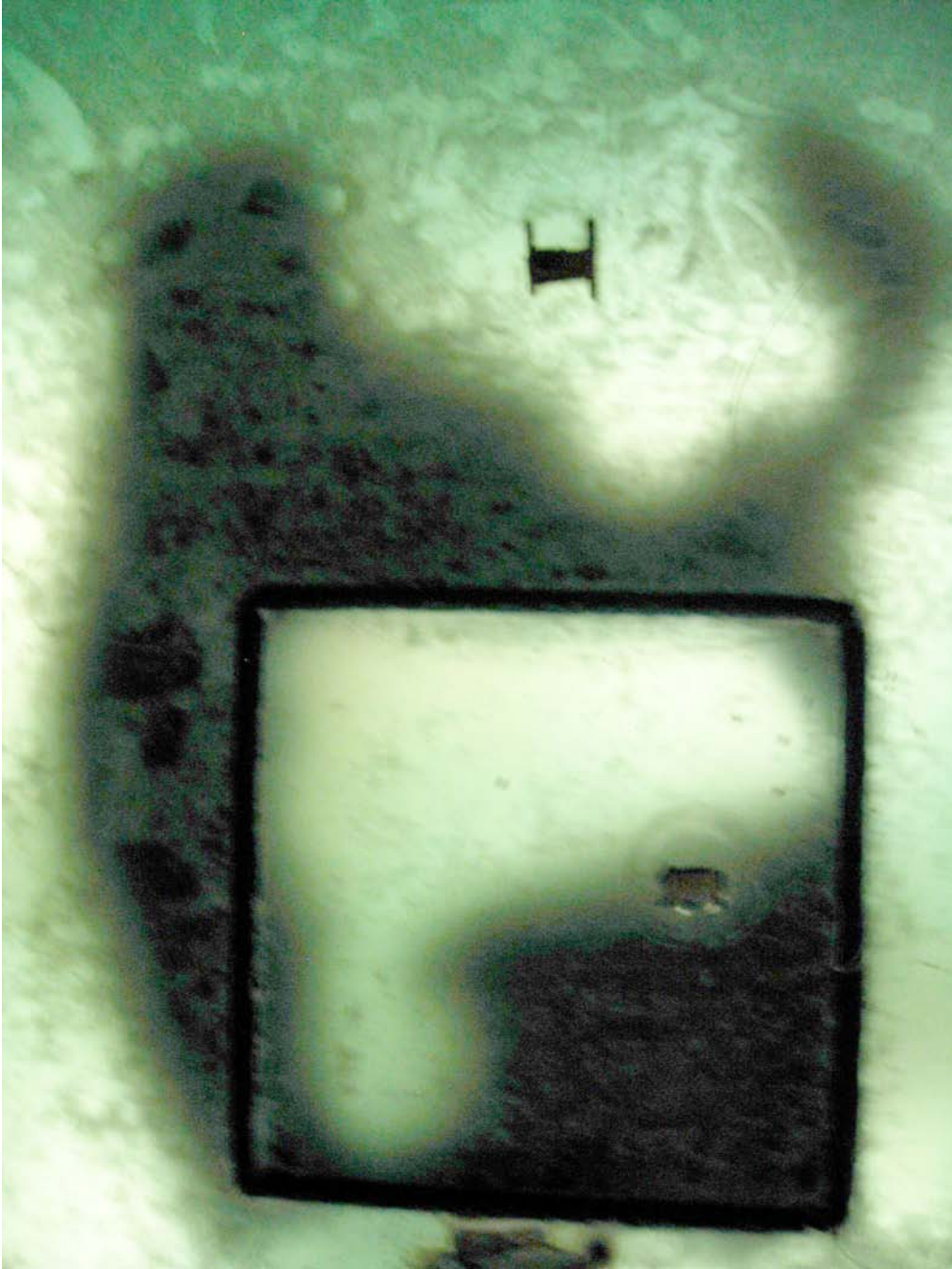
**Test Site 2-2:** Vertical backlit view showing oil under the ice, Nov 18. Skirt box is 2.43 m (8 ft) on each side. Photo is close to vertical. Blacker tones in lower half (South) half of the test area may indicate thicker oil. Note lobe of definite oil under the ice outside the skirt at the SE corner. It also appears that thin films of oil may have escaped outside the skirt at the NE corner. "Fuzzy" oil boundary may be the result of a thin skim of new ice crystals growing from the clean ice into the oil (as shown in underwater video and coring on Nov 19). Black distinct patch outside skirt on the south side is the original trench cut to insert the oil (a small amount of oil flowed out of the end of the pipe when it was withdrawn).



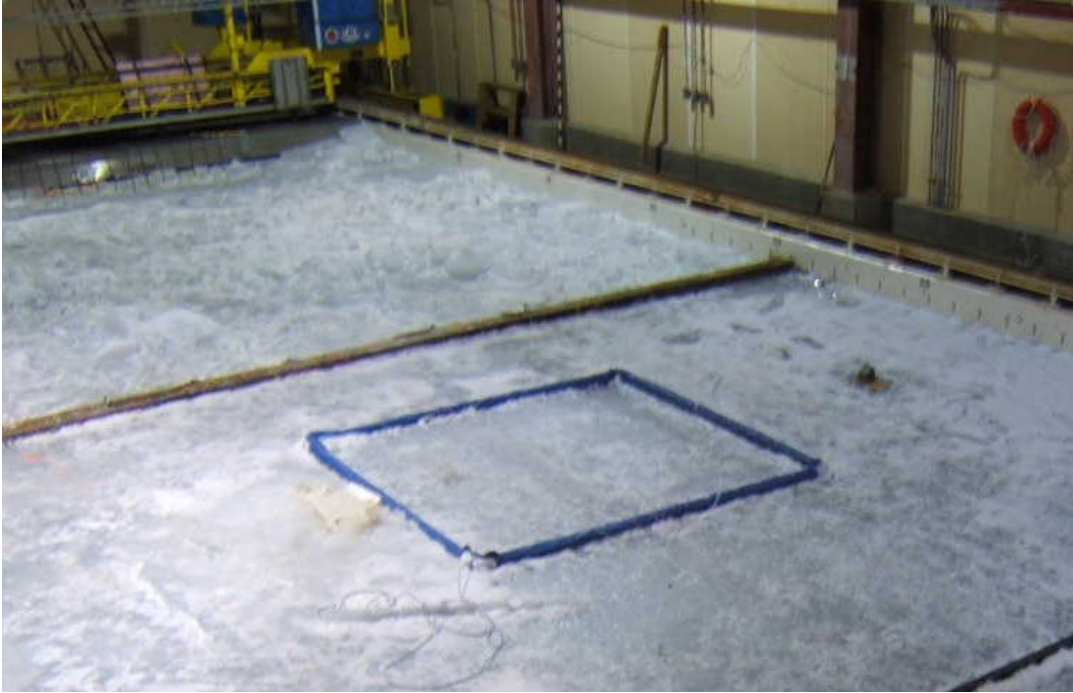
**Test Site 2-2:** Overall view of surface appearance of Site 2-2, Nov 17. Note oiled insertion trench outside of the skirt shown clearly in the backlit vertical photograph (above). There was no visible leakage of oil to the surface within the skirted area.



**Test Site 2-2:** Oiled core taken Nov 19. Oil layer far right. No evidence of oil in the upper ice section. Total core length recovered 23 cm. Oil migrated internally within the ice for 17 cm above the spill. Measurements in the hole indicated up to 7 cm of new ice growth beneath the oil (too fragile to be recovered by the core barrel).



**Test Site 2-3:** Vertical backlit view showing oil under the ice, Nov 18 (enhanced to clarify oil boundaries). Skirt box is 2.43 m (8 ft) on each side. Note lobes of oil under the ice outside the skirt on the north and west sides. "Fuzzy" oil boundary may be the result of a thin skim of new ice crystals growing from the clean ice into the oil (as shown in underwater video and coring on Nov 19).



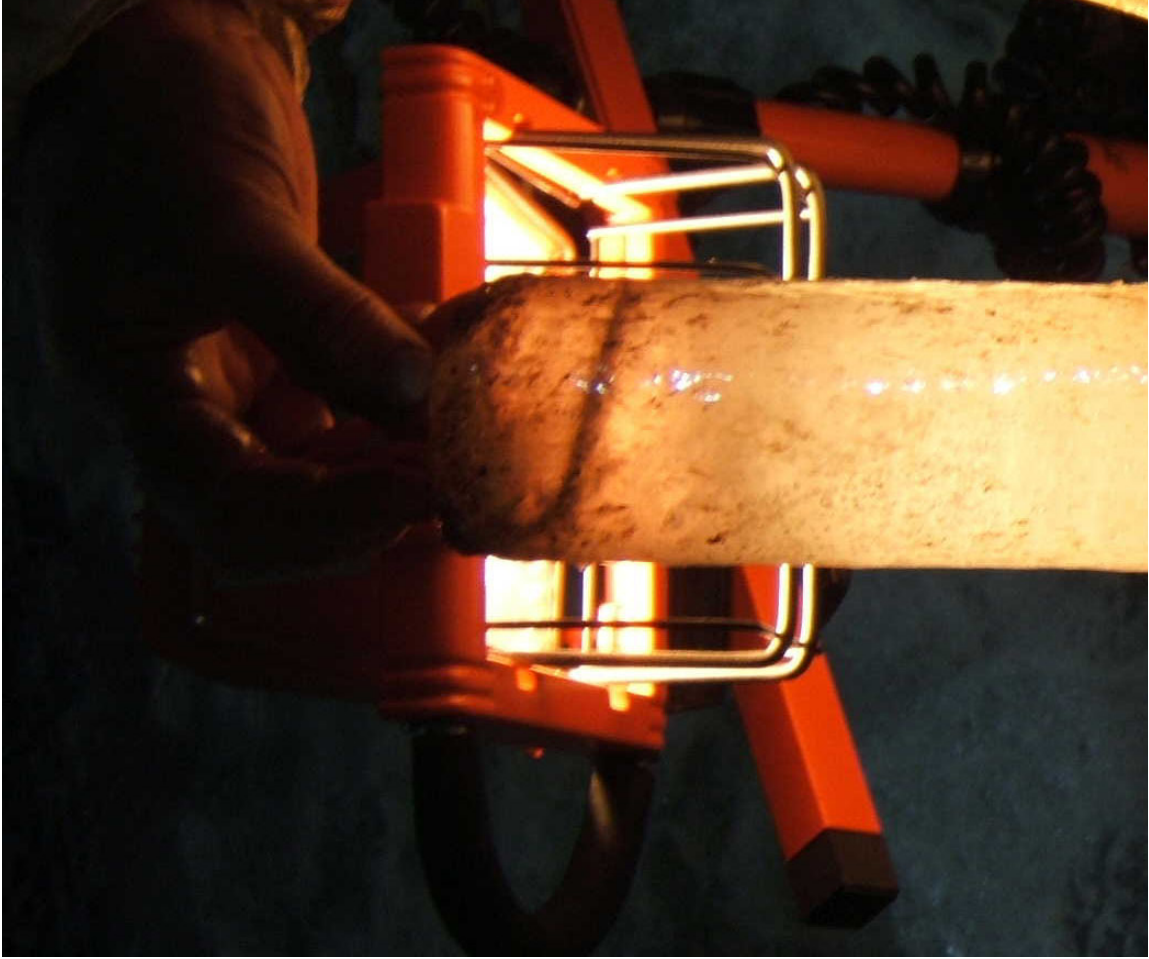
**Site 2-3:** Surface view showing lack of any oil leakage to surface, Nov 17.



**Test Site 2-3:** Two cores taken Nov 19. Upper core extracted within skirted area, bottom core from the lobe of oil extending outside the NW corner of the site. Both cores 35-36 cm in length with similar extent of vertical migration above the oil pool (far right). Concentration of oil within the ice appears denser within the lower core, potentially reflecting the thicker oil pool at that location (2.8 vs. 1.7 cm - see Table C-2). Radar signature also much more pronounced over the oil outside of the skirt.



**Test Site 2-4:** Oiled core taken through the rubble ice inside the skirt of Test site 2-4 (actual skirt outline not visible on the surface). Total core length 69 cm. Oil appears to have formed a thin layer, flowing between two blocks at an angle. See close-up below.



**Test Site 2-4:** Close up of well-defined oil band, likely marking the contact between different blocks making up the rubble field.

# **Appendix D**

## **Independent Hydrocarbon Analysis of Oil, Air, Water, Ice Samples**

Victor Jones  
Exploration Technologies Inc.

## Notes to Appendix D

Refer to accompanying test map for sample locations and tank layout.

### Oil Chemistry

Table 3 in Appendix D contains the analytical light gas headspace data for the saturated vapors in the South Louisiana Crude Oil samples (from drums as delivered, and from oil spilled under the ice). For these tests, the saturated vapor was generated by placing 2 ml (0.06 f.oz) of the oil in a closed 125 ml (4.22 f.oz) bottle and analyzing the saturated vapors in the headspace at room temperature. As shown by the analytical data, the headspace ethane concentrations in the original oil samples are significant and uniform, ranging from 4000 to 5000 ppmv in the saturated vapor headspace in contact with the six oils. These concentrations are in the upper quartile when compared with other oils that have been analyzed in ETI's laboratory (See main report Table 2-1). Consequently, the South Louisiana oil was judged to an excellent candidate for this study.

In addition to ethane, these oils also contained large quantities of other volatile components, such as methane (600 ppm), propane (29,000 ppm), butanes (52,000 ppm) and a full complement of C5+ gasoline range hydrocarbons. Complete analytical data for the C5+ and C15+ components are contained in Appendix D.

Because of the similarity of all six oils, only two of these seven oil samples from the ice, OC5 and OV6 were analyzed.

### Ice Cores Analyzed for Trapped Hydrocarbon Gases

The ice core samples were collected in 40 ml (1.35 f.oz) VOA vials on Nov 24, and kept frozen until transported to ETI for analysis of light C1 – C4 and C5+ hydrocarbons. Detection limits for this data are in the 5 to 10 ppbv (0.005 to 0.010 ppmv) range, and each of these ice core samples was run in triplicate in order to define the variance between samples. The analytical data from the melted core segments is contained in Table 2 in Appendix D with further explanatory notes.

Table 2 shows that ethane, propane, iso and normal-butane exhibited significant concentration increases with depth in all cores. Ethylene and propylene, which are not oil related components, did not change from the top to the bottom of these core samples. In contrast, it is important to note that propane and butanes demonstrated a similar increase in concentration with depth as ethane. The lack of olefins and presence of the C3 and C4 associated components confirms all these measured gases (including ethane) as oil-related hydrocarbons.

It is also interesting to note that the propane and butane components were well above background in the very shallowest cores collected in all three of the cored areas. A much more significant difference between the background area (GC-1) and the other two oil

spill areas (GC-2 and GC-3) is shown by the much larger vertical gradient that occurs in the vicinity of the oil spill areas. Note that the maximum propane and normal-butane concentrations are more than an order of magnitude greater at GC-2 and GC-3 as compared to GC-1. Clearly, both the overall magnitudes and the vertical increase in concentration with depth does show a relationship to the proximity of the injected oils. This is amplified even more by sample 1-3D from area GC-2, which had an encapsulated oil bubble, producing exceptionally high concentrations. Although, the shallowest sample from GC-3 was broken in transit, it can be assumed that it would probably have been similar to the other shallow cores, all of which have small, but above background concentrations.

There was no visual evidence showing how these light hydrocarbons may have migrated into the ice at these locations. As noted above, ice core sample GC-1 was collected within the NE corner of the ice-testing tank in an area that was thought to represent a clean background (the closest free oil was located in skirt 1-3 more than 3.5 m (11.5 ft) away). In addition, an ethane flux chamber measurement at site 01, about 1 m (3.3 ft) away from GC-1 produced a null value, further confirming the assumption that this area was at background when compared to the skirts, which contained free oil.

## **Water Samples**

Water samples collected from holes drilled in the melting ice sheet on Dec 17 were received on Jan 3, 2005 and analyzed for their light C1 – C4 hydrocarbons on Jan 6 -7. The water sample analysis and ambient air data is shown in Table 4, Appendix D.

With the exception of one invalid leaking sample (Serial AH361465 Lot B), the remaining water samples contained large headspace concentrations. These samples were analyzed by creating a 10 ml (0.34 f.oz) nitrogen headspace in the 40 ml (1.35 f.oz) VOA vials by displacing 10 ml of water with nitrogen, and then analyzing the headspace gases at room temperature. Laboratory detection limits for these samples is ~30 ppb.

The very large measured concentrations of the light C1 – C4 gases suggested that it might be interesting to also analyze the water samples for their C5+ gasoline range hydrocarbons. With the exception of BTEX (benzene, toluene, ethylbenzene and xylenes), these C5+ hydrocarbons are much less volatile and soluble than the light gases. If components of the oil had migrated away from the spill sites as water-soluble hydrocarbons, then the more soluble BTEX components would tend to dominate the C5+ signatures. Both the individual C5+ component magnitudes and the high-resolution capillary chromatograms are included in Appendix D for evaluation (Table 6). This C5+ data is very striking. All the component signatures found in the headspace waters are very similar to the whole oil sample analysis. The fact that these water samples are dominated by the less degradable and less soluble gasoline range components implies that the source of the h.c. vapors in these water samples are probably very small droplets of free oil that has migrated to the locations where the water samples were collected. Both

the ice core and water headspace data suggests that the oil spilled under the ice inside the skirts contaminated the entire undersurface of the ice sheet.

In addition to the C5+ having a whole-oil, rather than a dissolved phase signature, it is also very interesting to note that the components missing from the headspace C5+ chromatograms are only the most degradable components, such as the normal C6 and C7 alkanes. These normal alkanes have been nearly removed from the water headspace samples by biodegradation. Note also that the iso to normal-pentane ratios have changed from 1 to 1 to approximately 2 to 1. It is well known that the normal alkanes are always the first components to be biodegraded, and normal-pentane is degraded before iso-pentane.

This selective biodegradation of the normal alkanes may have occurred in the water under the ice, although it is possible that some portion, or all, of the degradation could have occurred after the water samples had been warmed to room temperature and had their nitrogen headspace added for analysis. Unfortunately, the C5+ analysis was conducted on Nov 20, 2005, 13 days after the C1 – C4 analysis was completed. It is generally accepted that biodegradation requires about 14 days to get started. Biodegradation also requires the presence of oxygen, which would have been present in the water when the samples were collected.

Apart from the uncertainty regarding whether the biodegradation took place in the ice, or in the samples after receipt at the lab, there is no question that very small quantities (micro-drops) of free oil mist have migrated out and impacted both the water and the ice over the entire tank.

## **Air Samples**

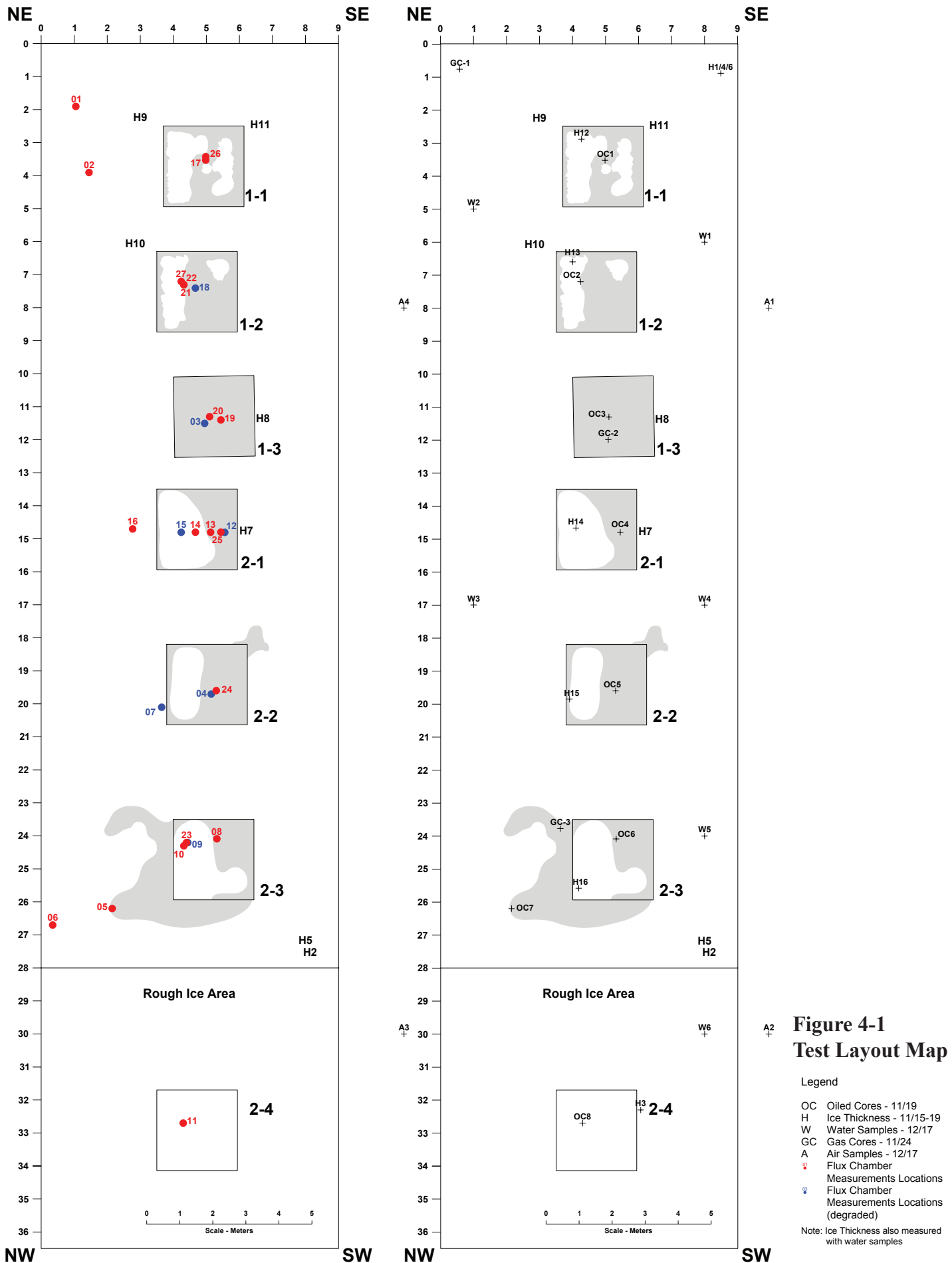
Due to the reliable performance of the Shell LightTouch™ system, only a few ambient air samples were collected during the field-testing. A series of seven air samples were collected in 125 ml (4.3 f.oz) glass bottles during the first two days of field testing for analysis by conventional GC technologies. Light C1 – C4 hydrocarbon gas chromatographs have the ability to measure ethane directly in the ambient air in the 5 to 10 ppbv range, using a flow-through analysis method that can be conducted on sample sizes as small as 125 ml (4.3 f.oz).

These results for C1 – C4 hydrocarbons are contained in Table 1 in Appendix D, with data listed in the date/time order collected, allowing easy correlation with the ethane flux data (App. B). As shown by Table 1 (Appendix D) the initial ambient air sample collected in the ice test tank had a concentration of 115 ppbv, with values subsequently dropping to 67 ppb on the following day, and to 34 ppb on the last day. A trip blank included with the initial ambient air data confirms that the ethane concentrations in the ETI sample bottles are below the 10 ppb detection level. Conformational gas chromatographs are also included for review in Appendix D.

One ambient air sample was also collected in the main entry hall adjacent to the stored oil barrels. This sample contained only 38 ppbv, indicating that there was no significant contamination in the test area where the oil filled barrels of oil were stored during the field testing phase.

In addition to ethane, ETI's ambient air analysis also confirmed the presence of several other light hydrocarbons, such as: methane, propane, iso-butane and normal-butane. This multi-component data provides additional confirmation that the ethane found in the ambient air was likely sourced from the spilled oil (ethane never occurs by itself - methane, propane and butanes are always present in any real petrogenic sample). Although the magnitudes of these light gases can change rapidly over short distances, the compositions are source related, and are much more stable. Their presence and relative concentrations confirm the source of these gases as oil-related.

A second set of four ambient air samples was also collected following completion of field-testing. These ambient air samples were received coincident with the water samples on Jan 3 and were also analyzed for light C1 – C4 hydrocarbons on Jan 6-7, 2005. A direct comparison of these four ambient air samples (Table 5) with the initial air samples (Table 1) shows that the ambient air in the chamber had become considerably more contaminated, particularly by the propane and butanes, during the collection of the ice core and water samples.





# Exploration Technologies, Inc.

7755 Synott Rd., Houston, TX 77083; Tel (281) 530-4300; Fax: (281) 530-4308

## 04 - 1509 Oil In Ice Project

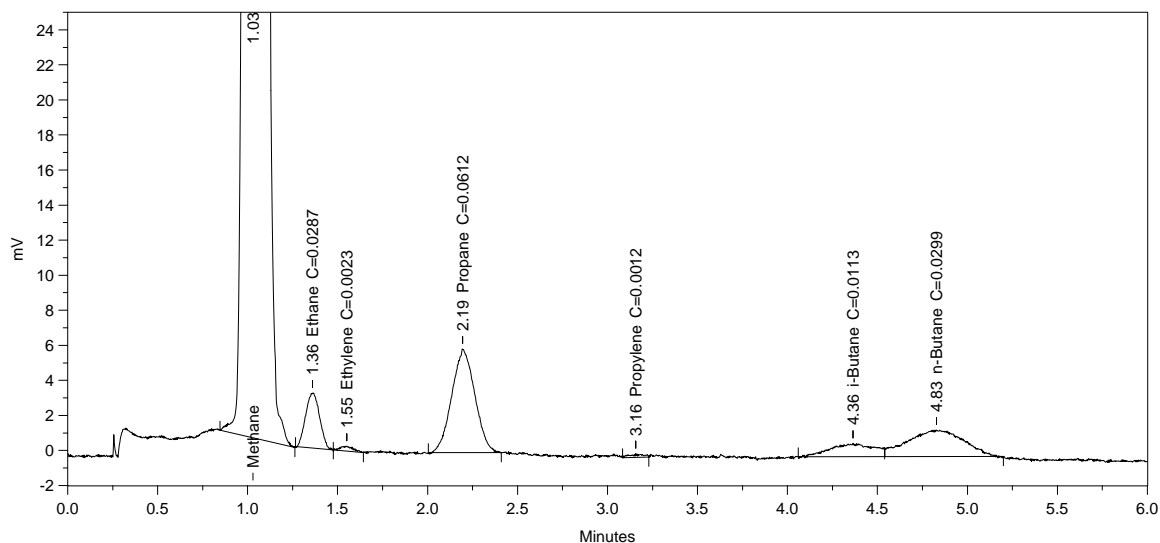
CRREL - Hanover, NH.

TABLE 1  
LIGHT C1-C4 HYDROCARBONS (ppmv)

ANALYZED DURING FILED TESTING - (NOVEMBER 17th - 18th, 2004)

SAMPLE NO.	DATE	BAR CODE	METHANE	ETHANE	ETHYLENE	PROPANE	PROPYLENE	I-BUTANE	N-BUTANE
Lab Air	Nov. 17, 2004 10:00am	152264	3.836	0.029	0.002	0.061	0.001	0.011	0.030
Trip Blk	Nov. 17, 2004 10:10am	152265	0.170	0.000	0.000	0.000	0.000	0.000	0.000
Air In Ice Tank	Nov. 17, 2004 10:10am	152266	4.267	0.115	0.002	0.241	0.001	0.060	0.203
Site 003 Air Sample	Nov. 17, 2004 2:10pm	152267	4.431	0.067	0.003	0.151	0.003	0.035	0.115
Lab Air Blk	Nov. 18, 2004 9:15am	152268	4.265	0.017	0.006	0.039	0.001	0.004	0.012
Site Air In Ice Tank	Nov. 18, 2004 9:20am	152269	3.934	0.034	0.003	0.094	0.001	0.025	0.079
Air In Oil Storage Area	Nov. 18, 2004 10:00am	152270	4.244	0.038	0.003	0.084	0.000	0.017	0.037

ND = Not Detected



Sample Name: **Lab Air**  
 Acquired from Chrom2--Det2A via port 3 on 12/8/04 03:06:36pm by Sharon  
 04-1509  
 FID 08DCAM1F.CAL

Data File: **G:\AMDATA\04-1509\FID\152264F.01R**  
 Date Stamp: 12/8/04 03:16:38pm  
 Method File: **!C:\AMDATA\04-1509\08DCAM1F.MET**  
 Bound Version 1. Date Stamp: 12/8/04 12:06:18pm  
 Calibration File: **!C:\AMDATA\04-1509\08DCAM1F.CAL**  
 Bound Version 2. Date Stamp: 12/8/04 03:16:38pm

Run Time = 6.0 min Sample Rate = 5.0 per sec.  
 Amount Inj. = 1.000 Dilution Factor = 1.000  
 Sample Weight = 1.000 Int Std Amount = 1.000

Starting Peak Width = 1.0 min. Peak Threshold = 0 Area Reject = 100

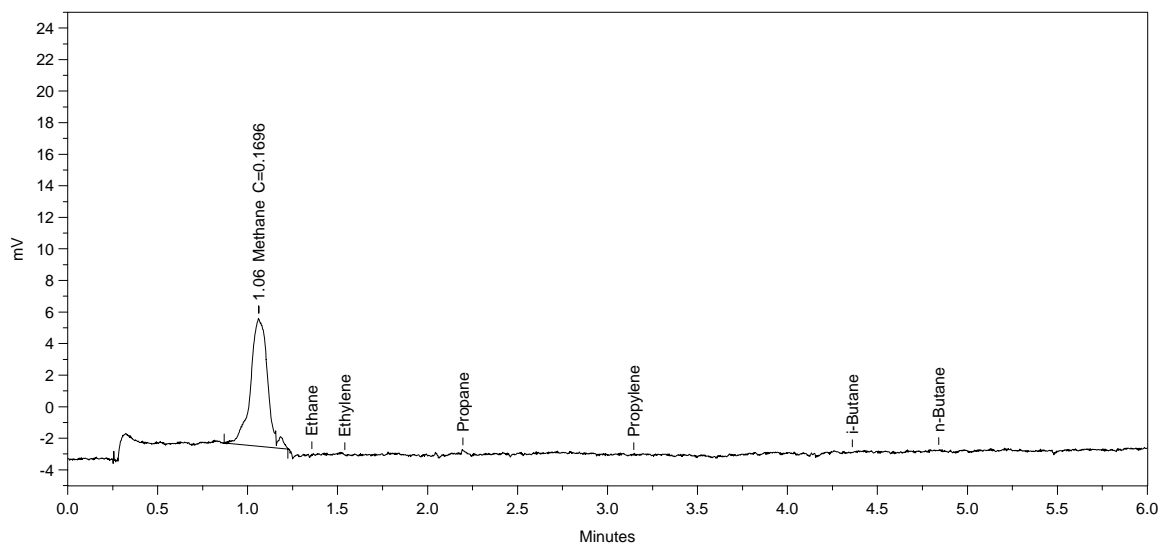
\* Some peaks have been manually integrated.

PK#	Ret Time	Name	Amount	Amount%	Area	Area%	Type	Width	Height	Height%
1	1.030	Methane	3.8364	96.613	1202262.0	91.129	BB	0.097	205516.50	94.554
2	1.361	Ethane	0.0287	0.722	16919.5	1.282	BV	0.090	3133.33	1.442
3	1.551	Ethylene	0.0023	0.057	1331.3	0.101	VB	0.078	285.08	0.131
4	2.194	Propane	0.0612	1.541	52621.1	3.989	BB	0.148	5923.77	2.725
5	3.157	Propylene	0.0012	0.030	1001.5	0.076	BB	0.078	214.04	0.098
6	4.363	i-Butane	0.0113	0.284	12501.9	0.948	BV	0.275	756.97	0.348
7	4.827	n-Butane	0.0299	0.753	32659.3	2.476	VB	0.357	1523.56	0.701

Total Area = 1319296.0, Total Amount = 3.971, Total Height = 217353.2

\* Some peaks have been manually integrated,

Trip Blk



Sample Name: **Trip Blk**  
Acquired from Chrom2--Det2A via port 3 on 12/8/04 02:51:21pm by Sharon  
04-1509  
FID 08DCAM1F.CAL

Data File: **G:\AMDATA\04-1509\FID\152265F.01R**  
Date Stamp: 12/8/04 02:58:30pm  
Method File: **!C:\AMDATA\04-1509\08DCAM1F.MET**  
Bound Version 1. Date Stamp: 12/8/04 12:06:18pm  
Calibration File: **!C:\AMDATA\04-1509\08DCAM1F.CAL**  
Bound Version 2. Date Stamp: 12/8/04 02:58:30pm

Run Time = 6.0 min Sample Rate = 5.0 per sec.  
Amount Inj. = 1.000 Dilution Factor = 1.000  
Sample Weight = 1.000 Int Std Amount = 1.000

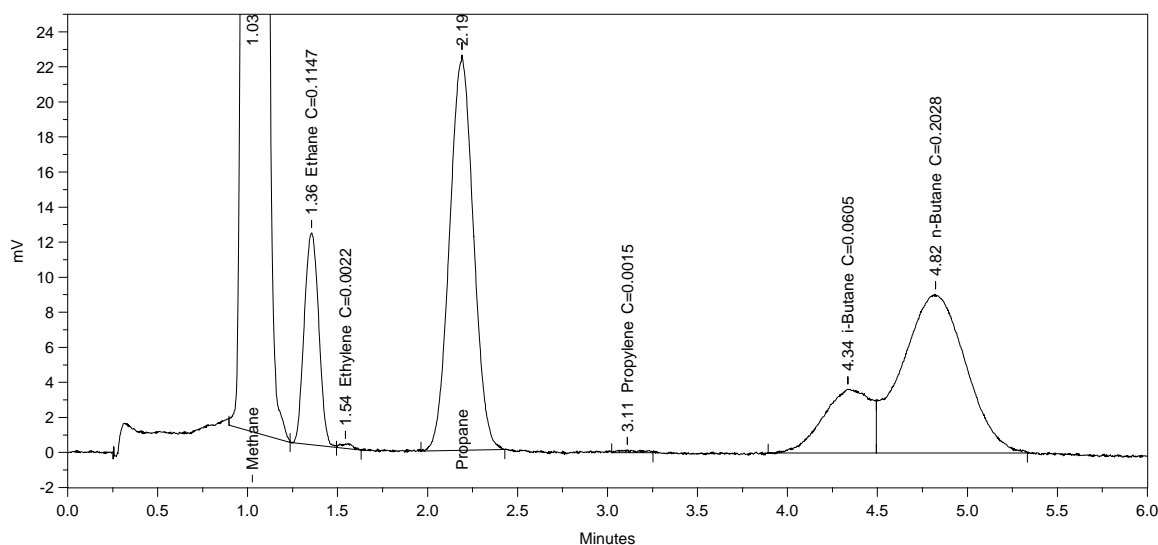
Starting Peak Width = 1.0 min. Peak Threshold = 0 Area Reject = 100

\* Some peaks have been manually integrated.

PK#	Ret Time	Name	Amount	Amount%	Area	Area%	Type	Width	Height	Height%
1	1.061	Methane	0.1696	100.000	53142.6	100.000	BB	0.109	8104.52	100.000

Total Area = 53142.6, Total Amount = 0.17, Total Height = 8104.52

\* Some peaks have been manually integrated.



Sample Name: **Air In Ice Tank**  
 Acquired from Chrom2--Det2A via port 3 on 12/8/04 03:34:27pm by Sharon  
 04-1509  
 FID 08DCAM1F.CAL

Data File: **G:\AMDATA\04-1509\FID\152266F.02R**  
 Date Stamp: 12/8/04 03:57:10pm  
 Method File: **!C:\AMDATA\04-1509\08DCAM1F.MET**  
 Bound Version 1. Date Stamp: 12/8/04 12:06:18pm  
 Calibration File: **!C:\AMDATA\04-1509\08DCAM1F.CAL**  
 Bound Version 2. Date Stamp: 12/8/04 03:57:10pm

Run Time = 6.0 min Sample Rate = 5.0 per sec.  
 Amount Inj. = 1.000 Dilution Factor = 1.000  
 Sample Weight = 1.000 Int Std Amount = 1.000

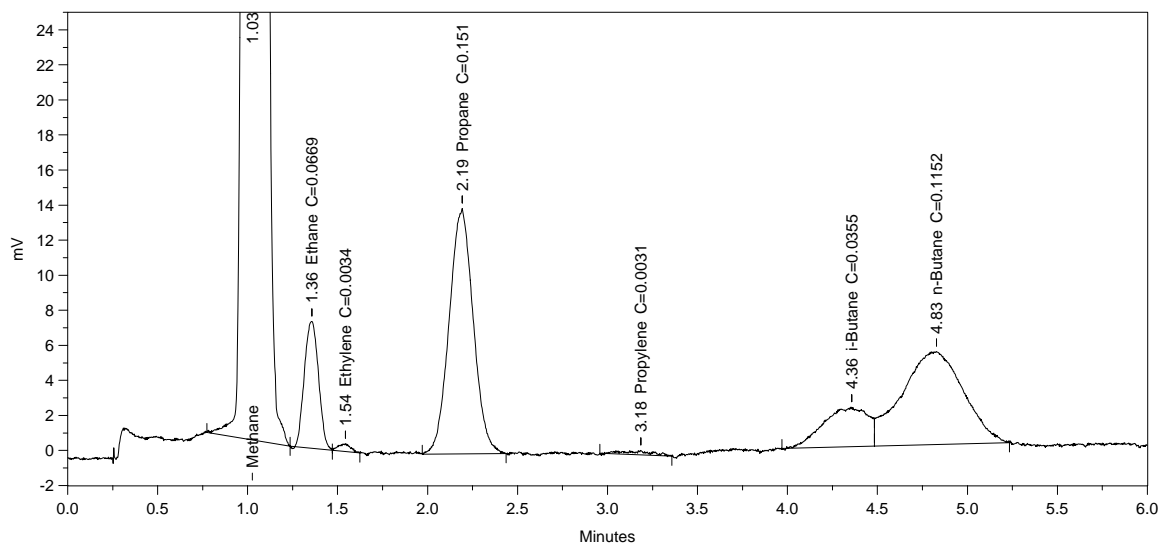
Starting Peak Width = 1.0 min. Peak Threshold = 0 Area Reject = 100

\* Some peaks have been manually integrated.

PK#	Ret Time	Name	Amount	Amount%	Area	Area%	Type	Width	Height	Height%
1	1.026	Methane	4.2667	87.261	1337091.0	70.250	BB	0.097	230275.50	82.802
2	1.356	Ethane	0.1147	2.345	67709.4	3.557	BV	0.093	12107.29	4.354
3	1.544	Ethylene	0.0022	0.046	1315.2	0.069	VB	0.077	283.29	0.102
4	2.191	Propane	0.2412	4.933	207424.4	10.898	BB	0.153	22560.54	8.112
5	3.110	Propylene	0.0015	0.030	1236.2	0.065	BB	0.126	163.62	0.059
6	4.335	i-Butane	0.0605	1.237	67126.3	3.527	BV	0.307	3644.47	1.310
7	4.823	n-Butane	0.2028	4.148	221434.0	11.634	VB	0.407	9067.63	3.261

Total Area = 1903337.0, Total Amount = 4.89, Total Height = 278102.3

\* Some peaks have been manually integrated,



Sample Name: **Site 003 Air Sample**  
 Acquired from Chrom2--Det2A via port 3 on 12/8/04 03:43:10pm by Sharon  
 04-1509  
 FID 08DCAM1F.CAL

Data File: **G:\AMDATA\04-1509\FID\152267F.01R**  
 Date Stamp: 12/8/04 04:59:48pm  
 Method File: **!C:\AMDATA\04-1509\08DCAM1F.MET**  
 Bound Version 1. Date Stamp: 12/8/04 12:06:18pm  
 Calibration File: **!C:\AMDATA\04-1509\08DCAM1F.CAL**  
 Bound Version 2. Date Stamp: 12/8/04 04:59:48pm

Run Time = 6.0 min Sample Rate = 5.0 per sec.  
 Amount Inj. = 1.000 Dilution Factor = 1.000  
 Sample Weight = 1.000 Int Std Amount = 1.000

Starting Peak Width = 1.0 min. Peak Threshold = 0 Area Reject = 100

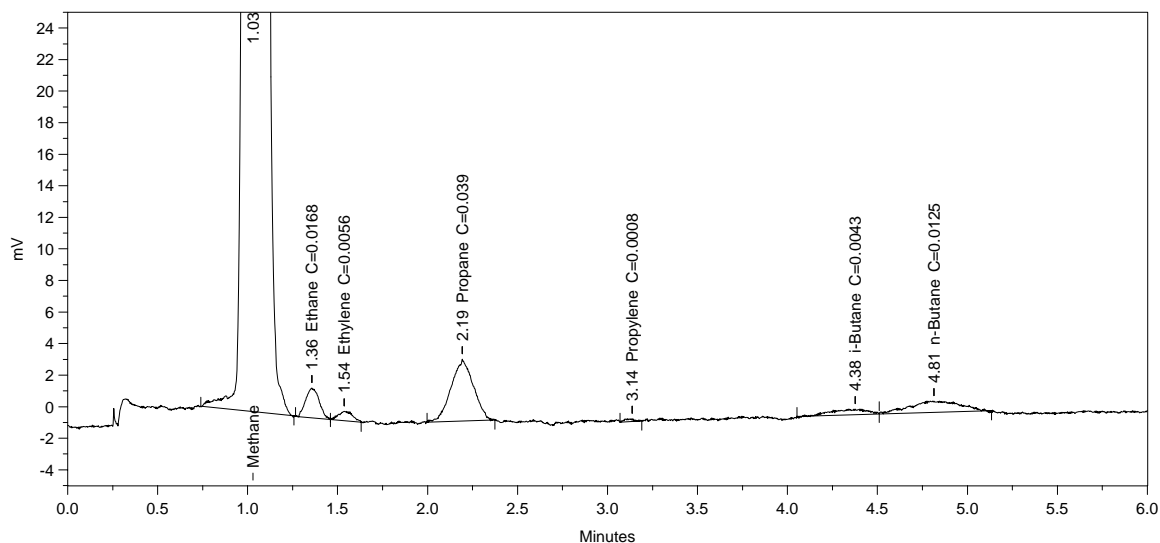
\* Some peaks have been manually integrated.

PK#	Ret Time	Name	Amount	Amount%	Area	Area%	Type	Width	Height	Height%
1	1.026	Methane	4.4311	92.196	1388635.0	80.371	BB	0.097	239395.50	89.022
2	1.356	Ethane	0.0669	1.392	39496.2	2.286	BV	0.091	7240.74	2.693
3	1.543	Ethylene	0.0034	0.071	1993.2	0.115	VB	0.076	436.12	0.162
4	2.192	Propane	0.1510	3.142	129873.9	7.517	BB	0.154	14015.90	5.212
5	3.184	Propylene	0.0031	0.064	2547.4	0.147	BB	0.159	266.80	0.099
6	4.357	i-Butane	0.0355	0.738	39397.9	2.280	BV	0.290	2262.84	0.841
7	4.827	n-Butane	0.1152	2.398	125828.2	7.283	VB	0.396	5299.99	1.971

Total Area = 1727772.0, Total Amount = 4.806, Total Height = 268917.8

\* Some peaks have been manually integrated,

Lab Air Blk



Sample Name: **Lab Air Blk**  
Acquired from Chrom2--Det2A via port 3 on 12/8/04 03:19:45pm by Sharon  
04-1509  
FID 08DCAM1F.CAL

Data File: **G:\AMDATA\04-1509\FID\152268F.01R**  
Date Stamp: 12/8/04 03:24:28pm  
Method File: **!C:\AMDATA\04-1509\08DCAM1F.MET**  
Bound Version 1. Date Stamp: 12/8/04 12:06:18pm  
Calibration File: **!C:\AMDATA\04-1509\08DCAM1F.CAL**  
Bound Version 2. Date Stamp: 12/8/04 03:24:28pm

Run Time = 6.0 min Sample Rate = 5.0 per sec.  
Amount Inj. = 1.000 Dilution Factor = 1.000  
Sample Weight = 1.000 Int Std Amount = 1.000

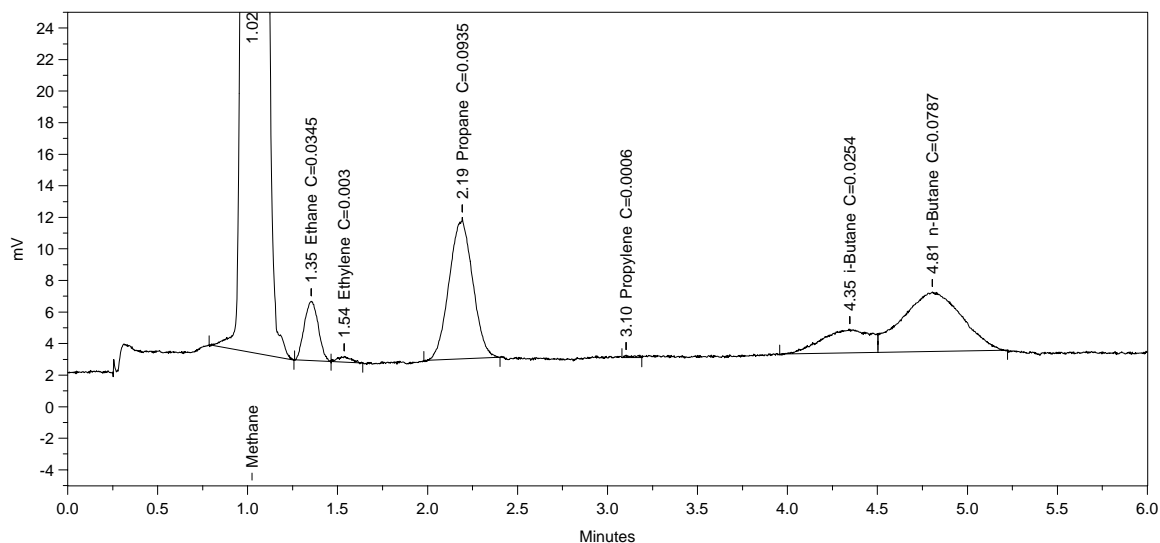
Starting Peak Width = 1.0 min. Peak Threshold = 0 Area Reject = 100

\* Some peaks have been manually integrated.

PK#	Ret Time	Name	Amount	Amount%	Area	Area%	Type	Width	Height	Height%
1	1.030	Methane	4.2652	98.182	1336641.0	95.306	BB	0.097	228638.10	96.742
2	1.356	Ethane	0.0168	0.386	9896.0	0.706	BV	0.087	1898.63	0.803
3	1.537	Ethylene	0.0056	0.129	3300.2	0.235	VB	0.093	593.49	0.251
4	2.193	Propane	0.0390	0.898	33538.9	2.391	BB	0.142	3933.22	1.664
5	3.136	Propylene	0.0008	0.019	699.4	0.050	BB	0.061	189.86	0.080
6	4.377	i-Butane	0.0043	0.099	4756.8	0.339	BV	0.219	361.73	0.153
7	4.813	n-Butane	0.0125	0.287	13637.4	0.972	VB	0.314	722.85	0.306

Total Area = 1402469.0, Total Amount = 4.344, Total Height = 236337.9

\* Some peaks have been manually integrated,



Sample Name: **Site Air In Ice Tank**  
 Acquired from Chrom2--Det2A via port 3 on 12/8/04 04:12:04pm by Sharon  
 04-1509  
 FID 08DCAM1F.CAL

Data File: **G:\AMDATA\04-1509\FID\152269F.01R**  
 Date Stamp: 12/8/04 04:51:58pm  
 Method File: **!C:\AMDATA\04-1509\08DCAM1F.MET**  
 Bound Version 1. Date Stamp: 12/8/04 12:06:18pm  
 Calibration File: **!C:\AMDATA\04-1509\08DCAM1F.CAL**  
 Bound Version 2. Date Stamp: 12/8/04 04:51:58pm

Run Time = 6.0 min Sample Rate = 5.0 per sec.  
 Amount Inj. = 1.000 Dilution Factor = 1.000  
 Sample Weight = 1.000 Int Std Amount = 1.000

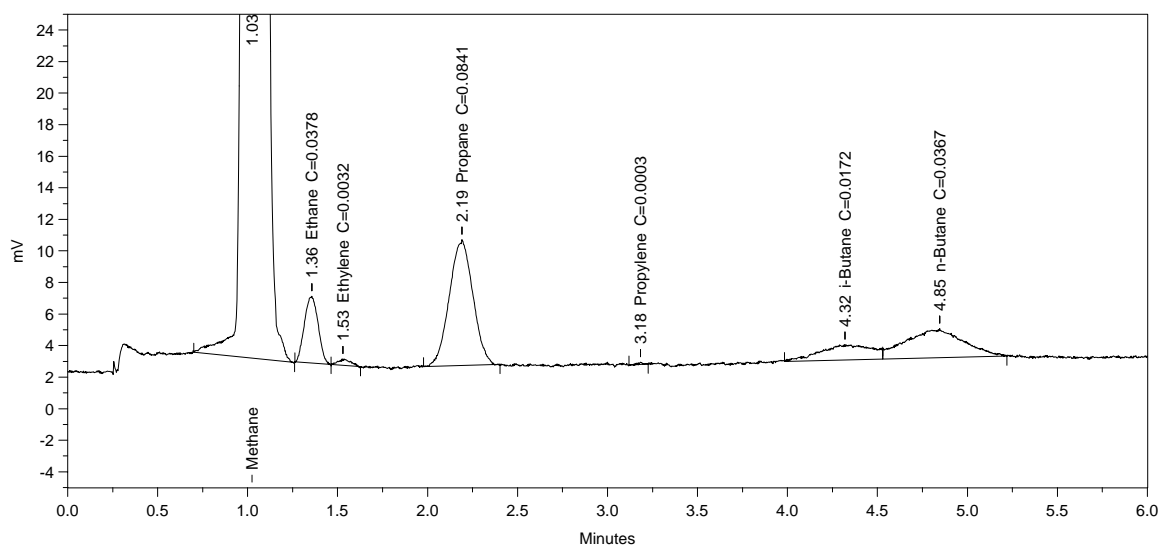
Starting Peak Width = 1.0 min. Peak Threshold = 0 Area Reject = 100

\* Some peaks have been manually integrated.

PK#	Ret Time	Name	Amount	Amount%	Area	Area%	Type	Width	Height	Height%
1	1.024	Methane	3.9336	94.347	1232723.0	85.021	BB	0.097	212670.10	91.982
2	1.353	Ethane	0.0345	0.827	20351.9	1.404	BV	0.090	3753.34	1.623
3	1.537	Ethylene	0.0030	0.073	1783.0	0.123	VB	0.081	364.78	0.158
4	2.193	Propane	0.0935	2.243	80440.0	5.548	BB	0.149	8974.32	3.881
5	3.103	Propylene	0.0006	0.014	490.7	0.034	BB	0.054	150.96	0.065
6	4.346	i-Butane	0.0254	0.608	28152.0	1.942	BV	0.310	1515.58	0.656
7	4.806	n-Butane	0.0787	1.888	85957.4	5.929	VB	0.379	3780.18	1.635

Total Area = 1449898.0, Total Amount = 4.169, Total Height = 231209.3

\* Some peaks have been manually integrated,



Sample Name: **Air In Oil Storage Area**  
 Acquired from Chrom2--Det2A via port 3 on 12/8/04 04:32:17pm by Sharon  
 04-1509  
 FID 08DCAM1F.CAL

Data File: **G:\AMDATA\04-1509\FID\152270F.01R**  
 Date Stamp: 12/8/04 04:49:38pm  
 Method File: **!C:\AMDATA\04-1509\08DCAM1F.MET**  
 Bound Version 1. Date Stamp: 12/8/04 12:06:18pm  
 Calibration File: **!C:\AMDATA\04-1509\08DCAM1F.CAL**  
 Bound Version 2. Date Stamp: 12/8/04 04:49:38pm

Run Time = 6.0 min Sample Rate = 5.0 per sec.  
 Amount Inj. = 1.000 Dilution Factor = 1.000  
 Sample Weight = 1.000 Int Std Amount = 1.000

Starting Peak Width = 1.0 min. Peak Threshold = 0 Area Reject = 100

\* Some peaks have been manually integrated.

PK#	Ret Time	Name	Amount	Amount%	Area	Area%	Type	Width	Height	Height%
1	1.025	Methane	4.2441	95.949	1330029.0	89.513	BB	0.098	226505.70	93.566
2	1.356	Ethane	0.0378	0.854	22293.1	1.500	BV	0.088	4238.68	1.751
3	1.530	Ethylene	0.0032	0.073	1897.4	0.128	VB	0.077	409.13	0.169
4	2.191	Propane	0.0841	1.901	72324.6	4.868	BB	0.151	7984.45	3.298
5	3.183	Propylene	0.0003	0.006	214.4	0.014	BB	0.026	139.28	0.058
6	4.320	i-Butane	0.0172	0.388	19051.5	1.282	BV	0.329	963.91	0.398
7	4.847	n-Butane	0.0367	0.829	40038.8	2.695	VB	0.363	1838.93	0.760

Total Area = 1485849.0, Total Amount = 4.423, Total Height = 242080.1

\* Some peaks have been manually integrated,



# Exploration Technologies, Inc.

7755 Synott Rd., Houston, TX 77083; Tel (281) 530-4300; Fax: (281) 530-4308

## 04 - 1509 Oil In Ice Project

CRREL - Hanover, NH.

TABLE 2  
LIGHT C1-C4 HYDROCARBONS (ppmv) in ICE CORES

SAMPLE NO.	RUN	BAR CODE	METHANE	ETHANE	ETHYLENE	PROPANE	PROPYLENE	I-BUTANE	N-BUTANE	
<b>GC1 - Control, NE Corner of Tank, Bills Control Area</b>										
C-A	48.0mm	1	140921	4.423	0.022	0.021	0.155	0.000	0.052	0.100
C-A	48.0mm	2	140921	4.422	0.024	0.021	0.156	0.000	0.048	0.103
C-A	48.0mm	3	140921	4.423	0.023	0.021	0.158	0.000	0.049	0.102
C-B	40.5mm	1	140922	4.304	0.026	0.032	0.187	0.004	0.060	0.115
C-B	40.5mm	2	140922	4.351	0.026	0.031	0.186	0.003	0.057	0.118
C-B	40.5mm	3	140922	4.402	0.024	0.030	0.185	0.003	0.064	0.121
C-C	43.0mm	1	140923	4.434	0.039	0.045	0.229	0.005	0.064	0.101
C-C	43.0mm	2	140923	4.427	0.037	0.046	0.228	0.005	0.064	0.106
C-C	43.0mm	3	140923	4.444	0.035	0.045	0.232	0.003	0.062	0.099
C-D	33.6mm	1	140924	4.477	0.093	0.022	0.276	0.003	0.082	0.159
C-D	33.6mm	2	140924	4.552	0.096	0.023	0.276	0.003	0.082	0.165
C-D	33.6mm	3	140924	4.474	0.092	0.022	0.273	0.002	0.085	0.167
C-E	42.5mm	1	140925	4.625	0.149	0.030	0.381	0.012	0.101	0.210
C-E	42.5mm	2	140925	4.586	0.150	0.029	0.381	0.011	0.102	0.213
C-E	42.5mm	3	140925	4.154	0.148	0.029	0.360	0.009	0.108	0.212
C-F	46.5mm	1	140926	4.113	0.179	0.002	0.375	0.000	0.113	0.305
C-F	46.5mm	2	140926	4.075	0.179	0.006	0.372	0.000	0.111	0.307
C-F	46.5mm	3	140926	4.043	0.180	0.002	0.370	0.007	0.108	0.301
<b>GC2 - Inside Hoop 1-3</b>										
1-3A	49.8mm	1	140930	4.024	0.028	0.022	0.155	0.000	0.075	0.152
1-3A	49.8mm	2	140930	4.093	0.026	0.020	0.158	0.005	0.072	0.156
1-3B	43.0mm	1	140931	4.171	0.024	0.017	0.159	0.000	0.064	0.123
1-3B	43.0mm	2	140931	4.165	0.027	0.022	0.155	0.000	0.067	0.128
1-3B	43.0mm	3	140931	4.091	0.026	0.015	0.152	0.000	0.059	0.116
1-3C	52.8mm	1	140932	5.372	4.103	0.031	23.940	0.009	12.411	40.157
1-3C	52.8mm	2	140932	5.304	4.087	0.037	23.861	0.008	12.469	39.686
1-3C	52.8mm	3	140932	5.386	4.088	0.040	23.900	0.013	12.405	40.049
1-3D*	56.5mm	1	140933	6.749	41.733	0.147	263.935	0.000	147.378	482.920
<b>GC3 - Outside Hoop 2-3 NE Corner</b>										
2-3B	48.0mm	1	140928	4.045	0.021	0.013	0.142	0.000	0.063	0.124
2-3B	48.0mm	2	140928	4.023	0.024	0.015	0.141	0.000	0.061	0.131
2-3B	48.0mm	3	140928	4.029	0.021	0.013	0.140	0.000	0.059	0.130
2-3C	58.6mm	1	140929	3.993	0.176	0.005	1.377	0.000	0.937	3.134
2-3C	58.6mm	2	140929	3.912	0.163	0.008	1.358	0.000	0.915	3.110
2-3C	58.6mm	3	140929	3.897	0.164	0.003	1.356	0.000	0.956	3.078

\* = Encapsulated Oil Bubble



# Exploration Technologies, Inc.

7755 Synott Rd., Houston, TX 77083; Tel (281) 530-4300; Fax: (281) 530-4308

## 04 - 1509 Oil In Ice Project

CRREL - Hanover, NH.

TABLE 3  
LIGHT C1-C4 HYDROCARBONS (ppmv)

SAMPLE NO.	METHANE	ETHANE	PROPANE	I-BUTANE	N-BUTANE
<b>Oil Products - Before Injection Under the Ice</b>					
Site #0	610.918	4576.170	26190.896	13718.243	35846.176
Site #1	479.290	4302.999	25211.492	13278.614	34957.152
Site #2	570.864	4631.730	26366.154	13794.865	36028.824
Site #3	561.758	5184.273	29213.242	15594.613	39145.070
Site #4	469.164	4810.876	27963.973	14973.289	38070.621
Site #5	639.416	5279.375	29100.705	15323.624	38607.133
<b>Oil Samples - Collected from Skirts Under the Ice</b>					
OC5	198.136	3222.091	17322.310	8780.723	23067.020
OC6	155.044	3279.003	16180.620	8220.811	20733.780

\* = Encapsulated Oil Bubble



# Exploration Technologies, Inc.

7755 Synott Rd., Houston, TX 77083; Tel: (281) 530-4300; Fax: (281) 530-4308

## 04 - 1509 Oil In Ice Project

CRREL - Hanover, NH.

TABLE 4  
LIGHT C1-C4 HYDROCARBONS (ppmv) - WATER HEADSPACE

SAMPLE NO.	SERIAL NO.	METHANE	ETHANE	PROPANE	I-BUTANE	N-BUTANE
<b>Water Samples Collected Under Ice After Field Testing</b>						
W-1	15cm SERIAL AH 361478 LO	13.501	32.900	66.636	14.049	32.189
W-2	15cm SERIAL AH 361380 LO	15.894	33.021	60.472	11.672	27.749
W-3	20cm SERIAL AH 361393 LO	11.086	23.197	43.746	9.330	20.504
W-4	17cm SERIAL AH 361320 LO	13.058	35.692	79.819	15.819	36.304
*W-5	23cm SERIAL AH 361465 LO	2.684	0.072	0.053	0.018	0.044
W-6	42cm SERIAL AH 361441 LO	13.476	25.717	46.786	8.816	21.016

\* = Water leaked out of sample.



# Exploration Technologies, Inc.

7755 Synott Rd., Houston, TX 77083; Tel (281) 530-4300; Fax: (281) 530-4308

## 04 - 1509 Oil In Ice Project

CRREL - Hanover, NH.

TABLE 5  
LIGHT C1-C4 HYDROCARBONS (ppmv), HELIUM (ppmv), & HYDROGEN (ppmv)

SAMPLE NO.		METHANE	ETHANE	ETHYLENE	PROPANE	PROPYLENE	I-BUTANE	N-BUTANE	HELIUM	HYDROGEN
A1-SE	8m	4.096	0.061	0.013	0.479	0.006	0.296	0.992	46.478	10.143
A2-SW	30m	4.061	0.112	0.004	0.868	0.000	0.503	1.583	48.741	8.438
A3-NW	30m	4.111	0.090	0.006	0.723	0.000	0.423	1.347	49.476	8.560
A4-NE	8m	4.094	0.137	0.005	1.034	0.000	0.596	1.838	48.249	6.466



# Exploration Technologies, Inc.

7755 Synott Rd., Houston, TX 77083 (281) 530-4300 Fax: (281) 530-4308

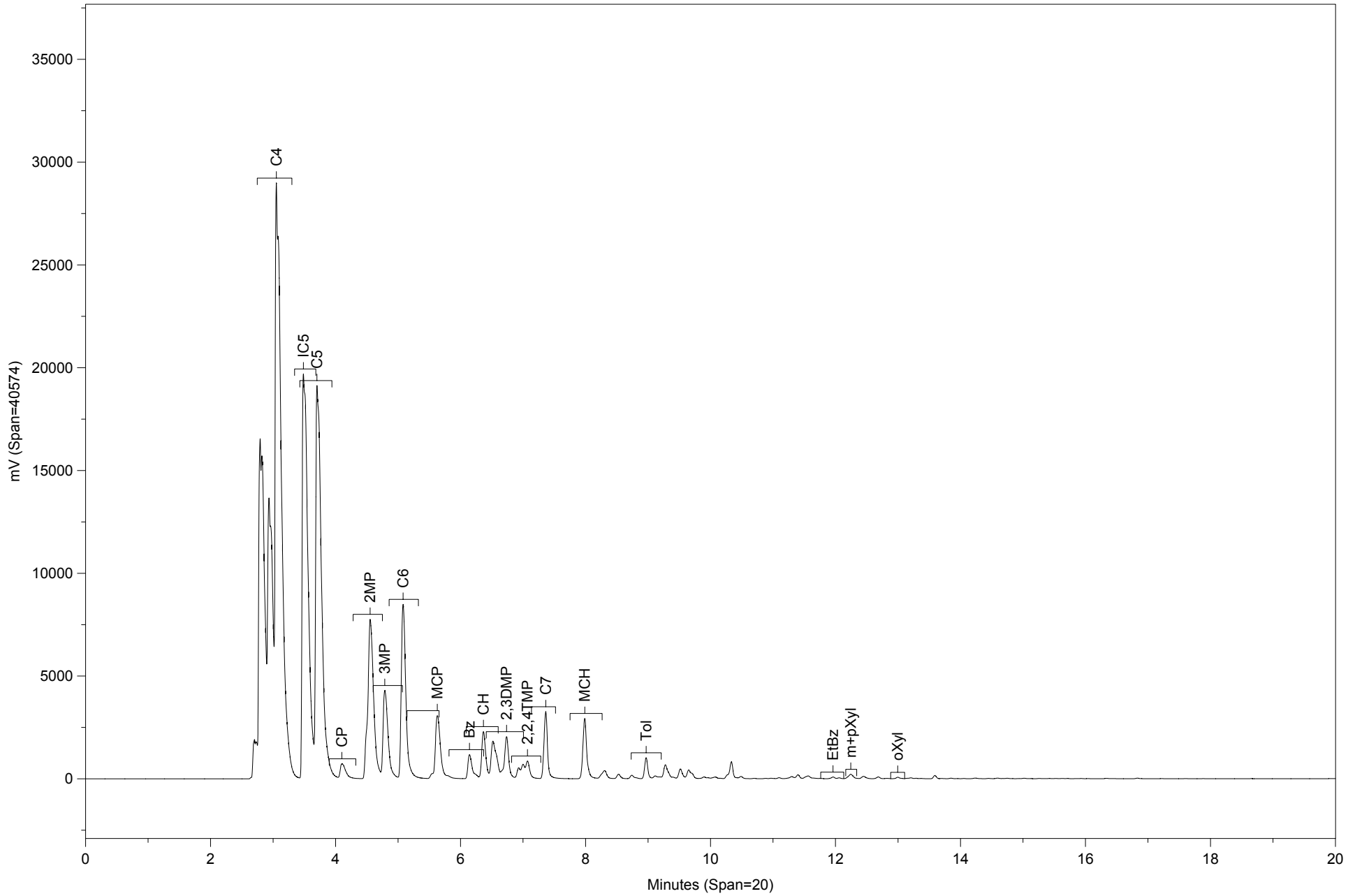
## 04 - 1509 Oil In Ice Project

CRREL - Hanover, NH.

TABLE 6  
C5+ GASOLINE RANGE HYDROCARBONS (ppmv) in HEADSPACE SAMPLES

SAMPLE NO.		IC5	NC5	CP	2-MP	3-MP	C6	MCP	BZ	CH	2,3-DMP	2,2,4-TMP	C7	MCH	TOL	EB	m,p-XYL	o-XYL
<b>Oil Samples - Collected from Skirts Under the Ice</b>																		
OC5	Site 5	10327.990	8922.855	322.769	5463.967	2359.610	4503.908	1381.496	353.777	802.191	713.952	324.106	1148.827	826.078	215.864	14.666	78.484	22.594
OC6	Site 6	9833.368	8315.837	439.975	5270.938	2274.738	4375.005	1355.641	384.535	814.135	724.639	354.573	1253.022	859.410	238.441	23.449	95.139	28.567
<b>Water Samples Collected Under Ice After Field Testing</b>																		
W-1	SERIAL AH 361478	7.031	3.672	0.217	7.656	2.776	0.182	5.355	0.367	6.097	3.293	0.647	0.000	6.065	0.000	0.536	0.028	0.125
W-2	SERIAL AH 361380	10.158	4.877	0.185	10.168	5.042	0.214	4.899	0.492	4.226	6.052	2.139	0.000	8.244	0.090	0.789	0.289	0.149
W-3	SERIAL AH 361393	7.535	3.632	0.187	5.171	1.936	0.147	2.894	0.389	3.209	2.107	0.805	0.000	3.124	0.000	0.328	0.023	0.061
W-4	SERIAL AH 361320	10.145	5.230	0.204	6.318	2.182	0.201	3.803	0.474	4.158	2.325	0.885	0.091	3.457	0.087	0.234	0.026	0.091
W-6	SERIAL AH 361441	6.442	4.126	0.278	4.109	1.423	0.227	2.129	0.690	2.448	1.649	0.568	0.078	2.290	0.111	0.305	0.312	0.066

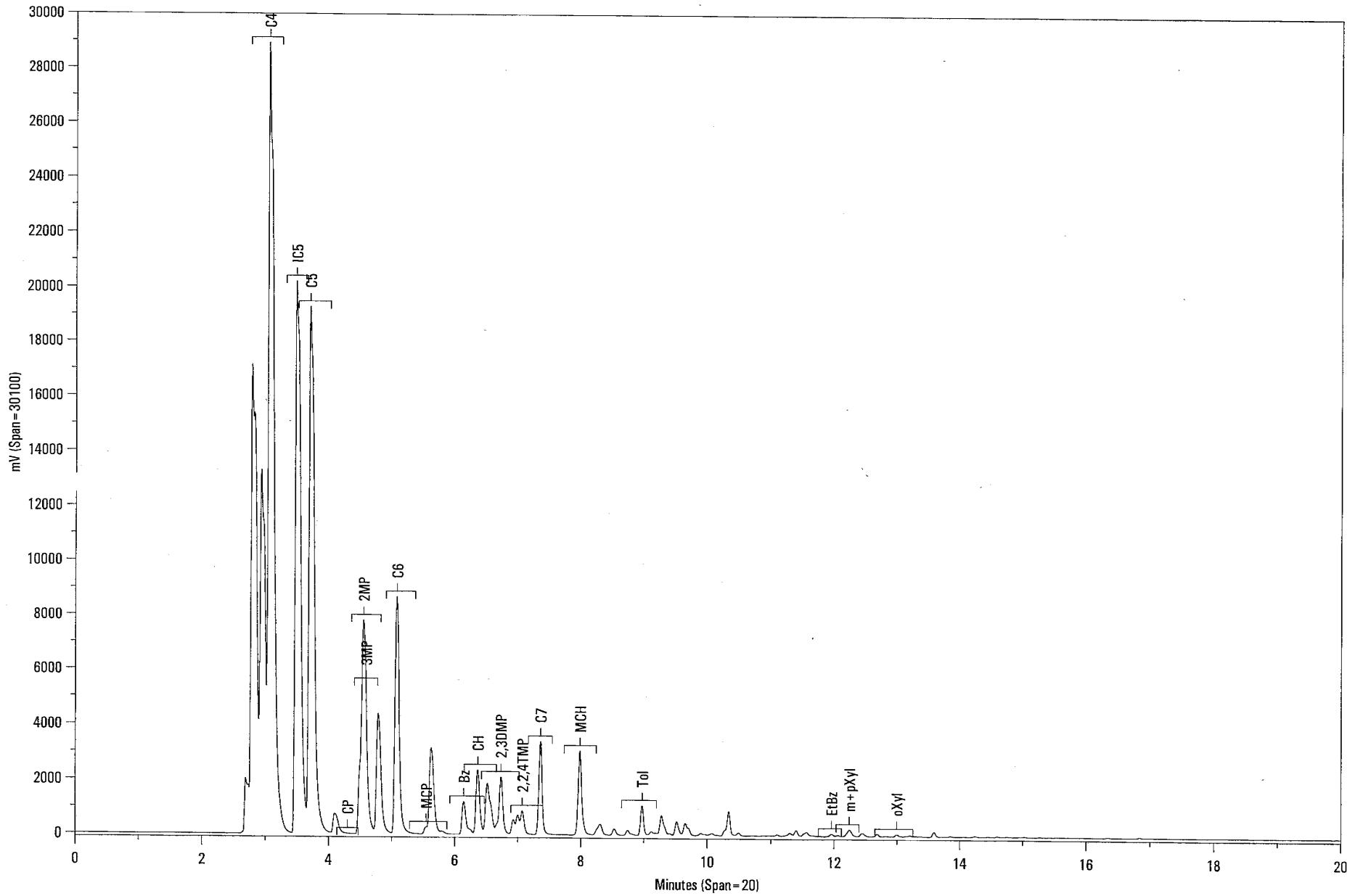
\* = Encapsulated Oil Bubble

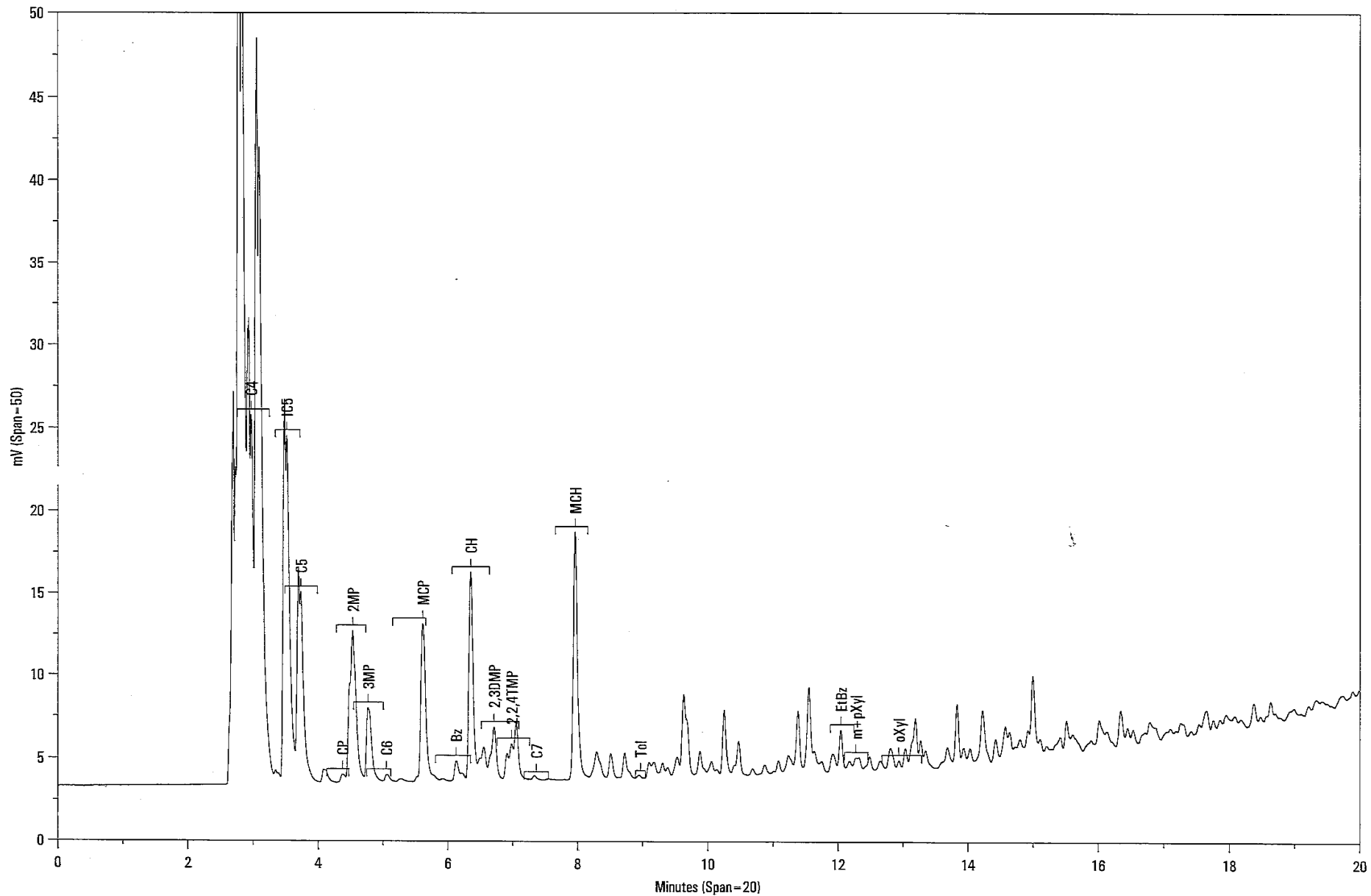


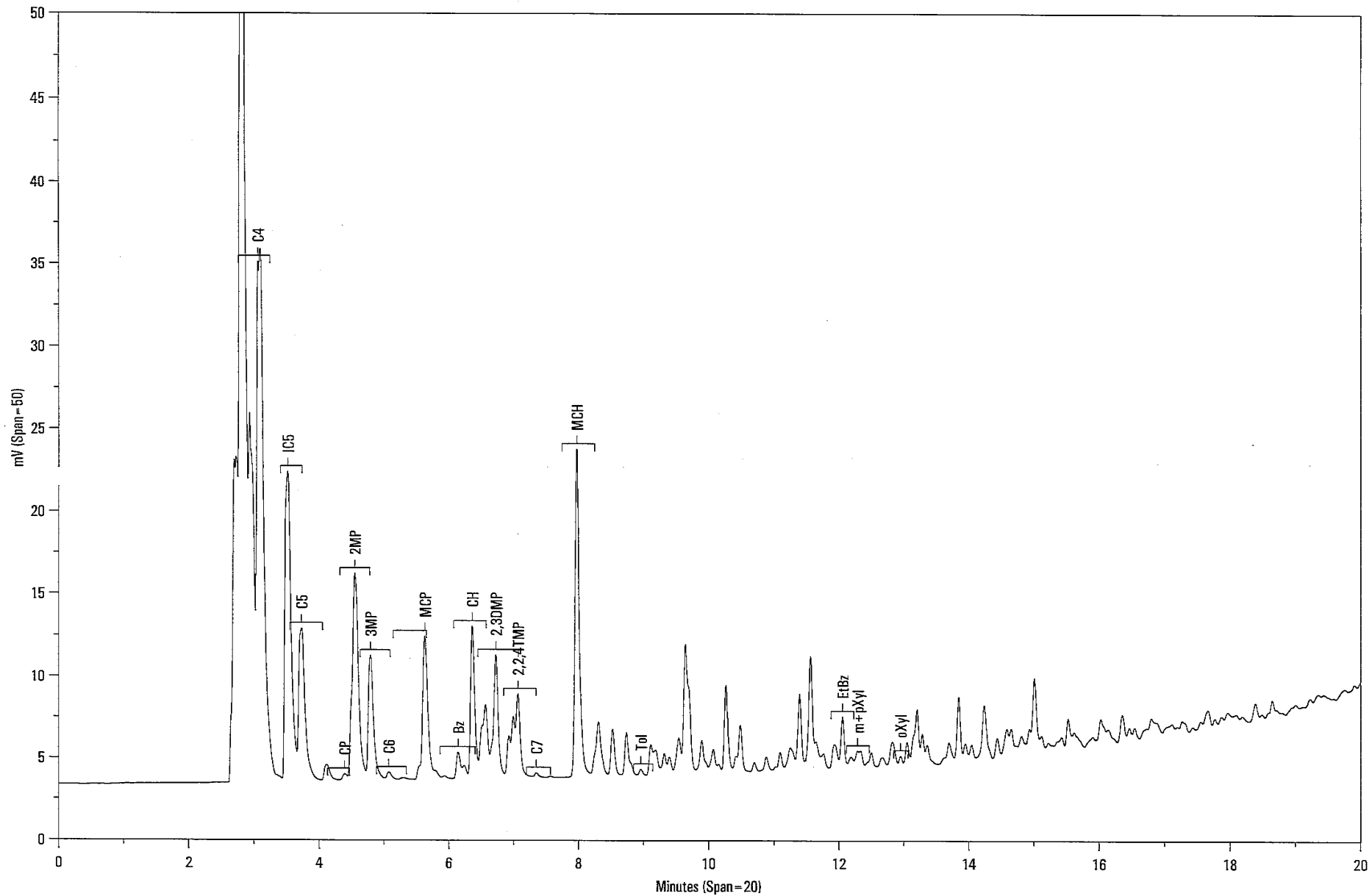
Site 6 500ul (non cryo)

Site 6 500ul (non cryo)

C:\HPDATA\04-1509\FID\140906.01R

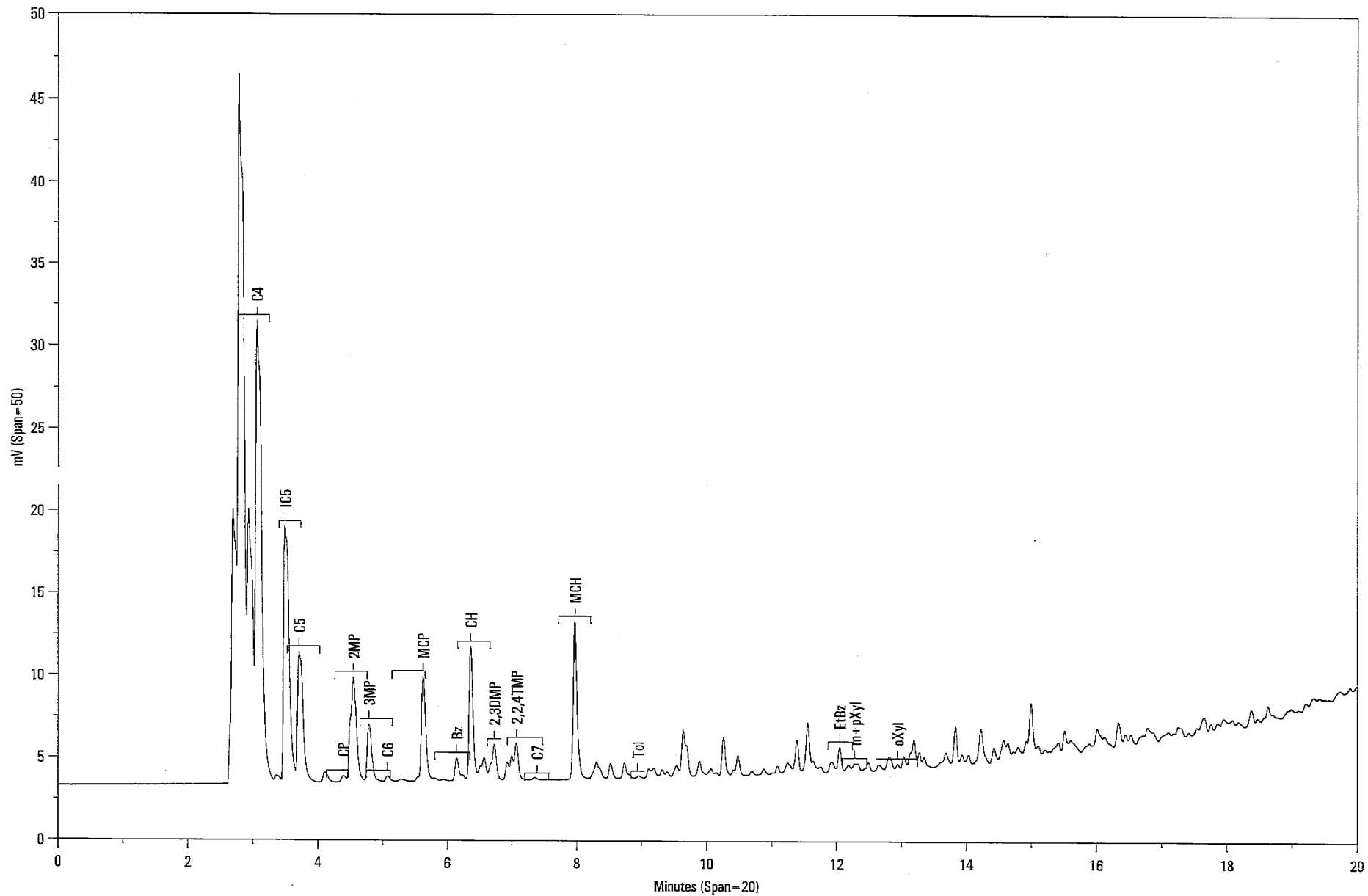


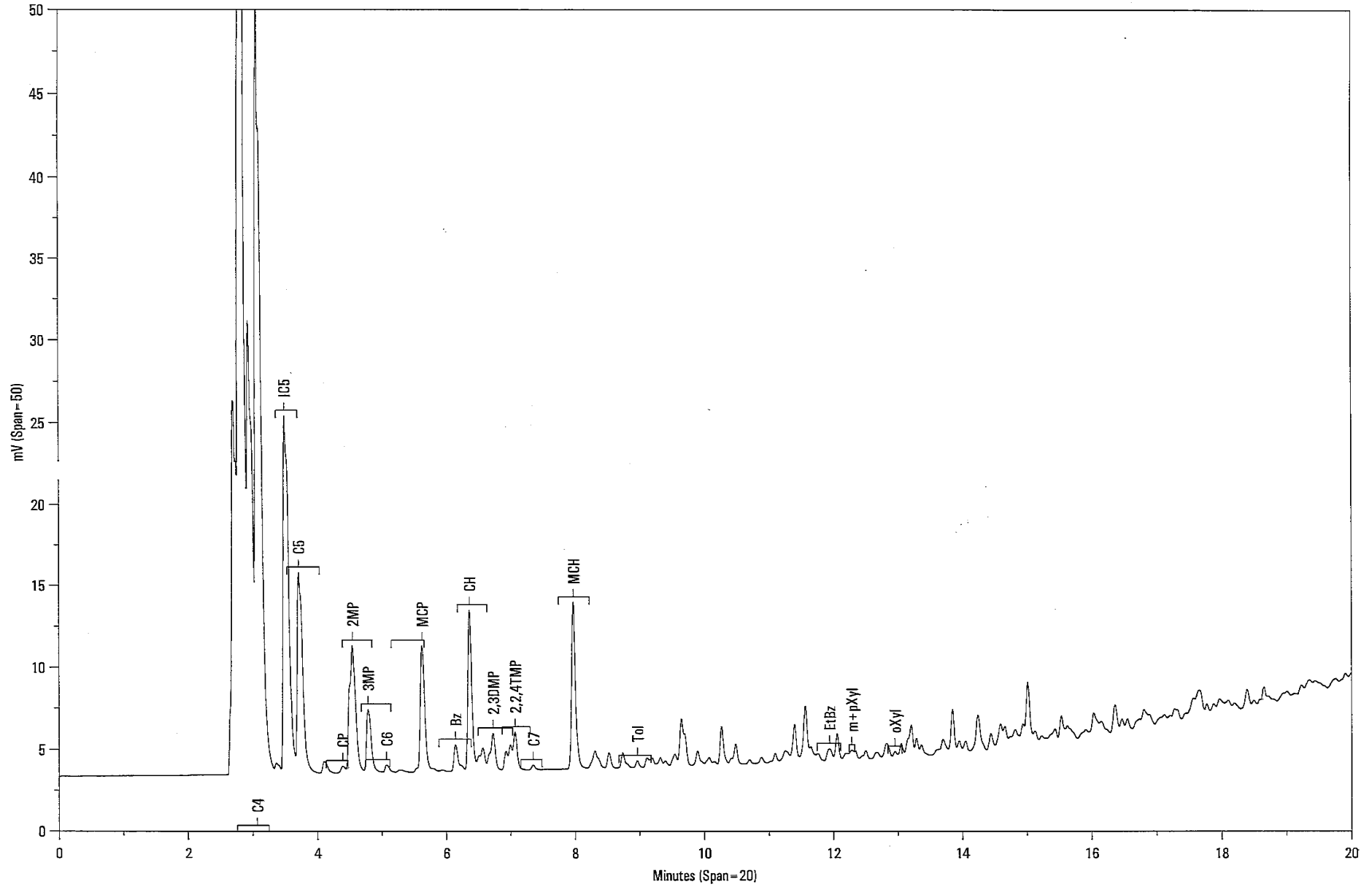


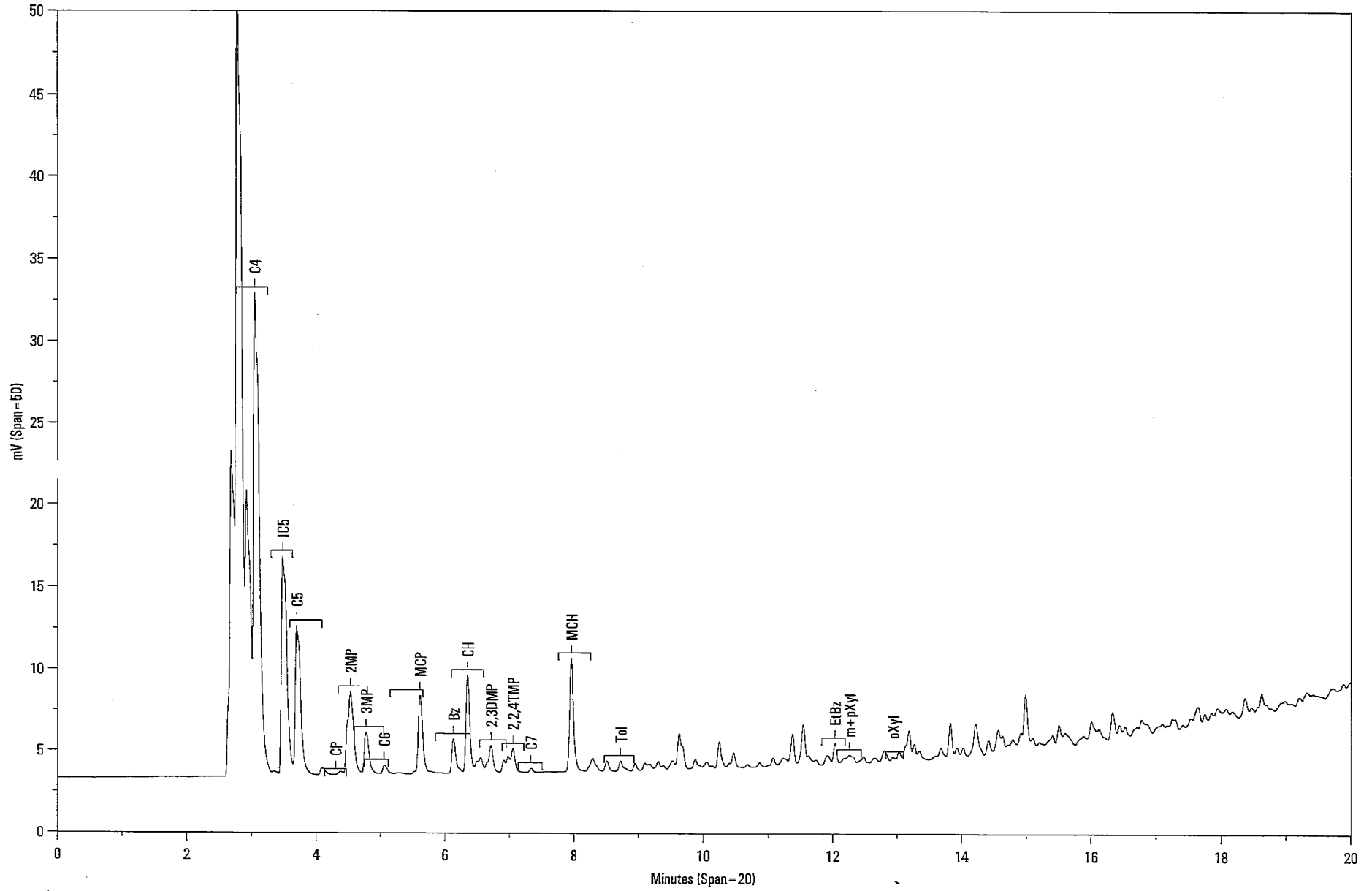


Serial AH361393 500ul (non cryo)

C:\HPDATA\04-1509\FID\140938.01R







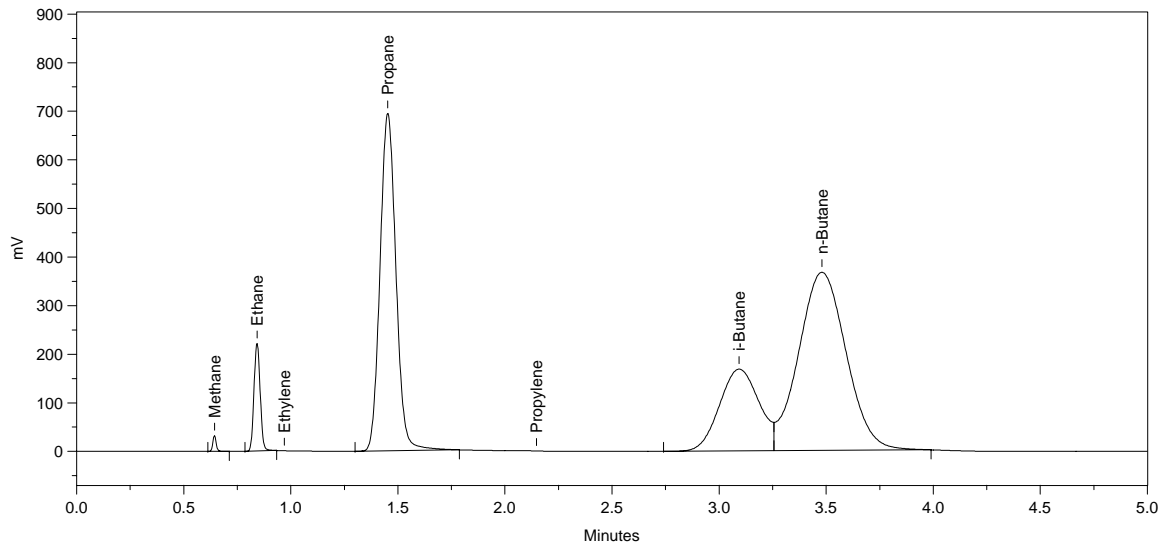


<b>04-1509B Oil in Ice Detection</b>								
<b>Amounts in P.P.M.:</b>								
<b>File name</b>	<b>Sample Name</b>	<b>Methane</b>	<b>Ethane</b>	<b>Ethylene</b>	<b>Propane</b>	<b>Propylene</b>	<b>i-Butane</b>	<b>n-Butane</b>
140895	Site 5 (1/10cc)	639.416	5279.375	0.000	29100.705	0.000	15323.624	38607.133
140894	Site 4 (1/10cc)	469.164	4810.876	0.000	27963.973	0.000	14973.289	38070.621
140891	Site 3 (1/10cc)	561.758	5184.273	0.000	29213.242	0.000	15594.613	39145.070
140892	Site 2 (1/10cc)	570.864	4631.730	0.000	26366.154	0.000	13794.865	36028.824
140889	Site 1 (1/10cc)	479.290	4302.999	0.000	25211.492	0.000	13278.614	34957.152
140888	Site 0 (1/10cc)	610.918	4576.170	0.000	26190.896	0.000	13718.243	35846.176



C5+ Components		Summary	Table											
Sample Name	C4	IC5	C5	CP	C6	MCP	Bz	CH	C7	MCH	Tol	EtBz	m+pXyl	oXyl
Site 0 500ul	29197.860	11562.380	10464.790	0.000	5613.818	1745.738	481.012	974.558	1655.332	1049.497	282.237	28.619	112.278	34.016
Site 1 500ul	29144.040	11695.170	10130.600	0.000	5370.652	1700.069	420.673	964.225	1595.656	1045.853	287.148	30.438	124.726	37.685
Site 3 500ul	19938.420	11630.330	10298.160	0.000	5362.421	1661.048	455.802	923.635	1504.023	961.844	258.032	25.563	99.958	30.482
Site 2 500ul	29689.080	11441.180	10350.550	0.000	5381.632	1653.629	401.313	918.746	1538.354	975.560	260.191	26.358	103.545	32.662
Site 4 500ul	21271.380	11496.810	10384.950	0.000	5486.882	1701.992	472.234	947.609	1623.494	1030.351	281.741	28.987	115.380	35.676
Site 5 500ul	23348.540	11428.250	10490.560	0.000	5392.491	1627.221	448.308	898.801	1508.844	945.893	250.332	24.656	95.071	29.306

Site 0 (1/10cc)



Sample Name: **Site 0 (1/10cc)**

Acquired from Chrom1--Det1A via port 1 on 10/21/04 03:08:02pm by Sharon

4-1509 B

Range -9

Data File: **F:\D2DATA\4-1509B\140888.02R**

Method File: **!C:\D2DATA\4-1509B\23JND22.MET**

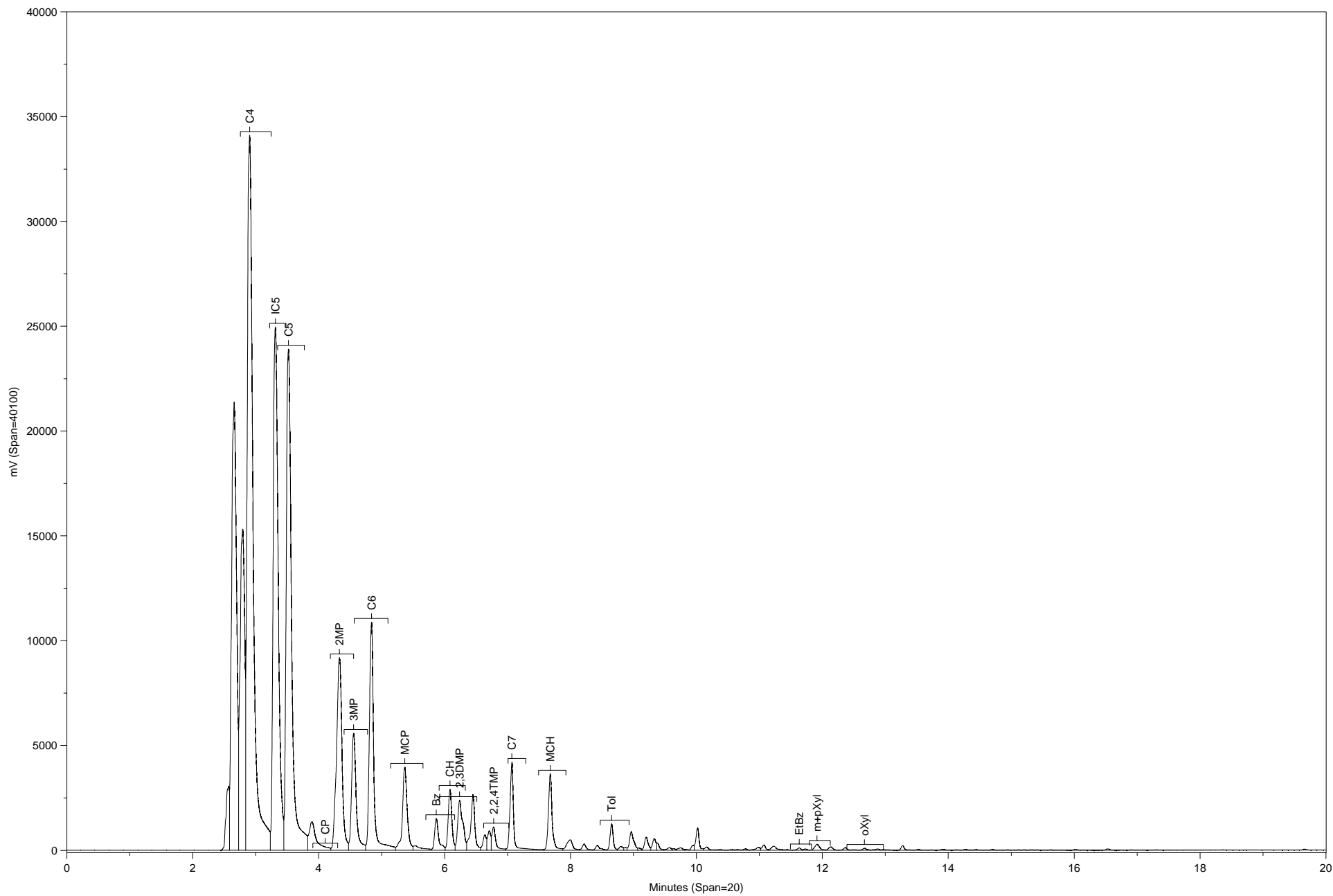
Calibration File: **!C:\D2DATA\4-1509B\23JND22.CAL**

\* Some peaks have been manually integrated.

PK#	Ret Time	Name	Amount	Amount%	Area	Area%	Type	Width	Height	Height%
1	0.643	Methane	610.9181	0.755	35761.6	0.301	BB	0.018	32284.55	2.175
2	0.842	Ethane	4576.1700	5.654	446649.1	3.755	BB	0.034	222133.90	14.968
3	1.453	Propane	26190.9000	32.357	3585137.0	30.142	BB	0.086	694524.90	46.799
4	3.094	i-Butane	13718.2400	16.948	2174223.0	18.280	BV	0.215	168381.00	11.346
5	3.480	n-Butane	35846.1800	44.286	5652512.0	47.523	VB	0.257	366742.80	24.712

Total Area = 11894280.0, Total Amount = 80942.41, Total Height = 1484067.0

\* Some peaks have been manually integrated.





Sample Name: **Site 0 500ul (non cryo)**  
Acquired from HP2--FID via port 2 on 10/21/04 02:48:29pm by Sharon  
F17DEC.MET  
F17DEC.CAL

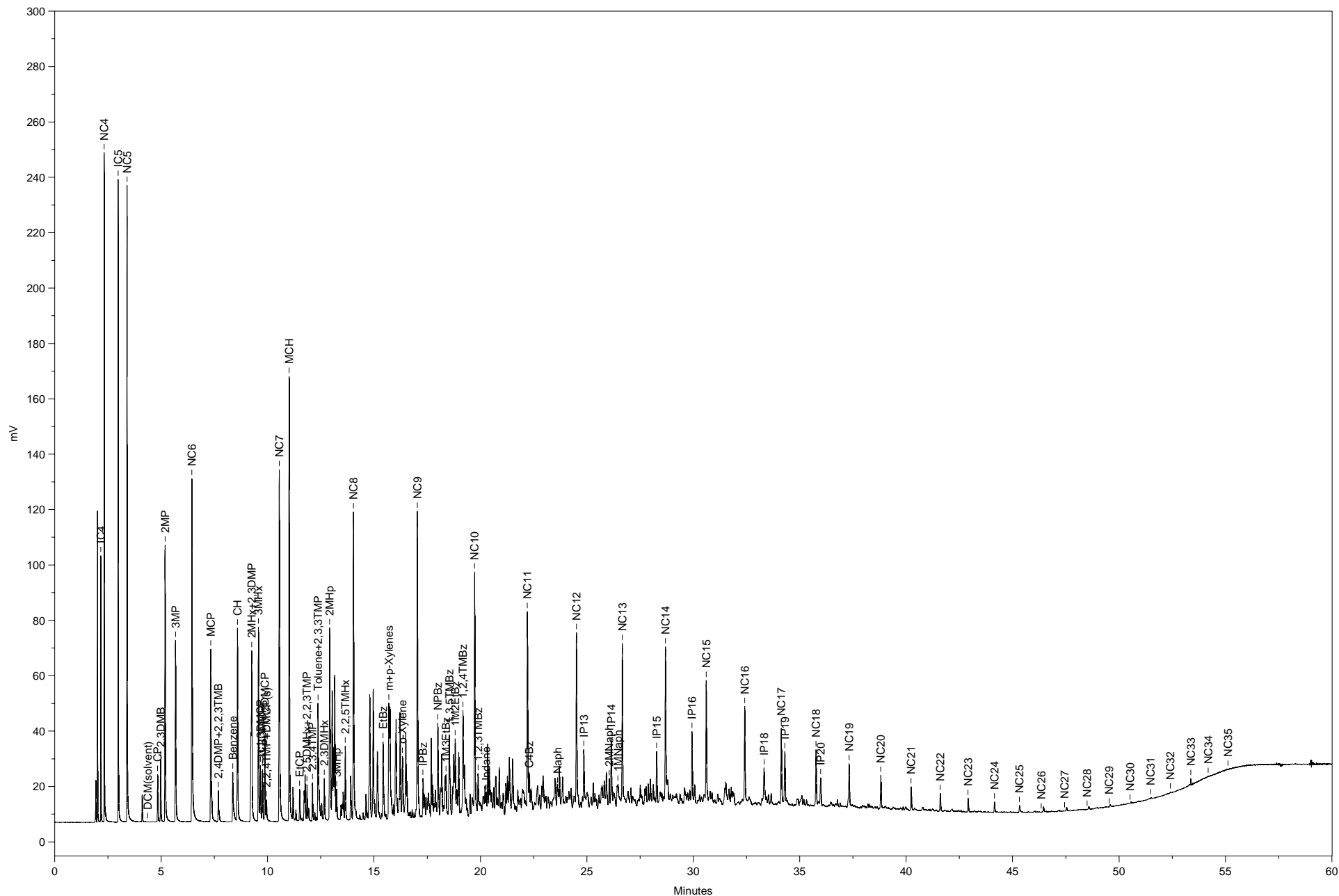
Data File: **E:\HPDATA\4-1509B\FID\140888F.01R**  
Method File: **!E:\HPDATA\4-1509B\F17DEC.MET**  
Calibration File: **!E:\HPDATA\4-1509B\F17DEC.CAL**

PK#	Ret Time	Name	Amount	Amount%	Area	Area%	Type	Width	Height	Height%
1	2.570		0.0000	0.000	11331340.0	1.120	BV	0.062	3063962.00	1.669
2	2.658		0.0000	0.000	116747600.0	11.538	VV	0.09121392170.00	11.649	
3	2.793		0.0000	0.000	79061070.0	7.813	VV	0.08615318900.00	8.342	
4	2.904 C4		29197.8600	39.560	222777200.0	22.016	VV	0.10934100850.00	18.570	
5	3.312 IC5		11562.3800	15.666	140240000.0	13.859	VV	0.09424955750.00	13.590	
6	3.520 C5		10464.7900	14.179	143082000.0	14.140	VV	0.10023907220.00	13.019	
7	3.891		0.0000	0.000	11150730.0	1.102	VV	0.137	1355808.00	0.738
8	4.330 2MP		6173.2040	8.364	55790340.0	5.514	VV	0.101	9190734.00	5.005
9	4.554 3MP		2935.5940	3.977	28766450.0	2.843	VV	0.086	5580726.00	3.039
10	4.839 C6		5613.8180	7.606	52294940.0	5.168	VV	0.08010882210.00	5.926	
11	5.367 MCP		1745.7380	2.365	20830580.0	2.059	VV	0.087	3968188.00	2.161
12	5.532		0.0000	0.000	1966402.0	0.194	VV	0.154	213502.10	0.116
13	5.868 Bz		481.0121	0.652	7053436.0	0.697	VV	0.078	1514340.00	0.825
14	6.086 CH		974.5579	1.320	11869010.0	1.173	VV	0.068	2904377.00	1.582
15	6.239 2,3DMP		1012.2690	1.372	13421580.0	1.326	VV	0.094	2383303.00	1.298
16	6.452		0.0000	0.000	12258050.0	1.211	VV	0.077	2648604.00	1.442
17	6.638		0.0000	0.000	2781584.0	0.275	VV	0.063	740489.60	0.403
18	6.708		0.0000	0.000	3220754.0	0.318	VV	0.058	926757.40	0.505
19	6.778 2,2,4TMP		483.7660	0.655	4872716.0	0.482	VV	0.073	1106681.00	0.603
20	7.069 C7		1655.3320	2.243	16649830.0	1.645	VV	0.066	4194477.00	2.284
21	7.679 MCH		1049.4970	1.422	15087580.0	1.491	VV	0.069	3640758.00	1.983
22	7.996		0.0000	0.000	3345559.0	0.331	VV	0.111	500797.70	0.273
23	8.214		0.0000	0.000	1373522.0	0.136	VV	0.077	295479.00	0.161
24	8.425		0.0000	0.000	1152165.0	0.114	VV	0.083	231589.70	0.126
25	8.653 Tol		282.2368	0.382	4320087.0	0.427	VV	0.057	1257464.00	0.685
26	8.801		0.0000	0.000	777297.0	0.077	VV	0.071	183525.70	0.100
27	8.865		0.0000	0.000	400041.3	0.040	VV	0.051	129542.00	0.071
28	8.965		0.0000	0.000	4160051.0	0.411	VV	0.079	882571.80	0.481
29	9.081		0.0000	0.000	345166.2	0.034	VV	0.053	108803.30	0.059
30	9.202		0.0000	0.000	2592997.0	0.256	VV	0.069	628222.80	0.342
31	9.330		0.0000	0.000	2149303.0	0.212	VV	0.064	557126.90	0.303
32	9.376		0.0000	0.000	960467.1	0.095	VV	0.046	346321.80	0.189
33	9.571		0.0000	0.000	588280.6	0.058	VV	0.077	127205.80	0.069
34	9.638		0.0000	0.000	234697.4	0.023	VV	0.053	73830.23	0.040
35	9.751		0.0000	0.000	615277.8	0.061	VV	0.088	117189.70	0.064

PK#	Ret Time	Name	Amount	Amount%	Area	Area%	Type	Width	Height	Height%
36	9.824		0.0000	0.000	114795.6	0.011	VV	0.051	37348.80	0.020
37	9.944		0.0000	0.000	712756.7	0.070	VV	0.050	238667.10	0.130
38	10.018		0.0000	0.000	3750922.0	0.371	VV	0.059	1058063.00	0.576
39	10.162		0.0000	0.000	742625.4	0.073	VV	0.081	153618.30	0.084
40	10.371		0.0000	0.000	181064.9	0.018	VV	0.086	35185.16	0.019
41	10.488		0.0000	0.000	26335.5	0.003	VV	0.039	11146.96	0.006
42	10.557		0.0000	0.000	130764.9	0.013	VV	0.070	31004.24	0.017
43	10.648		0.0000	0.000	172937.5	0.017	VV	0.079	36290.19	0.020
44	10.776		0.0000	0.000	261144.5	0.026	VV	0.063	68544.23	0.037
45	10.981		0.0000	0.000	706724.6	0.070	VV	0.083	141671.00	0.077
46	11.071		0.0000	0.000	954759.7	0.094	VV	0.064	247897.10	0.135
47	11.230		0.0000	0.000	1196246.0	0.118	VV	0.105	189435.30	0.103
48	11.434		0.0000	0.000	133047.8	0.013	VV	0.086	25743.95	0.014
49	11.633 EtBz		28.6190	0.039	455044.2	0.045	VV	0.069	110317.50	0.060
50	11.729		0.0000	0.000	228251.1	0.023	VV	0.064	59306.62	0.032
51	11.914 m+pXyl		112.2779	0.152	1561808.0	0.154	VV	0.093	279142.00	0.152
52	12.131		0.0000	0.000	790796.9	0.078	VV	0.084	157502.80	0.086
53	12.365		0.0000	0.000	493081.4	0.049	VV	0.068	120517.40	0.066
54	12.493		0.0000	0.000	151659.5	0.015	VV	0.105	24128.94	0.013
55	12.667 oXyl		34.0155	0.046	422521.3	0.042	VV	0.074	95223.43	0.052
56	12.879		0.0000	0.000	320876.3	0.032	VV	0.090	59363.61	0.032
57	12.962		0.0000	0.000	110293.2	0.011	VV	0.058	31718.03	0.017
58	13.033		0.0000	0.000	91475.4	0.009	VV	0.082	18638.60	0.010
59	13.274		0.0000	0.000	738053.2	0.073	VV	0.057	216900.60	0.118
60	13.369		0.0000	0.000	74500.9	0.007	VV	0.073	16979.28	0.009
61	13.521		0.0000	0.000	143924.4	0.014	VV	0.065	36683.52	0.020
62	13.622		0.0000	0.000	47734.3	0.005	VV	0.067	11852.33	0.006
63	13.732		0.0000	0.000	63586.0	0.006	VV	0.067	15878.74	0.009
64	13.909		0.0000	0.000	226813.9	0.022	VV	0.085	44445.73	0.024
65	14.128		0.0000	0.000	97214.6	0.010	VV	0.080	20236.07	0.011
66	14.270		0.0000	0.000	169671.3	0.017	VV	0.068	41529.25	0.023
67	14.351		0.0000	0.000	40958.2	0.004	VV	0.051	13304.24	0.007
68	14.434		0.0000	0.000	168864.7	0.017	VV	0.086	32635.22	0.018
69	14.621		0.0000	0.000	51665.3	0.005	VV	0.067	12764.90	0.007
70	14.701		0.0000	0.000	146243.6	0.014	VV	0.068	36073.43	0.020
71	14.806		0.0000	0.000	28846.1	0.003	VV	0.070	6842.19	0.004
72	14.944		0.0000	0.000	82372.0	0.008	VV	0.065	21073.44	0.011
73	15.015		0.0000	0.000	35172.3	0.003	VV	0.055	10659.58	0.006
74	15.112		0.0000	0.000	71058.5	0.007	VV	0.075	15739.79	0.009
75	15.201		0.0000	0.000	79265.9	0.008	VV	0.061	21728.21	0.012
76	15.322		0.0000	0.000	109389.6	0.011	VV	0.081	22426.95	0.012
77	15.404		0.0000	0.000	70859.0	0.007	VV	0.058	20347.05	0.011
78	15.529		0.0000	0.000	44727.2	0.004	VV	0.059	12627.02	0.007

PK#	Ret Time	Name	Amount	Amount%	Area	Area%	Type	Width	Height	Height%
79	15.624		0.0000	0.000	66764.4	0.007	VV	0.064	17338.32	0.009
80	15.713		0.0000	0.000	38271.6	0.004	VV	0.087	7343.43	0.004
81	15.830		0.0000	0.000	19928.9	0.002	VV	0.086	3878.97	0.002
82	16.018		0.0000	0.000	150421.9	0.015	VV	0.068	36967.14	0.020
83	16.137		0.0000	0.000	42111.9	0.004	VV	0.068	10268.11	0.006
84	16.242		0.0000	0.000	9897.0	0.001	VB	0.066	2508.97	0.001
85	16.423		0.0000	0.000	7936.0	0.001	BV	0.072	1824.93	0.001
86	16.531		0.0000	0.000	253791.0	0.025	VV	0.066	64371.66	0.035
87	16.750		0.0000	0.000	9532.4	0.001	VV	0.085	1867.47	0.001
88	16.806		0.0000	0.000	4792.0	0.000	VV	0.050	1598.59	0.001
89	16.907		0.0000	0.000	58020.8	0.006	VV	0.063	15297.94	0.008
90	17.028		0.0000	0.000	22644.4	0.002	VV	0.073	5203.81	0.003
91	17.308		0.0000	0.000	79041.6	0.008	VV	0.093	14189.66	0.008
92	17.471		0.0000	0.000	17371.1	0.002	VV	0.064	4554.07	0.002
93	17.580		0.0000	0.000	35971.9	0.004	VV	0.059	10120.10	0.006
94	17.677		0.0000	0.000	28040.4	0.003	VV	0.067	6990.60	0.004
95	17.837		0.0000	0.000	48225.2	0.005	VV	0.092	8691.55	0.005
96	17.980		0.0000	0.000	12980.0	0.001	VV	0.070	3085.34	0.002
97	18.061		0.0000	0.000	27747.2	0.003	VV	0.085	5441.46	0.003
98	18.210		0.0000	0.000	8707.6	0.001	VV	0.062	2334.52	0.001
99	18.354		0.0000	0.000	55316.4	0.005	VV	0.081	11382.91	0.006
100	18.468		0.0000	0.000	22189.9	0.002	VV	0.058	6404.10	0.003
101	18.580		0.0000	0.000	27162.9	0.003	VV	0.055	8167.18	0.004
102	18.658		0.0000	0.000	17802.2	0.002	VV	0.054	5482.23	0.003
103	18.715		0.0000	0.000	16249.7	0.002	VV	0.050	5416.06	0.003
104	18.780		0.0000	0.000	28193.9	0.003	VB	0.058	8041.79	0.004
105	18.910		0.0000	0.000	19101.8	0.002	BV	0.067	4726.47	0.003
106	19.100		0.0000	0.000	18371.7	0.002	VV	0.150	2041.23	0.001
107	19.243		0.0000	0.000	16871.8	0.002	VB	0.067	4195.36	0.002
108	19.374		0.0000	0.000	7276.4	0.001	BV	0.056	2162.55	0.001
109	19.452		0.0000	0.000	16656.2	0.002	VV	0.072	3836.60	0.002
110	19.536		0.0000	0.000	11344.6	0.001	VV	0.060	3143.49	0.002
111	19.658		0.0000	0.000	185518.3	0.018	VV	0.063	48731.66	0.027
112	19.806		0.0000	0.000	8062.3	0.001	VB	0.055	2422.64	0.001
113	19.911		0.0000	0.000	8876.6	0.001	BB	0.050	2963.23	0.002

Total Area = 1011870000.0, Total Amount = 73806.96, Total Height = 183633600.0, Sample Units = ppm



Sample Name: **Site 0 0.1ul (Cryo)**  
 Acquired from HP1--FID via port 1 on 10/20/04 05:03:28pm by Sharon  
 Split -12/0,2/0/0,7/340/7 t=60 min, 0.1 ul  
 hp 16.5 (flow 1.65 ml/min) ; sv=150 ml/min  
 Data File: **E:\HPDATA\04-1509\PRODUC~1\140888.01R**  
 Method File: **!C:\HPDATA\04-1509\11MARCH.MET**  
 Calibration File: **!C:\HPDATA\04-1509\11MARCH.CAL**

PK#	Ret Time	Name	Amount	Amount%	Area	Area%	Type	Width	Height	Height%
1	1.931		0.0000	0.000	19262.0	0.194	BV	0.021	15216.98	0.373
2	2.009		0.0000	0.000	126138.8	1.270	VV	0.019	113121.50	2.771
3	2.168	IC4	1.5834	0.335	101292.2	1.020	VV	0.018	96336.53	2.360
4	2.325	NC4	3.3052	0.700	271265.2	2.732	VV	0.019	241915.90	5.926
5	2.983	IC5	1.4617	0.310	305135.6	3.073	VV	0.022	232187.80	5.688
6	3.396	NC5	0.7315	0.155	340985.8	3.434	VV	0.025	230793.70	5.653
7	4.109		0.0000	0.000	21117.5	0.213	VV	0.035	10010.07	0.245
8	4.835	CP	0.0693	0.015	32304.0	0.325	VV	0.031	17202.72	0.421
9	4.974	2,3DMB	0.0936	0.020	43640.8	0.439	VV	0.032	22547.59	0.552
10	5.184	2MP	0.4484	0.095	209022.7	2.105	VV	0.035	100034.40	2.450
11	5.674	3MP	0.3240	0.069	151017.1	1.521	VV	0.038	65634.76	1.608
12	6.445	NC6	0.8492	0.180	326140.8	3.284	VV	0.044	124005.30	3.038
13	7.328	MCP	0.4042	0.086	155237.4	1.563	VV	0.041	62403.25	1.529
14	7.690	2,4DMP+2,2,3TMB	0.3125	0.066	31807.1	0.320	VB	0.047	11195.32	0.274
15	8.360	Benzene	0.5484	0.116	55817.4	0.562	BV	0.052	17869.14	0.438
16	8.586	CH	0.4913	0.104	161004.4	1.621	VB	0.038	69938.54	1.713
17	9.252	2MHx+2,3DMP	0.6457	0.137	211606.8	2.131	BB	0.057	61699.03	1.511
18	9.570	3MHx	0.4421	0.094	144885.8	1.459	BV	0.035	69965.53	1.714
19	9.662	c1,3DMCP	0.1339	0.028	43898.0	0.442	VV	0.037	19833.56	0.486
20	9.760	t1,3DMCP	0.1141	0.024	37382.8	0.376	VB	0.034	18124.58	0.444
21	9.872	t1,2DMCP	0.1714	0.036	56169.2	0.566	BB	0.032	29347.31	0.719
22	10.549	NC7	0.9539	0.202	312608.9	3.148	BB	0.041	127147.30	3.115
23	11.015	MCH	0.2010	0.043	345264.0	3.477	BV	0.036	160455.50	3.930
24	11.193		0.0000	0.000	26122.2	0.263	VB	0.036	11942.67	0.293
25	11.505	EtCP	0.0121	0.003	23691.7	0.239	BB	0.035	11257.29	0.276
26	11.760		0.0000	0.000	52835.3	0.532	BV	0.054	16242.91	0.398
27	11.850	2,5DMHx+2,2,3TMP	0.0124	0.003	24226.1	0.244	VB	0.033	12371.15	0.303
28	12.107	2,3,4TMP	0.0140	0.003	27375.5	0.276	BB	0.033	13690.14	0.335
29	12.365	Toluene+2,3,3TMP	0.0675	0.014	131957.9	1.329	BV	0.052	42087.90	1.031
30	12.662	2,3DMHx	0.3201	0.068	36157.6	0.364	VB	0.040	15043.02	0.368
31	12.914	2MHP	1.7723	0.375	200169.2	2.016	BV	0.049	68757.85	1.684
32	13.031		0.0000	0.000	96418.3	0.971	VV	0.036	45230.46	1.108
33	13.099		0.0000	0.000	51608.4	0.520	VV	0.036	24096.11	0.590
34	13.151		0.0000	0.000	114362.9	1.152	VB	0.038	49878.55	1.222
35	13.444		0.0000	0.000	8350.6	0.084	BB	0.030	4579.65	0.112

PK#	Ret Time	Name	Amount	Amount%	Area	Area%	Type	Width	Height	Height%
36	13.646	2,2,5TMHx	0.4763	0.101	53790.6	0.542	BB	0.034	26021.69	0.637
37	13.902		0.0000	0.000	40447.5	0.407	BV	0.043	15781.75	0.387
38	14.033	NC8	2.3845	0.505	269314.5	2.712	VB	0.040	110995.70	2.719
39	14.491		0.0000	0.000	7624.2	0.077	BB	0.050	2530.29	0.062
40	14.620		0.0000	0.000	20168.8	0.203	BB	0.038	8766.91	0.215
41	14.798		0.0000	0.000	128185.9	1.291	BB	0.048	44400.23	1.088
42	14.960		0.0000	0.000	117774.0	1.186	BB	0.042	46268.26	1.133
43	15.154		0.0000	0.000	71990.1	0.725	BB	0.051	23749.40	0.582
44	15.424	EtBz	0.0592	0.013	74328.9	0.748	BB	0.046	27059.76	0.663
45	15.690	m+p-Xylenes	0.1111	0.024	44910.5	0.452	BB	0.029	25426.94	0.623
46	15.748		0.0000	0.000	34910.1	0.352	BB	0.029	19928.92	0.488
47	16.034		0.0000	0.000	127184.1	1.281	BB	0.062	34395.91	0.843
48	16.222		0.0000	0.000	91669.8	0.923	BB	0.043	35947.94	0.881
49	16.335	o-Xylene	0.0818	0.017	55638.3	0.560	BB	0.046	19943.94	0.489
50	16.489		0.0000	0.000	97655.8	0.983	BB	0.056	28976.87	0.710
51	17.032	NC9	0.7463	0.158	294614.1	2.967	BB	0.044	110476.60	2.706
52	17.300	IPBz	0.0809	0.017	29367.2	0.296	BB	0.040	12366.79	0.303
53	17.479		0.0000	0.000	10166.1	0.102	BB	0.035	4889.29	0.120
54	17.556		0.0000	0.000	25524.9	0.257	BB	0.063	6794.76	0.166
55	17.688		0.0000	0.000	54311.9	0.547	BB	0.035	26215.15	0.642
56	17.758		0.0000	0.000	14394.3	0.145	BB	0.030	8126.01	0.199
57	17.874		0.0000	0.000	17945.1	0.181	BB	0.045	6661.56	0.163
58	17.995	NPBz	0.2417	0.051	90386.4	0.910	BB	0.046	32468.38	0.795
59	18.177		0.0000	0.000	74064.3	0.746	BB	0.059	21100.57	0.517
60	18.380	1M3EtBz	0.2987	0.063	55116.7	0.555	BB	0.069	13217.66	0.324
61	18.536	1,3,5TMBz	0.2536	0.054	99877.1	1.006	BB	0.059	28411.75	0.696
62	18.740		0.0000	0.000	30194.4	0.304	BB	0.039	12780.33	0.313
63	18.809	1M2EtBz	0.1059	0.022	42254.0	0.425	BB	0.036	19645.11	0.481
64	18.977		0.0000	0.000	45488.2	0.458	BB	0.037	20469.57	0.501
65	19.177	1,2,4TMBz	0.4941	0.105	176785.4	1.780	BB	0.079	37231.83	0.912
66	19.510		0.0000	0.000	22391.2	0.225	BB	0.050	7528.84	0.184
67	19.607		0.0000	0.000	15995.9	0.161	BB	0.060	4469.80	0.109
68	19.726	NC10	0.2812	0.060	203474.7	2.049	BB	0.040	85017.02	2.083
69	19.883	1,2,3TMBz	0.1313	0.028	50697.7	0.511	BB	0.063	13493.25	0.331
70	20.123		0.0000	0.000	14015.6	0.141	BB	0.058	4012.84	0.098
71	20.339		0.0000	0.000	43968.7	0.443	BB	0.033	21950.46	0.538
72	20.412		0.0000	0.000	33243.7	0.335	BB	0.045	12286.22	0.301
73	20.627		0.0000	0.000	16568.7	0.167	BB	0.037	7434.57	0.182
74	20.715		0.0000	0.000	33658.9	0.339	BB	0.051	10923.31	0.268
75	20.879		0.0000	0.000	34169.8	0.344	BB	0.040	14195.80	0.348
76	21.060		0.0000	0.000	22809.6	0.230	BB	0.059	6391.25	0.157
77	21.190		0.0000	0.000	18012.5	0.181	BB	0.034	8951.38	0.219
78	21.263		0.0000	0.000	19887.8	0.200	BB	0.034	9732.68	0.238

PK#	Ret Time	Name	Amount	Amount%	Area	Area%	Type	Width	Height	Height%
79	21.354		0.0000	0.000	50148.6	0.505	BB	0.049	17156.96	0.420
80	21.506		0.0000	0.000	59427.1	0.598	BB	0.055	18038.80	0.442
81	21.749		0.0000	0.000	18152.9	0.183	BB	0.045	6700.00	0.164
82	21.977		0.0000	0.000	35892.8	0.361	BB	0.097	6145.36	0.151
83	22.203	NC11	0.4429	0.094	159733.4	1.608	BB	0.039	68011.30	1.666
84	22.372		0.0000	0.000	16790.3	0.169	BB	0.051	5449.46	0.133
85	22.678		0.0000	0.000	27527.6	0.277	BB	0.065	7017.34	0.172
86	22.782		0.0000	0.000	11460.5	0.115	BB	0.044	4359.84	0.107
87	22.934		0.0000	0.000	49873.9	0.502	BB	0.078	10608.88	0.260
88	23.171		0.0000	0.000	18460.4	0.186	BB	0.075	4084.51	0.100
89	23.495		0.0000	0.000	32531.9	0.328	BB	0.064	8527.85	0.209
90	23.706		0.0000	0.000	26452.3	0.266	BB	0.037	12043.03	0.295
91	23.853		0.0000	0.000	29472.9	0.297	BB	0.050	9785.69	0.240
92	24.253		0.0000	0.000	15255.3	0.154	BB	0.047	5414.41	0.133
93	24.392		0.0000	0.000	13376.5	0.135	BB	0.074	2992.89	0.073
94	24.506	NC12	0.3472	0.074	164885.4	1.660	BB	0.045	61544.82	1.508
95	24.851	IP13	0.1258	0.027	59727.0	0.601	BB	0.051	19531.57	0.478
96	25.011		0.0000	0.000	17408.3	0.175	BB	0.079	3674.65	0.090
97	25.197		0.0000	0.000	13622.9	0.137	BB	0.073	3109.20	0.076
98	25.295		0.0000	0.000	17639.8	0.178	BB	0.039	7467.19	0.183
99	25.567		0.0000	0.000	12337.9	0.124	BB	0.053	3902.61	0.096
100	25.708		0.0000	0.000	20927.7	0.211	BB	0.065	5354.41	0.131
101	25.807		0.0000	0.000	14029.7	0.141	BB	0.038	6231.81	0.153
102	25.909		0.0000	0.000	27887.7	0.281	BB	0.045	10268.97	0.252
103	26.049	2MNaph	0.0452	0.010	21477.7	0.216	BB	0.040	9003.13	0.221
104	26.139	IP14	0.0982	0.021	60152.6	0.606	BB	0.044	22675.59	0.555
105	26.453	1MNaph	0.0728	0.015	44626.0	0.449	BB	0.102	7278.97	0.178
106	26.662	NC13	67.2894	14.257	148024.0	1.491	BB	0.043	57062.46	1.398
107	26.932		0.0000	0.000	16600.5	0.167	BB	0.071	3897.84	0.095
108	27.068		0.0000	0.000	15224.5	0.153	BB	0.048	5330.85	0.131
109	27.504		0.0000	0.000	10351.0	0.104	BB	0.033	5209.49	0.128
110	27.721		0.0000	0.000	7711.6	0.078	BB	0.034	3805.11	0.093
111	27.880		0.0000	0.000	16099.5	0.162	BB	0.042	6362.74	0.156
112	27.982		0.0000	0.000	19688.8	0.198	BB	0.042	7864.67	0.193
113	28.118		0.0000	0.000	14477.4	0.146	BB	0.041	5821.45	0.143
114	28.276	IP15	19.3054	4.090	42468.2	0.428	BB	0.039	18260.08	0.447
115	28.441		0.0000	0.000	24770.3	0.249	BB	0.115	3604.44	0.088
116	28.691	NC14	56.3797	11.945	124024.7	1.249	BB	0.039	52768.31	1.293
117	29.370		0.0000	0.000	14824.5	0.149	BB	0.070	3525.96	0.086
118	29.581		0.0000	0.000	23611.0	0.238	BB	0.076	5186.10	0.127
119	29.831		0.0000	0.000	7526.5	0.076	BB	0.034	3702.70	0.091
120	29.939	IP16	29.1227	6.170	64064.6	0.645	BB	0.043	24717.76	0.605
121	30.063		0.0000	0.000	14892.2	0.150	BB	0.041	6033.12	0.148

PK#	Ret Time	Name	Amount	Amount%	Area	Area%	Type	Width	Height	Height%
122	30.606	NC15	56.5427	11.980	124383.3	1.253	BB	0.048	43524.08	1.066
123	30.789		0.0000	0.000	10478.4	0.106	BB	0.059	2948.91	0.072
124	31.150		0.0000	0.000	8203.7	0.083	BB	0.048	2876.63	0.070
125	31.522		0.0000	0.000	39041.2	0.393	BB	0.092	7052.31	0.173
126	31.679		0.0000	0.000	13404.2	0.135	BB	0.053	4213.83	0.103
127	31.777		0.0000	0.000	10112.1	0.102	BB	0.037	4564.32	0.112
128	32.416	NC16	39.6195	8.394	87155.5	0.878	BB	0.043	34078.90	0.835
129	33.322	IP18	17.2141	3.647	37867.7	0.381	BB	0.054	11607.94	0.284
130	33.526		0.0000	0.000	7648.9	0.077	BB	0.042	3047.81	0.075
131	33.653		0.0000	0.000	12856.0	0.129	BB	0.055	3896.37	0.095
132	34.131	NC17	31.4743	6.669	69237.5	0.697	BB	0.043	26956.68	0.660
133	34.297	IP19	23.2861	4.934	51225.0	0.516	BB	0.047	18011.81	0.441
134	35.101		0.0000	0.000	18605.7	0.187	BB	0.093	3340.83	0.082
135	35.762	NC18	23.7418	5.030	52227.5	0.526	BB	0.044	19930.01	0.488
136	35.977	IP20	12.5849	2.666	27684.4	0.279	BB	0.048	9518.92	0.233
137	37.318	NC19	22.5308	4.774	49563.6	0.499	BB	0.053	15491.19	0.379
138	38.806	NC20	14.7619	3.128	32473.5	0.327	BB	0.045	11964.49	0.293
139	40.230	NC21	10.2165	2.165	22474.5	0.226	BB	0.044	8461.94	0.207
140	41.601	NC22	7.8407	1.661	17248.2	0.174	BB	0.045	6419.30	0.157
141	42.906	NC23	6.0705	1.286	13353.9	0.134	BB	0.045	4912.19	0.120
142	44.146	NC24	4.9457	1.048	10879.7	0.110	BB	0.048	3787.47	0.093
143	45.323	NC25	4.6133	0.977	10148.4	0.102	BB	0.067	2519.81	0.062
144	53.374	NC33	2.0818	0.441	4579.5	0.046	BB	0.031	2485.73	0.061
145	57.397		0.0000	0.000	474857.3	4.782	BB	4.816	1643.45	0.040

Total Area = 9930606.0, Total Amount = 471.984, Total Height = 4082388.0

# **Appendix E**

## **Technical Note: Oil Recovery**

Len Zabilansky  
US Army Cold Regions Research Engineering Laboratory

## OIL RECOVERY

To limit the clean up procedure, the experiment was designed for the oil to be spilled within containment hoops. The approach was very simple and effective except for two oversights, of neither which affected the overall outcome of the experiment: oil delivery in hoop 2-3 and the hoop in the rough ice. The oil delivery J pipe used to inject the oil in hoop 2-3 was oriented horizontal, and therefore, oil was released outside the containment hoop. The confusion on the orientation of the delivery piping could be avoided using a straight delivery pipe facilitating easier orientation on the pipe from the surface. In the rough ice, the PVC frame was encapsulated into the irregular bottom of the ice and the containment skirts did not extend through the entire ice depth. As the ice melted non-uniformly around the hoop, the oil floated over the top of the flotation frame and escaped to the rest of the tank. This problem could be avoided in future tests with full depth skirts.

As the first test involving oil and ice at the CRREL facilities, there was an inevitable learning curve associated with the clean-up process. The oil recovery system used previously at the OHMSETT facility was used as a starting point, but the ice impeded the oil recovery at CRREL. Eventual recovery procedures were developed using trial and error with a mix of equipment brought in as required. The disposal of the oil and absorbent pads followed guidelines established by the U.S. Army and CRREL.

The following points can be considered "lessons learned" that could be used to develop more effective recovery procedures for future oil and ice test programs at CRREL.

1. Immediately following the test, the free oil should be recovered where possible.
2. Accelerate the ice melting by elevating the room temperature and circulating the air with high volume fans. The wind vector should be parallel with the water surface to improve the heat exchange, but not impinge on the surface causing emulsification of the oil.
3. The wind generated by the fans on the melt tank cover, west end of the tank, pushes the free oil to the east end of the tank as the ice melts.
4. The belt type oil skimmer located at the east end of the tank can run continuously and recover the oil as it is pushed across the surface by the wind. This approach removes 95% of the oil.
5. The oil film that accumulates to the tank walls should be wiped off with oil absorbing pads prior to pressure washing the side of the tank.
6. Any oil films on the water surface can be recovered effectively using oil absorbent booms.

# **Appendix F**

## **Technical Note: Potential for Seismic Methods**

Lee Liberty

Boise State University

Center for Geophysical Investigation of the Shallow Subsurface

## SEISMIC METHODS

Seismic reflection methods have shown promise in imaging through sea ice (e.g., Jones and Kwan, 1984; Jones et al., 1986). The primary challenge in acquisition comes from the need to couple the source and receiver to the ice surface. Once achieved, seismic frequencies upwards of 200 kHz, that produce cm-scale wavelengths, have been documented to penetrate sea ice (e.g., Jones et al., 1986). Although these earlier studies concluded that simple reflection methods to identify amplitude anomalies due to the presence of oil under sea ice was not possible, improvements in acquisition and processing technologies have prompted us to revisit the potential use of seismic methods to address this problem. Here, we discuss the physical properties of each material involved and we model the response of the presence of oil under sea ice under various conditions.

### Physical Properties

To examine the theoretical use of seismic reflection methods to identify the presence of oil under a layer of sea ice, we begin by defining the seismic properties of water, oil, and ice. The seismic reflection coefficient (R) defines the relative amplitude of energy reflected back toward the source. Under plane wave conditions (valid under the model conditions), this equation requires both seismic velocity and density values of the contrasting media. The reflection coefficient is defined as:

$$R = (\rho_2 V_2 - \rho_1 V_1) / (\rho_2 V_2 + \rho_1 V_1)$$

Where  $\rho$  is the density in  $\text{g/cm}^3$  for the top (1) and bottom (2) layers, and  $V$  is the velocity in  $\text{m/s}$  of layers 1 and 2. A negative reflection coefficient implies a decrease in the velocity-density contrast across an interface.

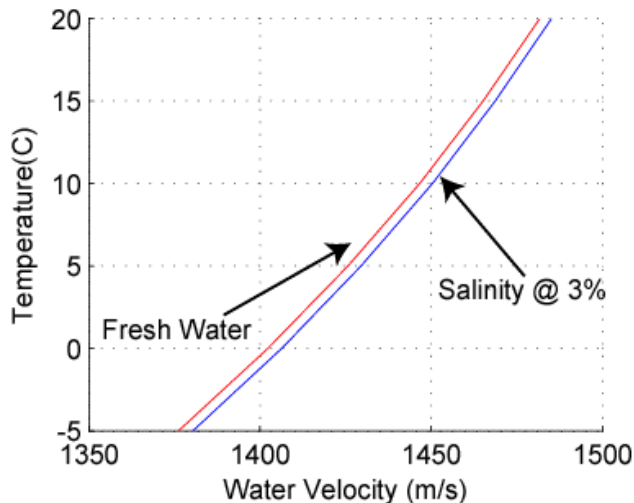


Figure 1. Water velocity vs. temperature for fresh water and salt water conditions.

### Water

The seismic velocity in water varies as a function of water temperature, depth, and salinity. The equation that governs water velocity (Sheriff, 2002) is as follows:

$$v_{\text{water}} = 1449.2 + 4.6T - 0.055T^2 + 0.0003T^3 + (1.34 - 0.01T)(S - 35) + 0.016Z$$

where  $v_{\text{water}}$  represents water velocity in  $\text{m/s}$ ,  $T$  represents temperature in Celcius,  $S$  represents salinity in ppm, and  $Z$  represents water depth in meters. Figure 1 shows seismic velocity

curves for both fresh water and salt water conditions over a range of temperatures. Note the water velocity at 0° C for 3 ppm salt water is 1,406 m/s. Water densities for fresh water and salt water are 1.0 g/cm<sup>3</sup> and approximately 1.025 g/cm<sup>3</sup> respectively.

### Oil

Oil velocity varies as a function of oil density, pressure, and temperature. Oil densities are often measured using American Petroleum Institute values where:

$$API\ gravity = (141.5/\rho_0)-131.5$$

Batzle and Wang (1992) define ultrasonic seismic velocity for oil as the following:

$$v_{oil}=15450(77.1+API)^{-1/2} - 3.7T+4.64P+0.0115(0.36API^{1/2}-1)TP;$$

where P is pressure. Since pressure at surface conditions approaches 0, oil velocity for our analysis simplifies to:

$$v_{oil} = 15450(77.1+API)^{-1/2} - 3.7T;$$

Figure 2 shows the relationship between oil density and API value and also seismic velocity for oil as a function of density for a range of temperatures. Here, we will not be concerned with the condition of heavy oil that is denser than salt water. The seismic velocity at 0° C for a medium crude oil of 33 API is 1,472 m/s.

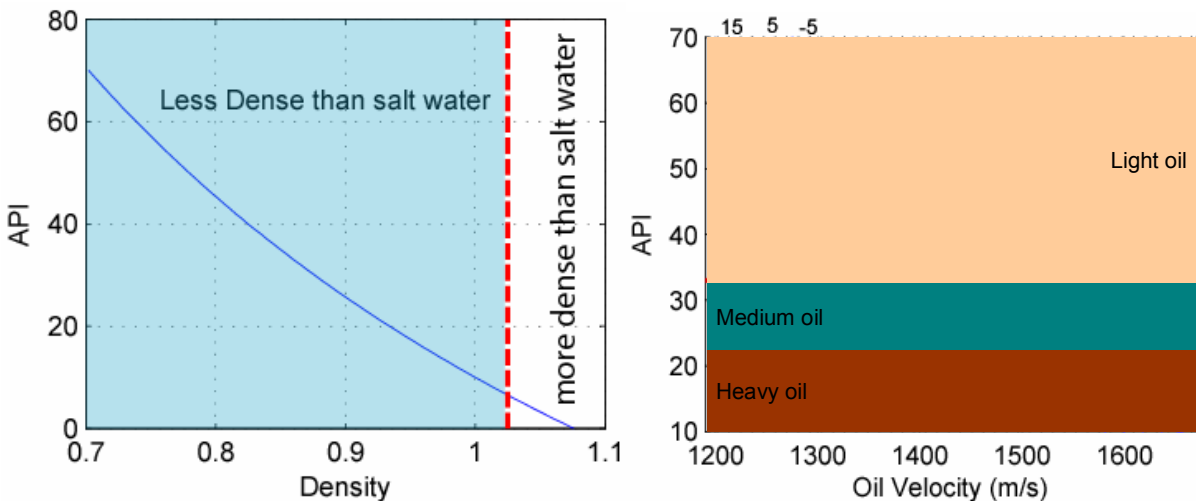


Figure 2 (A) Oil density vs. API gravity curve. Note that API values less than 10 are less dense than fresh water ( $\rho = 1$ ). (B) Seismic velocity of oil vs. API. Each curve represents constant temperature with the bold line representing 0° C

### Sea Ice

Seismic properties for sea ice can vary widely as parameters such as ice age and origin vary. Jones et al. (1986) define seismic values for first year salt water ice as follows:

*P-wave velocity=3300 m/s*  
*Density=0.9 g/cc*

Since the seismic velocity for sea ice is significantly greater than either oil or water, the precise seismic velocity for an ice/water or ice/oil interface will not significantly change the models presented below. Therefore, we use these published values for sea ice properties in this study.

### Modeled results

We model two possible scenarios to determine whether seismic methods can assist in identifying the presence of oil under sea ice. The first condition is where an ice/water interface is present and no oil appears (2-layer model). The second condition models oil present immediately below an ice layer and water is present below the oil interface (3-layer model).

The seismic properties defined above for water, oil, and ice all suggest that a large negative reflection coefficient will appear at either an ice/oil or an ice/water contact with more than 40 percent (reflection coefficient <-0.40) of the seismic energy returning to the ice surface under most modeled conditions. The question we will address is whether the oil/water contact will appear as an identifiable reflection or amplitude effect.

Figure 3 shows the reflection coefficient for a range of oil and salt water conditions. This figure shows that high density oil (low API) will record a negative reflection coefficient.

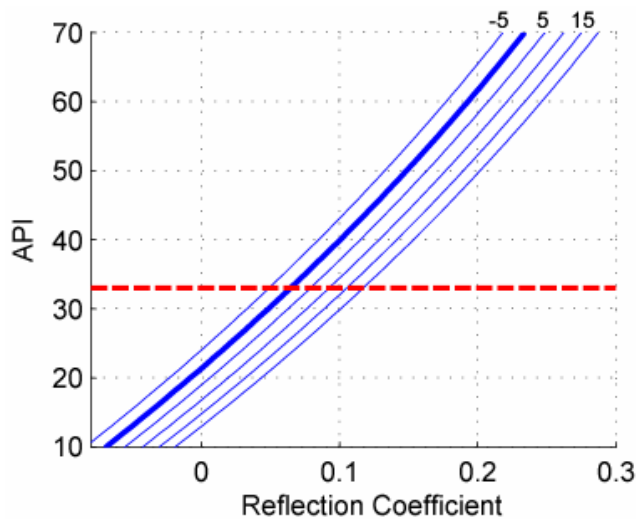


**Figure 3. Reflection coefficients for a range of oil densities and salt water temperatures. The bold line curve represents 0° C.**

Under these conditions (less than 22 API for 0° C), oil is denser than salt water (Figure 2) and oil will not float. For medium and light oil conditions (>22 API), reflection coefficients are greater than 0. This figure shows that larger API values and larger temperatures increase the reflection coefficient. Hence, seismic methods to identify the presence of oil under ice improve as the oil density decreases.

Figure 4 shows the results of an acoustic finite difference model under a variety of oil under sea ice conditions. We use a 100 kHz

seismic source and velocity and density values discussed above to produce the results. We show the seismic response of the presence of oil thicknesses that range from 1 cm to 5 cm for two different oil densities, 33 API (medium-weight oil) and 50 API (light-weight oil). Figure 4 shows there is a clear separation of the wavelets from oil/water

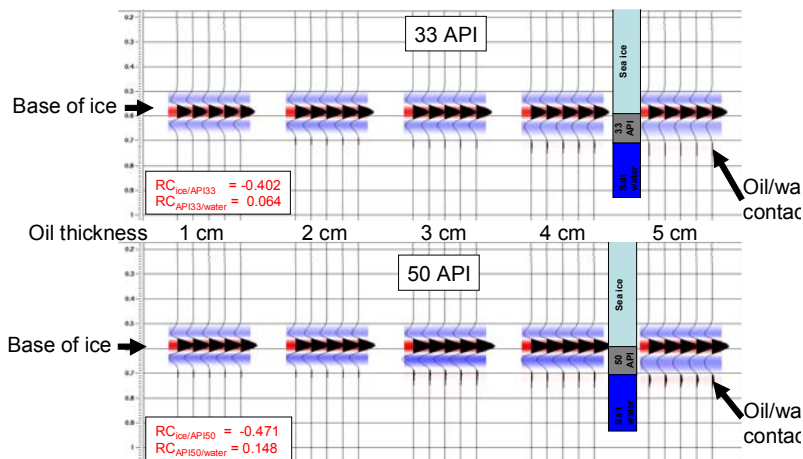


**Figure 3. Finite difference response to the presence of oil under sea ice. Each 5 trace set represents changing oil thicknesses for 33 API oil (top) and 50 API oil (bottom). Density and velocity values are discussed in the text. RC=reflection coefficient**

interface and the ice/oil interface under the range of oil thicknesses. This is in contrast to the radar methods where the wavelengths are much larger and we rely on thin-bed methods to characterize oil properties. These modeled results suggest if we can couple the seismic source to the ice surface, we can use seismic methods to identify the presence of oil under ice.

## Results

The modeled results presented here show that seismic methods can identify the presence of oil under sea ice. Although the amplitude effects diminish when oil thicknesses or oil densities decrease, increased dynamic range of new acquisition systems coupled with advanced processing routines to address thin bed problems should provide adequate resolution to distinguish the presence of oil under ice when compared to an ice/water interface. The challenge to the use of seismic methods now turns to the challenge of efficiently and quickly coupling the seismic source and receivers to the ice surface.

## References

- Betzle, M. and Wang, Z., 1990, Seismic properties of pore fluids, *Geophysics*, 57 (11), p. 1396-1408.
- Jones, H.W., and Kwan, H.W., 1982, The detection of oil spills under arctic ice by ultrasound, in *Proceedings of the 5<sup>th</sup> annual arctic marine oil spill program technical seminar* (Environmental Protection Service, Ottawa), p. 391-411.
- Jones, H.W., Kwan, H.W., Hayman, T., and Yeatman, E.M., 1986, The detection of liquids and viscoelastic substances trapped under solid surfaces, *Journal of Acoustical Society of America*, 79(1), p. 84-90.

